Makassar Strait Intraseasonal Variability

Kandaga Pujiana

Submitted in partial fulfillment of the
requirements for the degree
of Doctor of Philosophy
in the Graduate School of Arts and Sciences

COLUMBIA UNIVERSITY

2012

ABSTRACT

Makassar Strait Intraseasonal Variability

Kandaga Pujiana

The intraseasonal variability (ISV; 20-90 days) in Makassar Strait, the primary pathway for Pacific water flow into the Indian Ocean and a waveguide for transmitting subinertial energy from the tropical Indian Ocean to Indonesian seas, is investigated, using the 2004-2006 *International Nusantara Stratification and Transport* (INSTANT) observations. The INSTANT current and temperature timeseries in the Labani Channel, a narrow constriction in Makassar Strait, are used to identify the ISV. Additionally, insitu current measurements along with satellite-derived wind and sea level anomaly data in the region are employed to track the transmission of ISV from their likely origin.

We find that the Makassar Strait ISV can be classified as locally or remotely forced features. Local winds and shear flow instability-generated eddies within Makassar Strait control the locally forced ISV component, while the remotely forced part is linked to equatorial Indian Ocean Kelvin waves and Sulawesi Sea eddies. The oceanic response to the local wind stress varying at periods of 45-90 days, with 60-day oscillation showing the strongest coherence, is constrained to along-strait flow primarily within the upper 50 m of the water column. At depths greater than 50 m, we observe that the 20-40 day variability reflects locally generated eddy signatures, while the 60-90 day variability agrees with remotely forced Kelvin wave characteristics. Moreover the Sulawesi Sea ISV, signifying eddy signatures, and along-strait flow across the Makassar Strait pycnocline of 50-450 m display significant coherence at periods of 45-90 days.

The observed 60-90 day variability at depths of 100-450 m, coinciding with weaker Makassar Strait throughflow, exhibits Kelvin wave signatures including vertical energy propagation, energy equipartition, non-dispersive relationship and semi-geostrophic balance. Current meters at 750 m and 1500 m further provide evidence that the vertical

structure of the Kelvin waves resembles that of a second baroclinic mode. We propose that the intraseasonal Kelvin waves emanate from the tropical Indian Ocean as wind-forced equatorial Kelvin waves and propagate along a waveguide which extends from the south-western coasts of the Indonesian archipelago to Makassar Strait, via Lombok Strait. From Lombok Strait to Makassar Strait, the Kelvin waves navigate along the 100-m isobath. The intraseasonal Kelvin waves induce increased vertical shear of the along-strait flow across the pycnocline, which potentially leads to instability with a vertical mixing rate of 1-5x 10^{-5} m^2s. Moreover the intraseasonal Kelvin waves also force the ITF transport anomalies in Makassar Strait.

The 20-40 day variability is most evident in the across-strait flow, and in the across-strait gradient of the along-strait flow as well as in the vertical displacements of isotherms observed at depths of 100-300 m. The flow fields at 20-40 days are approximated by a vortex velocity structure, and the corresponding isotherm displacements signify potential vorticity conservation. We propose that southward-advected eddies, generated in the northern Makassar Strait at latitudes of 0.5°-2°S due to background flow instability, likely explain the 20-40 day variability observed in the Labani Channel.

Table of Contents

List of Figures

Acknowledgments

I gratefully acknowledge my advisor, Arnold L. Gordon, for his advice and tremendous support throughout. My gratitude also extends to my committee members, Hsien-Wang Ou, Douglas Martinson, Raghu Murtugudde, and Andreas Thurnherr for their encouragement and stimulating discussions. I am also grateful for the contributions of Janet Sprintall, Joe Metzger, Amy Ffield, Dwi Susanto, and Bruce Huber. Debra Tillinger, Phil Orton, Zach Tessler, and Phil Mele thanks for patiently sharing the office module at Lamont.

Columbia University and project grants from the National Science Foundation generously supported my studies. Special thanks for the wonderful DEES and OCP ladies, Mia Leo, Missy Pinckert, Carol Mountain, Laura Litchblau, and Claudia Giulivi for their care.

Finally, my Bandung and Siantar family for their prayer: Hj. Elis Pudjaastuti, Inang Haloho, Kartika Juniastuti, Kanaga Pujiadi, and Kantika Noviastuti. And of course my beloved wife, Asmi Napitu, for her support and jokes. I dedicate this thesis to my late father, Kardana.

Chapter 1

Introduction

The Makassar Strait is located at the heart of the Indonesian seas, which are characterized by multitude of passages, shallow and deep basins with complex bathymetry; bordered by the Pacific and Indian Ocean (Figure 1.1). The geometry of the Makassar Strait deep passage (> 50-m) has an hourglass shape with a 45-km wide Labani Channel as its narrowest constriction, near 3°S, and the shallowest section, Dewakang Sill of ∼680 m, marks the southern Makassar Strait (Figure 1.1).

Makassar Strait is the primary inflow portal for the Indonesian Throughflow (ITF; Gordon *et al.*, 1999; Gordon, 2005; Gordon *et al.*, 2008). The ITF, which affects the heat and freshwater budgets of both oceans (Byrden and Imawaki, 2001), potentially exerts significant control over global climate in general and tropical climate in particular through modifying sea surface temperature in the Pacific and Indian Ocean (Schneider, 1998).

Mooring observations in the Labani Channel (Figure 1.1), from December 1996 to June 1998 during the *Arus Lintas Indonesia* (ARLINDO; Gordon and Susanto, 1999) program measured the ITF transport in Makassar Strait of 9.2±2.7 Sv (1 Sv = 10^6 m^3/s; Gordon *et al.*, 1999). The more extensive program of the throughflow observation, the *International Nusantara Stratification and Transport* (INSTANT) program (Sprintall *et al.*, 2004), during January 2004-November 2006 reported the Makassar Strait throughflow of 11.6±3.3 Sv (Gordon *et al.*, 2008), a 27% increase compared to that observed in the ARLINDO program. Both programs, however, consistently reveal that the throughflow transport anomaly shows large variability at subinertial timescales (>10 days; Gordon *et al.*, 2010). The Asia-

Australia monsoons affect the seasonal cycle of the Makassar Strait throughflow transport as the transport attains maximum values towards the end of the northwest and southeast monsoons with minimum transport in October-December (Gordon *et al.*, 2008). At longer timescales, the Makassar Strait throughflow transport variability demonstrates a significant correlation with El Niño-Southern Oscillation (ENSO) with a sustained high transport during La Niña phase and significantly reduced transport during El Niño (Gordon *et al.*, 1999; Gordon *et al.*, 2008; Tillinger and Gordon, 2010).

In addition, Makassar Strait is part of a planetary waveguide extending along the equatorial Indian Ocean to the southwestern coasts of Indonesia, entering Makassar Strait via Lombok Strait (Figure 1.1; Wijffels and Meyers, 2004). Analyzing the temperature time series inferred from expendable bathythermograph (XBT) sections between Java and Australia, Wijffels and Meyers(2004) hypothesize a wave pathway, spreading the equatorial Indian Ocean wind energy with timescales longer than semiannual cycle (180-day) into the Indonesian seas. Sprintall *et al.*(2000) argue that a semiannual coastally trapped Kelvin wave generated via an equatorial Kelvin wave impinging upon the west Sumatra coast propagates along the waveguide and forces the northward geostrophic flow in Lombok and Makassar Straits during the transition months from the northwest monsoon to southeast monsoon. Furthermore some numerical studies suggest that the waveguide is also a viable medium for channeling energy into internal Indonesian seas at shorter timescales such as intraseasonal periods (20-90 days; Qiu *et al.*, 1999; Schiller *et al.*, 2010). Thus, Makassar Strait is an intersection of the inflowing Pacific water into the Indian Ocean and a waveguide transmitting energy from the tropical Indian Ocean to Indonesian seas.

This study investigates the Makassar Strait intraseasonal features and their genesis. We classify the observed intraseasonal signatures in Makassar Strait into two types: locally and remotely generated. The local winds and eddies force the locally generated intraseasonal features, while the remotely forced ones are linked to Kelvin waves originating in the Indian Ocean and eddies from the Sulawesi Sea. Gordon *et al.*(1999) suggest that the episode when the ITF turned northward in May 1997 is likely attributed to an intraseasonal event, which indicates the influence of intraseasonal oscillations on the Makassar Strait throughflow transport. We examine if the theoretical Kelvin wave signatures can explain

the characteristics of the ITF reversal events occurring at every 2-3 months. The pathway guiding the Kelvin waves from Lombok Strait to Makassar Strait and the effect of the Kelvin waves on the transport variability and mixing environment in Makassar Strait are discussed as well. At the high end of the intraseasonal frequency band, Gordon *et al.*(2008) report strong monthly temperature fluctuations that do not correlate with the ITF transport in the Makassar Strait lower pycnocline. We determine that the observed monthly temperature variability is associated with the southward advected eddies, generated due to instability of the ITF in the northern Makassar Strait.

Chapter 2 aims to identify the dominant intraseasonal oscillations within the Makassar Strait pycnocline using the along-strait flow data from the INSTANT program. The along-strait flow time series consistently reveal the presence of the 45-90 day motions as the dominant oscillations throughout the Makassar Strait pycnocline, but point to three plausible different forcings: the dominant oscillations at the upper 50-m of the water column show a significant correlation with the local winds, while those at depths of 100-400 m may derive their energy from remote forcing in Sulawesi Sea and the equatorial Indian Ocean.

Chapter 3 focuses more on the relationship between the observed 60-90 day variability and theoretical Kelvin wave attributes. Using the along-strait flow and temperature dataset in Makassar Strait, we demonstrate that the data exhibit Kelvin wave characteristics including vertical energy propagation, energy equipartition, non-dispersive relationship and semi-geostrophic balance. We propose that the 100-m isobath acts as the waveguide for the Kelvin wave to propagate from Lombok Strait to Makassar Strait. The impact of the Kelvin wave on the Makassar Strait throughflow and mixing environment is presented.

Chapter 4 describes the 20-40 day variability trapped in the Makassar Strait lower pycnocline. Aside from the along-strait flow and temperature time series, we also include the across-strait flow data, a parameter that has been overlooked in previous studies, in our analysis. At the 20-40 day period band, the observed flow fields within the lower pycnocline depths can be approximated by the vortex velocity structure. The relationship between the vertical displacement of the isopycnal surfaces and the flow field signifies potential vorticity conservation. We thus propose that the 20-40 day motion observed in Makassar Strait is an eddy expression. Analyses of the model flow field suggest that the eddy is generated in

the northern Makassar Strait at the lower pycnocline depths where the eddy kinetic energy and the sheared ITF are most energetic. The eddy is advected southward along with the ITF and dissipates its energy in the southern Makassar Strait.

In Chapter 5 we present summary and discussion on possible future research to further advance our understanding on the dynamics of the intraseasonal variability in the region in general and in the Makassar Strait in particular.

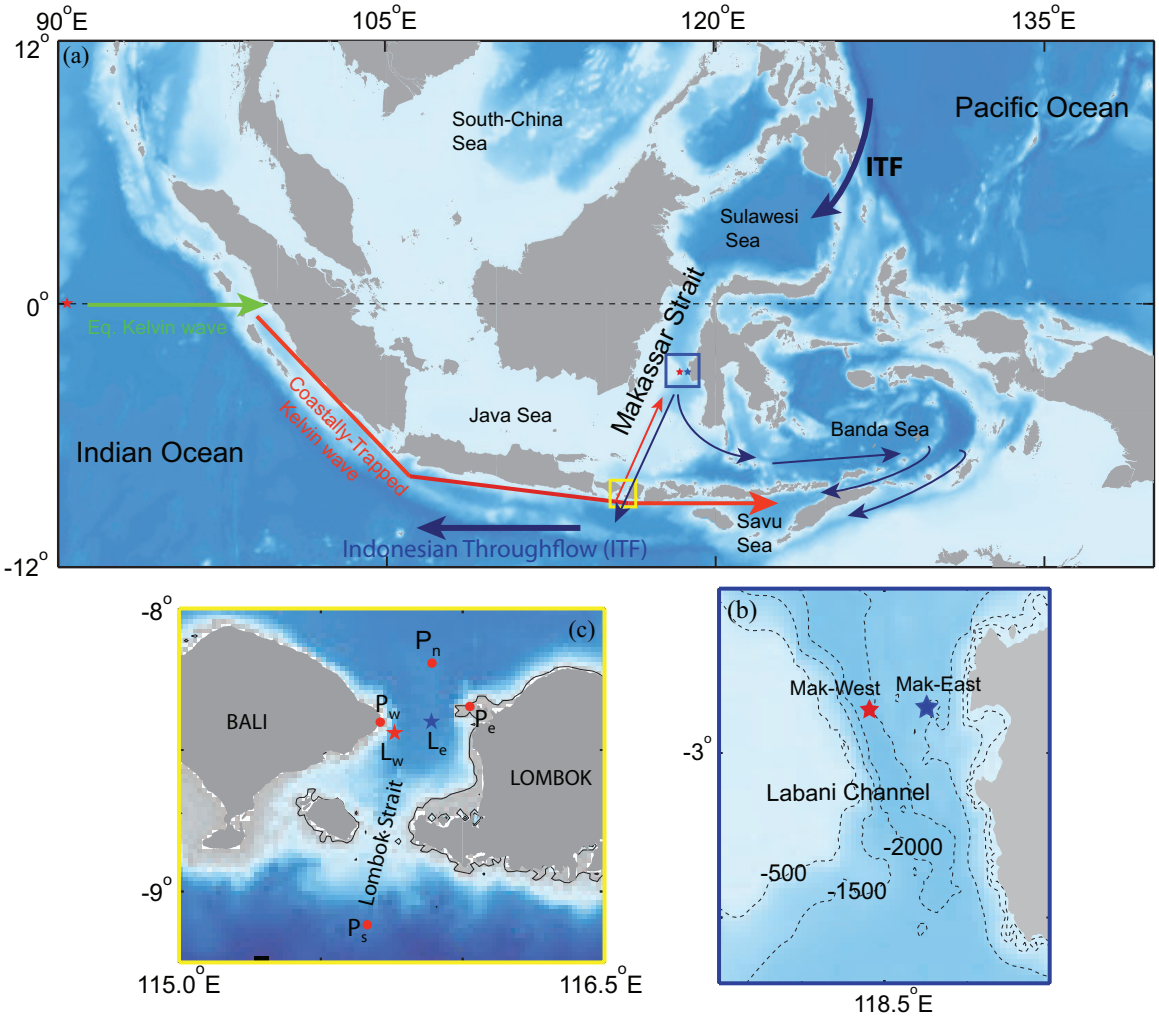

Figure 1.1: (a) The Makassar Strait location in the maritime continent, and the schematic of the Indonesian throughflow [ITF] pathways and of the waveguide for the Indian Ocean Kelvin wave. (b) An expanded view of the blue box in (a) showing the Labani Channel, the narrowest deep passage within Makassar Strait where the moorings [Mak-West and Mak-East] were deployed. (c) An expanded view of the yellow box in (a) displaying the Lombok Strait and corresponding mooring [Lw and Le], shallow pressure gauge [Pw and Pe] and altimeter measurement [Pn and Ps] sites.

Chapter 2

Intraseasonal Variability in the Makassar Strait Thermocline

Published as: Pujiana, K., Gordon, A. L., Sprintall, J., and Susanto, R.D. 2009. Intraseasonal Variability in the Makassar Strait Thermocline. Journal of Marine Research, 67.757-777.

Abstract Intraseasonal variability [ISV] in the Makassar Strait thermocline is examined through the analysis of along-channel flow, regional sea level anomaly and wind fields from January 2004 through November 2006. The dominant variability of 45-90 day in the Makassar Strait along-channel flow is horizontally and vertically coherent and exhibits downward energy propagation. The majority of the Makassar ISV is uncoupled to the energy exerted by the local atmospheric ISV: instead the Makassar ISV is due to the combination of a remotely forced baroclinic coastal Kelvin wave radiating from Lombok Strait and deep reaching ISV originating in the Sulawesi Sea. Thermocline depth changes associated with ENSO influence the ISV characteristics in the Makassar Strait lower thermocline, with intensified ISV during El Niño when the thermocline shallows, and weakened ISV during La Niña.

2.1 Introduction

The flow through Makassar Strait represents the primary inflow gateway of the Pacific water composing the Indonesian Throughflow [ITF] (Figure 2.1; Gordon and Fine, 1996). Gordon *et al.*(1999, 2008) showed that the Makassar throughflow is thermocline intensified, seasonally dependent, and modulated by El Niño-Southern Oscillation [ENSO] signals. Additionally, there are energetic fluctuations at tidal and intraseasonal [<90 day period] time scales (Susanto *et al.*, 2000).

The intraseasonal variability [ISV] within the atmosphere is a prominent feature of tropical climate, particularly in the region affected by the Asian and Australian-Indonesian monsoons (Mcbride and Frank, 1996). Two primary elements of ISV of the tropical atmosphere are the Madden-Julian Oscillation (MJO) and the convectively coupled equatorial Rossby waves (Madden and Julian, 1971; Wheeler *et al.*, 2000). Variances of MJO and equatorial Rossby waves are confined within the period bands of 30-80 days and 10-40 days respectively, and the motions of both features are primarily zonal in direction.

The oceanic ISV of the ITF is influenced by the remote wind variation in the Indian Ocean (Wijffels and Meyers, 2004; Sprintall *et al.*, 2000) and the Pacific Ocean (Cravette *et al.*, 2004; Qu *et al.*, 2008). For example, relaxation of the southward flow within Makassar Strait with current reversal in the lower thermocline during the monsoon transition period [April/May and October/November] is considered to be an intrusion of Indian Ocean semi-annual coastal Kelvin waves [CTKW] (Sprintall *et al.*, 2000; Syamsudin *et al.*, 2004; Iskandar *et al.*, 2005). Intraseasonal variability within the ITF inflow portal may also be indirectly influenced by the tropical intraseasonal wind in the Pacific Ocean. Cravette *et al.*(2004), utilizing altimeter data, demonstrated the dynamics of intraseasonal Rossby waves that likely imposed perturbations to the low latitude boundary currents in the Western Pacific Ocean. It has also been suggested that semi-annual Rossby waves originating in the central tropical Pacific force semiannual variation of Mindanao Current (Qu *et al.*, 2008). In addition to the ISV drawing most of its momentum from remote atmospheric perturbations, ISV formed within the Sulawesi Sea due to baroclinic Rossby wave resonance may also inject ISV energy into the Makassar Strait (Qiu *et al.*, 1999; Masumoto *et al.*, 2001).

The Susanto *et al.*(2000) study of the intraseasonal variability in the Makassar Strait, using a 1.5 year (1996-1998) time series of currents at 300 m and 450 m, showed two significant ISV peaks: 35-60 and 70-100 days. They speculated that the 35-60 day oscillations are associated with the Sulawesi Sea ISV (Qiu *et al.*, 1999; Kashino *et al.*, 1999) while the 70-100 day oscillations are related to a Kelvin wave from the Indian Ocean (Qiu *et al.*, 1999; Sprintall *et al.*, 2000).

This study investigates ISV features within Makassar Strait throughout the full thermocline depth. We first describe the data and method employed. This is then followed by discussions on the intraseasonal characteristics within Makassar Strait and how they are related to ISV within Sulawesi Sea to the north and ISV in Lombok Strait to the south of Makassar Strait.

2.2 Data and Method

The oceanic ISV characteristics in Makassar Strait were investigated through flow as recorded from two moorings: 2°51.9 S, 118° 27.3 E [MAK-West] and 2°51.5 S, 118° 37.7 E [MAK-East], within the 45 km wide Labani Channel (Gordon *et al.*, 2008; Figure 2.1). Each mooring consisted of an upward-looking RD Instruments Long Ranger 75 kHz Acoustic Doppler Current Profiler [ADCP] at depth 300 m and two current meters deployed at 200 m and 400 m that measured the variation of zonal and meridional velocity. The zonal and meridional velocity data were linearly interpolated onto a 25-m depth grid for each two-hour time step to produce the gridded current vectors from 25 m to 400 m. These gridded current vectors were subsequently used to compute the along-channel flow parallel to the along axis of Labani Channel, which is oriented along 170°.

To examine the links via Lombok Strait between the oceanic ISV recorded in Makassar Strait and that of the eastern equatorial Indian Ocean [EEIO], current meter data retrieved every two hours at 50 m and 350 m within Lombok Strait and at EEIO were analyzed. The data in Lombok Strait were recorded by the Lombok-East mooring deployed at 8°24.1 S, 115° 53.9 E, north of 300 m sill (Sprintall *et al.*, 2009) and in the EEIO at 0°, 90°E (Masumoto *et al.*, 2005; Figure 2.1). The time series, recovered from all moorings, extends

from early January 2004 to late November 2006 encompassing a period of weak El Niño from January 2004 until October 2005, followed by a La Niña until April 2006, with a mild El Niño until the end of observation period. The Makassar and Lombok moorings are part of the *International Nusantara Stratification and Transport* [INSTANT] program (Sprintall *et al.*, 2004).

The influence of remotely forced ISV to Makassar Strait ISV was evaluated using satellite altimeter JASON-1 derived Sea Level Anomaly [SLA] datasets in the Sulawesi Sea and Lombok Strait. The data were acquired from the database of sea surface height recorded every 10 days along the Jason-1 satellite altimetry tracks [http://podaac.jpl.nasa.gov/jason1]. In the Sulawesi Sea, the along-track SLA data derived from several Jason satellite passes were interpolated through an inverse distance weighted [IDW] method to yield the estimated SLA data at 3°N along longitudes from 118°E to 125° E. The principle premise of the IDW method is that the interpolating data are weighted by the inverse of their distance to the interpolated data (Fisher *et al.*, 1987).

The atmospheric ISV in Makassar Strait was assessed through the analysis of the local wind variability. Wind data were collected from a wind gauge placed 10 m above mean sea level at Balikpapan airport (Figure 2.1), and sampled every 2-hours coincident with the mooring time series.

The Makassar mooring data contained a short gap between recovery and deployment on 7-10 July 2005, and we applied a singular spectrum analysis (SSA) to reconstruct the data and fill in the gap. The application of SSA to fill in the missing data in this study adapted the procedure derived by Schoellhamer(2001). SSA decomposes the mooring time series into reconstructed components through the following steps.

1. A lagged autocovariance matrix is formed by $c_j = \frac{1}{N_l} \sum_{l \leq N-j} x_l x_{l+j}; 0 \leq j \leq M-1$ where c is a Toeplitz lagged correlation matrix, N is number of data, M (14 days) is window size, and x denotes data .[1]

2. The eigenvalues, λ_k, and eigenvectors, E_j^k, of the matrix are determined.

[1]For this lagged autocovariance matrix, we experimented with a variety of interpolants to fill the gap. Seeing no sensitivity to the interpolant, hence we used a linear interpolant.

3. The principle component is computed using $a_i^k = \frac{M}{N_l} \sum_{l \leq M} x_{i+1} E_l^k; 0 \leq i \leq N_l - M$

4. The reconstructed component is then given by $x_i^k = \frac{1}{M} \sum_{j=1}^{M} a_{i-j}^k E_j^k; M \leq i \leq N - M + 1$

Isolating the intraseasonal variability from the full dataset was accomplished through filtering of the data. The spectra of the data were firstly multiplied with a transfer function, adopting a cosine-recursive or a Butterworth filter shape, to remove data with frequencies higher than 1/20-day (a low-pass filter with a cut off frequency of 1/20-day). The spectra of the low-pass filtered data were subsequently multiplied with the same type transfer function but a different cut off frequency of 1/90-day in order to remove data with low frequencies, resulting in the intraseasonal data.

The intraseasonal characteristics of the datasets were then examined using spectral, coherence, wavelet, wavelet coherence, and complex EOF analyses. The dominant intraseasonal variability in the data was identified through spectrum analysis. The power spectra of the data were computed using the multi-taper method with adaptive weighing as follows:

$$P_X(f) = \frac{\sum_{k=1}^{K} b_k^2(f) \mu_k \left| X_k(f) \right|^2}{\sum_{k=1}^{K} b_k^2(f) \mu_k} \tag{2.1}$$

with K is the number of tapers, μ is the weight, b is a weighing function which prevents a broadband leakage, f is frequency, and X is the discrete fourier transform (DFT) of the tapered data (Percival and Walden, 1993). Multitaper analysis multiplies the overlapped and segmented data by several different windows or tapers and subsequently averages the estimates to get an averaged spectrum with a higher degree of freedom or smaller uncertainty. The type of orthogonal window applied in our study was the discrete prolate spheroidal sequence, and the chi-squared 95% confidence intervals approximation for the estimated spectra were computed as

$$\begin{aligned} c_{upper} &= \frac{1}{\left[1 - \frac{2}{9\nu} - 1.96\sqrt{\frac{2}{9\nu}}\right]^3} \\ c_{lower} &= \frac{1}{\left[1 - \frac{2}{9\nu} + 1.96\sqrt{\frac{2}{9\nu}}\right]^3} \end{aligned} \tag{2.2}$$

where ν denotes the degrees of freedom (DOF). We segmented the timeseries into 5 segments, which resulted in 10 DOF.

To investigate both the dominant intraseasonal variability in the mooring data and how the dominant variability varies in time, we applied wavelet analysis (Torrence and Compo, 1998). The wavelet transform of the data was defined as a convolution between DFT of the data and of a scaled and translated version of a wavelet function as follows:

$$W_n(s) = \sum_{k=0}^{N-1} \hat{x}_k \hat{\psi} * (s\omega_k) e^{i\omega_k n \delta t} \tag{2.3}$$

where s is wavelet scale, n is time index, and $\hat{x}$ and $\hat{\psi}$ are DFT of the data and wavelet function respectively. The Morlet shape was chosen as the wave function for the analysis. The likelihood that the true wavelet power is within a certain interval about the estimated wavelet power is given by the following:

$$\frac{2}{\chi_2^2(\frac{\alpha}{2})} |W_n(s)|^2 \leq W_n^2(s) \leq \frac{2}{\chi_2^2(1-\frac{\alpha}{2})} |W_n(s)|^2 \tag{2.4}$$

with χ_2^2 is chi-square distributed with 2 DOF.

The degree of correlation in frequency domain between two time series was examined using coherence analysis. The squared coherence magnitude was determined using the multi-taper method with adaptive weighing with the following formula:

$$C_{XY}(f) = \frac{\left|\sum_{k=1}^{K} \mu_k X_k(f).Y_k(f)\right|^2}{\sum_{k=1}^{K} \mu_k |X_k(f)|^2 \sum_{k=1}^{K} \mu_k |Y_k(f)|^2} \tag{2.5}$$

Where X and Y are DFT estimates of data tapered with k^{th} taper. The confidence limit of estimated coherence at a given α ($\alpha = 0.05$ for 95% level of significance) is computed as 1-$\alpha^{(1/K-1)}$. Meanwhile the phase information is $\phi_{XY}(f) = tan^{-1}\frac{im(C_{XY})}{re(C_{XY})}$. Like the spectrum analysis, we also segmented the mooring data into 5 segments for the coherence calculation.

To examine and illustrate in time-frequency space the coherence of the data, we applied wavelet coherence analysis. The wavelet coherence of two time series is defined as (Grinsted *et al.*, 2004)

$$R_n^2(s) = \frac{\left|\mu(s^{-1} w_n^{XY}(s))\right|^2}{\mu(s^{-1} |w_n^X(s)|^2).\mu(s^{-1} |w_n^Y(s)|^2)} \tag{2.6}$$

where s denotes scale, μ is a smoothing operator, and W_n^{XY} is cross wavelet transform of two time series X and Y. For the Morlet wavelet the smoothing operator is given as $\mu = \mu_{scale}(W_n(s) * c_2 \Pi(0.6s))$, where μ_{scale} denotes smoothing along the wavelet scale axis, c

is normalization constant, and the rectangle function. The significance level of the wavelet coherence is approximated using Monte Carlo methods (Grinsted *et al.*, 2004). A large ensamble consisting of ∼1000 surrogate data pairs with identical first order autoregresive process is generated, and wavelet coherence is applied to each data pair.

2.3 Intraseasonal features

2.3.1 ISV observed in the Makassar Strait

2.3.1.1 Along-channel flow features

ISV within the thermocline at Mak-West and Mak-East mooring sites is marked by oscillations within a wide spectrum of 45-90 days with a spectral peak at 60 days (Figure 2.2 a,b,c,d). A second peak within a band of 30-40 days occurs at both moorings, but it is not significantly different from the background at the 95% confidence limits (Figure 2.2 c,d). Figure 2.2 shows that the signature of the dominant ISV is characteristically stronger in the upper 100 m of water depth at both mooring sites, and it is discernable down to the base of the thermocline although with reduced energy. The Brunt-Väisällä frequency profiles (Figure 2.3) at the Mak-West and Mak-East thermocline, inferred from several Conductivity-Temperature-Depth [CTD] casts carried out during the Northwest monsoon [rainy season], indicate that the strongest stratification is observed at depth between 100-125 m. This strong stratification demarcates the upper thermocline [25 m-100 m] from the lower thermocline [125 m - 400 m] in Makassar Strait.

In the upper thermocline [25 m - 100 m] the 60-day oscillation at Mak-West is a half order more energetic than that at Mak-East (Figure 2.2 c,d), with 75% of the variance of both moorings being strongly coherent (Figure 2.4, left panel). The coherence of the 60-day variability at both moorings attains its maximum value at 25 m and declines below the significance level at 100 m. In terms of the relative phase relationship, the principal fluctuations in the upper thermocline of Mak-East lead that of Mak-West by 3°-19°, equivalent to 0.5-3 days; the lead is maximum at 25 m and minimum to 75 m (Figure 2.4, right panel). The phase lag is unreliable at 100 m because the coherence squared is below the significance level at that depth.

Within the lower thermocline (125 m - 400 m) the percentage of strongly correlated along-channel flow at Mak-West and Mak-East increases to 85% (Figure 2.4). The horizontal coherence is minimum at 125 m and substantially increases toward the base of thermocline at 400 m while the relative phase shift reveals the tendency of the ISV of Mak-West to lead that of Mak-East by 1-day. The zonally coherent along-channel flow at intraseasonal time scales as inferred from the two mooring sites is likely an indication that ISV length scale is much larger than the width separating the moorings.

We explored the vertical structure of ISV by considering the vertical coherence of intraseasonal along-channel flows at the Mak-West site. We focused on the Mak-West features as Figure 2.4 shows there is little difference between Mak-West and Mak-East at the ISV time scales that we are interested in. The results of a cross coherence method suggest that the significant 60-day upper thermocline feature is also quantitatively vertically coherent (Figure 2.5a). The vertically coherent feature observed in the upper thermocline is particularly energetic in 2004 and 2006 and less vigorous during a weak El Niño period in the first six months of 2005 (Figure 2.6a). We suggest that shear attenuation is due to the shoaling of the Makassar thermocline and less ITF transport during this El Niño phase (Gordon *et al.*, 1999; Ffield *et al.*, 2000). The weakening of the intraseasonal signatures in the upper thermocline was observed a couple of months after the sea surface temperature maximum marking the El Niño onset appeared in the central Pacific Ocean. The lag reflects the role of the baroclinic Rossby waves with a phase speed of 0.3 m/s that transmit variability in the central Pacific towards the western Pacific (Cravette *et al.*, 2004) and eventually into Makassar Strait. In the lower thermocline, the coherence persists over all depths (Figure 2.5b), and is consistently strong throughout the year (Figure 2.6b).

Apart from the strong coherence, another feature of the lower thermocline is the pattern of phase lags. The phase relation between the ISV at 200 m and deeper layers shows a linear trend of the vertical phase lags in the lower thermocline with a slope of $11^{\circ}/50$ m (Figure 2.5b, right panel). The lags (Figure 2.5b, right panel) signify that the vertically coherent signals found in the lower thermocline exhibit a 2-day shift for every 50 m of increasing depth, and are thus indicative of downward energy propagation. Downward energy propagation is a common expression of waveform propagation in a stratified ocean (Ped-

losky, 2003). Figure 2.5 shows that the dominant oscillations in the lower thermocline are weakly correlated with those in the upper thermocline. As the more substantial oscillations are confined to the upper thermocline, we argue that the stratification maximum at 120 m inhibits vertical energy propagation of oscillations originating above or below that depth.

Another important characteristic observed in the lower thermocline is the strong ISV signature in May and June of both 2004 and 2005 (Figure 2.2a,b). The onset of this distinct feature is consistent with the timing of a semiannual Kelvin wave forced by winds over the Indian Ocean (Sprintall *et al.*, 2000). The 2006 May-June ISV was markedly weaker. This period corresponds to a La Niña phase, when the ITF transport is increased and the thermocline deepens (Gordon *et al.*, 2008). The relatively weak intraseasonal oscillations during May-June 2006 most likely correspond with a reduction in forcing rather than the increased viscous dissipation associated with increased vertical shear. Substantial vertical shear is observed only in the upper 100 m of Makassar Strait thermocline (Figure 2.7). Since the vertical gradient of along-channel flow is significantly different from zero only within the upper thermocline, we conclude that the role of viscous dissipation is negligible in causing the differences observed between the ISV of May/June in 2004 and 2005, with that in May/June 2006 within the Makassar Strait lower thermocline.

So far, we have discussed the intraseasonal features in the upper thermocline and lower thermocline. We now investigate the common intraseasonal characteristics occupying the full range of the thermocline. A Complex Empirical Orthogonal Function [CEOF] method was applied to simplify the intricate along-channel flow observed at Mak-West mooring site into two dominant modes, which accounted for 90% of total variance. The first mode explains 70% of variance within the thermocline and a wavelet transform shows it is characterized by a persistent 2-month oscillation throughout the observation period (Figure 2.8a). Its amplitude attains maximum value at the surface, decreases to its lowest level at 75 m, and increases toward the lower thermocline (Figure 2.8c). Vertical structure of the first two modes implies the top thermocline depth of 25 m as a momentum source as indicated by its energetic amplitude. This large amplitude at the top thermocline level is not projected further in the thermocline layer due to viscous dissipation: Momentum transfer from the surface to deeper depths is attenuated because substantial amount of energy is dissipated

against friction due to viscosity. Instead of being further dissipated in the lower thermocline, the amplitude of the first mode increases slightly with depth down to 300 m, again indicative of downward energy propagation. As in the phase relationship for the 200 m along-channel flow ISV with deeper layers (Figure 2.5b, right panel), the vertical energy propagation is identified as a phase increase of 11°/50 m over the lower thermocline (Figure 2.8d). This implies that it takes about 2 days for a 60-day oscillation to radiate its energy from 150 m to 200 m.

2.3.1.2 Wind Variability

The wind field in Makassar Strait, as inferred from the local meridional wind measured at Balikpapan airport, reveals a substantial amount of ISV (Figure 2.9a). The seasonal cycle of local wind at Balikpapan station is driven by the monsoonal winds: northwesterly [southeasterly] winds prevail during boreal winter [summer]. On many occasions the amplitude of the meridional component of wind at intraseasonal time scales is very large, so energetic intraseasonal variations may override the seasonal cycle. Because of the nearly meridional orientation of the Labani channel, we do not include the characteristics of the zonal component of the wind in our analysis.

Furthermore, the spectrum estimate of the zonal wind does not indicate any distinct peaks in ISV periods centered at 60-days, but rather, resembles a red spectrum (not shown). In contrast, meridional wind at Balikpapan airport exhibits substantial variance at 60-day oscillation (Figure 2.9a). The 60-day oscillation is strong during the late summer and into the fall. A striking example of this oscillation is the anomalous southeasterly wind bursts recorded in August and October of each year, against the prevailing northwesterly monsoonal winds (Figure 2.9a). In the following section, we discuss whether the atmospheric ISV is projected onto the Makassar Strait thermocline.

2.3.1.3 Interaction of Atmospheric and Oceanic ISV

To ascertain the importance of the ISV in the atmosphere to the intraseasonal oscillations in the along-channel flow of the Makassar Strait thermocline, we employed a wavelet coherence method. The coherence shows the degree of correlation as well as how the correlation evolves

with time. Again, we show only the Mak-West data since the majority of the variance observed at Mak-East resembles that of Mak-West (Figure 2.4). The strong coherence between the meridional wind and the along-channel flow at 25 m within the 45-60 days band suggests that the momentum of the atmospheric ISV is partly transferred to force the variability at the top of the Makassar Strait upper thermocline (Figure 2.9b). The phase relationship (Figure 2.9b) implies that the along-channel flow reaches maximum velocity 5 days following the peak of the wind, and the coherence between the wind and the flow at 25 m strengthens during summer and fall months of 2004 and 2005 but is weakened during the same period of 2006. We suspect that the deepening of the thermocline associated with the La Niña of early 2006 inhibited wind derived momentum transfer from the ocean surface to depth of 25 m and deeper layers.

Analyzing the wind influence deeper in the water column, we find that the trace of wind signatures is no longer substantially observed below 25 m (not shown). The correlation between winds and current at 50 m drops to 60%, which is below the significance level. However, the along-channel flow at 25 m is well correlated with the flow at 125 m depth (Figure 2.5a). This finding suggests that the variability at intraseasonal time scales in the uppermost Makassar Strait thermocline is partly an oceanic response to energy from local wind forcing, but that the majority of ISV observed in the Makassar Strait thermocline is derived from a remote source. We now explore the potential remote sources of the Makassar Strait ISV.

2.3.2 Links between Makassar Strait ISV and Sulawesi Sea ISV

The first remote basin considered as the origin of ISV observed in Makassar Strait is Sulawesi Sea, located to the north of the INSTANT moorings (Figure 2.1). The analysis of intraseasonal variations in the Sulawesi Sea inferred from mooring data is not available although mooring sites off the Pacific entrance of the Sulawesi Sea [off the southeastern tip of Mindanao Island] indicated that the 50-day oscillation is dominant (Kashino *et al.*, 1999). The study of intraseasonal oscillations in Sulawesi Sea has been done through several numerical experiments. Qiu *et al.*(1999) suggested two principal mechanisms likely responsible for the dominant 50-day oscillation in the Sulawesi Sea. First, they argued that the geom-

etry of the Sulawesi Sea would support the intrinsic period of 50-days [the gravest Rossby wave period]. Second, the eddy shedding of the Mindanao Current was suggested to force 50-day oscillations in the Sulawesi Sea. In addition, Masumoto *et al.*(2001) hypothesized that westward propagating eddies generated at 40-days characterized the main ISV feature in the Sulawesi Sea. Both numerical experiments agreed that the ISV emanating from the Sulawesi Sea dissipated its energy along the pathway of ITF.

We examined the SLA variability measured by the Jason-1 altimetry satellite to obtain the main oscillations in Sulawesi Sea. We focused our analysis of SLA variability at 3°N and along longitudes from 118°E to 125° E in Sulawesi Sea (Figure 2.1) that corresponds to the locations where the majority of the ISV variance were numerically simulated (Qiu *et al.*, 1999; Masumoto *et al.*, 2001). The intraseasonal oscillations in the Sulawesi Sea vary from 45 to 90 days and contribute significantly to the overall variance (Figure 2.10a,b). Figure 2.10b shows that the ISV is stronger than the seasonal variability and is of comparable strength with the interannual variability (the interannual variation was marked with a period of suppressed [enhanced] SLA anomaly linked to a phase of a weak El Niño [La Niña]). The spatial variability of the ISV signature indicates the amplification towards the western boundary of the Sulawesi Sea (Figure 2.10a).

To further analyze the ISV characteristics in Sulawesi Sea, a CEOF method was applied to extract the most common pattern governing the SLA variability at intraseasonal time scales. The amplitude time series of the ISV patterns that accounts for 90% of the total intraseasonal SLA variance are given in Figure 2.10c. The leading mode, which explains 70% variance, reveals the importance of the 45-90 day variability as the dominant intraseasonal oscillation, and its zonal structure supports the energy intensification towards the western boundary of Sulawesi Sea (Figure 2.10d). The second mode, associated with the 20% of total variance, reveals another band of 30-40 day energy. The dominance of the 45-90 day and 30-40 day periods may be the expression of the cyclonic eddies which were well resolved in the numerical experiments of Qiu *et al.*(1999) and Masumoto *et al.*(2001). By analyzing the relative phase lags at several longitudes for the first orthogonal mode (Figure 2.10e), we argue that the 50-day oscillation propagates westward at a phase speed of 0.2 m/s, which is similar to the phase speed of a baroclinic Rossby wave as simulated through the numerical

experiments (Qiu *et al.*, 1999; Masumoto *et al.*, 2001).

To investigate whether the variability at the intraseasonal time scales observed in the Sulawesi Sea is related to the variability in Makassar Strait, we correlate SLA in the Sulawesi Sea and the along-channel flow in Makassar Strait (Figure 2.11). The dominant intraseasonal variability of the Sulawesi Sea SLA correlates significantly with the Makassar thermocline layer variability. The most coherent fluctuations of the Sulawesi and Makassar Strait ISV are within the period band of 50-70 days. The corresponding analysis of relative phase difference of the most coherent variability confirms that the features emanating from the Sulawesi Sea propagate and radiate energy into Makassar Strait with phase speeds of 0.2-0.3 m/s (Figure 2.11, right panel). Thorough discussion on the mechanisms or forms through which the energy originating from the Sulawesi Sea propagates into Makassar Strait is not within the framework of our present study, but will be investigated in the future.

2.3.3 Links between ISV in Makassar Strait and ISV in Lombok Strait and EEIO

Lombok Strait throughflow displays substantial intraseasonal variability (Arief and Murray, 1996; Wijffels and Meyers, 2004; Sprintall *et al.*, 2009). The remote wind fields, particularly wind variability in the equatorial Indian Ocean, are identified as the source of the ISV in Lombok Strait. Here we investigate the linkage of Lombok ISV to that of Makassar using the INSTANT data in Lombok Strait.

In the upper thermocline, the dominant intraseasonal fluctuations in Lombok Strait are more energetic than in Makassar Strait (Figure 2.12a). A wavelet-coherence revealed that the 60-90 days oscillations observed at both straits are coherent with a phase relationship that suggests a phase shift of about 40° (Figure 2.12b), suggesting a feature that radiates towards Makassar Strait at speeds of 1-1.5 m/s. By applying the Liouville-Green approximation (Gill, 1982) to the stratification profile in Makassar Strait (Figure 2.3), we find phase speeds for the lowest three ocean modes are 1.4 m/s, 0.7 m/s, and 0.5 m/s respectively. The phase speed of 1-1.5 m/s is commensurate with the first mode of baroclinic wave speed in a continuously stratified ocean. To investigate the possibility of a baroclinic wave propagating from Lombok Strait to Makassar Strait, we compute the theoretical lower bound

of the coastal trapping period. The coastal trapping period, (Allen and Romea, 1980), is a preliminary approach to estimate the shortest period of any coastal trapped waves possibly excited at a certain location. The coastal trapping period ($/itT$) is inversely proportional to the internal Rossby radius of deformation [Rm] and the variation of the Coriolis parameter with latitude (β). The baroclinic Rossby radius of deformation is a function of phase speed [c] and Coriolis parameter [f], and defined as (Gill, 1982; Pedlosky, 2003). We specified c in both Makassar Strait and Lombok Strait to be 1 m/s, the phase speed of a propagating feature inferred from observation. Using the given phase speed, $f_m = 7.5\text{x}10^{-6}$ s^{-1}, $f_L = 2.1\text{x}10^{-5}$ s^{-1}, $f_m = 2.3\text{x}10^{-11}$ m^{-1} s^{-1}, and $f_L = 2.28\text{x}10^{-11}$ m^{-1} s^{-1} [subscripts m and L denote Makassar and Lombok respectively], we determined that the theoretical lower bounds of the coastal trapping period in Makassar and Lombok Strait are 50-days and 129-days respectively. This suggests that the coherent 60-day oscillation observed in Lombok Strait can reasonably be classified as a baroclinic CTKW. Further evidence of the CTKW expression is that the upper thermocline along-channel flow in Lombok Strait is in geostrophic balance, as indicated through the surge [drop] of SLA corresponding to the northward [southward] along-channel flow (Figure 2.12a).

On the other hand, it is likely that the 60-day variability observed in the upper thermocline of Makassar Strait is not a trapped wave feature since its longest theoretical period at the Makassar moorings is 50-day, and another waveform such as baroclinic Rossby waves plausibly transmit the energy from Lombok Strait. To examine whether Rossby wave dynamics can explain the propagating feature from Lombok Strait to Makassar Strait, we employed the vertical propagation of equatorial Rossby waves theory as a preliminary measure. McCreary(1984) suggested that an equatorial Rossby wave would propagate vertically at an angle of where l is the wave mode. Provided $N = 0.0123$ s^{-1} [the largest N value observed in Makassar Strait, see Figure 2.3], $l = 1$ [first mode of a baroclinic wave], a distance of 673 km separating Lombok and Makassar moorings, a baroclinic wave oscillating at a period band of 60-90 days and emanating from the Lombok Strait surface would penetrate vertically into the Makassar Strait thermocline within a depth range of 130-200 m. The moorings data reveal that wave vertical propagation is evident as indicated by the strong coherency between the dominant variability at 50 m depth in Lombok Strait and that of the

Makassar Strait upper thermocline (Figure 2.12c). It is inferred from the phase relationship (Figure 2.12c) that the energy propagates vertically from 50 m depth in Lombok Strait to the Makassar Strait mid-thermocline although its signature weakens in the lower thermocline. The strong coherence between the dominant flow at 50 m depth in Lombok Strait and that of the Makassar Strait upper thermocline and the vertical propagation from Lombok Strait to Makassar Strait may indicate that baroclinic Rossby wave theory is applicable as a first approximation to describe how the energy of 60-90 day variability is transmitted from Lombok Strait to Makassar Strait.

As previously mentioned, the dominant oscillations at 50 m depth in the upper thermocline in Makassar Strait are not as strong as that in Lombok Strait. The attenuation of the 45-90 days energy in Makassar Strait is probably due to the spreading of the horizontal wave scale associated with the augmentation of internal Rossby deformation radius [R_m] towards the equator. Given $R_{1m} = 275$ km and $R_{1L} = 66$ km, the ratio between the internal Rossby radii in Makassar to Lombok Strait is 3, leading to the amplification of the horizontal wave scale in Makassar Strait. Since conservation of energy flux is needed, the amplification of the horizontal wave scale in Makassar Strait requires decreasing of the wave amplitude, as reflected in the weakening of the along-channel speed in Makassar Strait. Another possible mechanism related to the attenuation of the 45-90 days energy in Makassar Strait is that the wave path is not only from Lombok Strait to Makassar Strait, but also from Lombok Strait to Java Sea and to Flores Sea (Figure 2.1). In other words, a baroclinic wave in Lombok Strait could possibly scatter its energy into three different outlets: Java Sea, Flores Sea, and Makassar Strait leading to the observed weaker along-channel flow in Makassar Strait.

In the lower thermocline of Lombok Strait at 350 m, the variance is less energetic than at 350 m depth in Makassar Strait (Figure 2.13a). Nevertheless the dominant fluctuations observed at 350 m in Lombok and in Makassar Strait are coherent, particularly in the 45-55 days band from January to September 2005 (Figure 2.13b). The phase shift of the coherent oscillations indicates the propagation of a non-dispersive perturbation towards Makassar Strait with a phase speed of 1 m/s. The coherent motion found at 350 m is well below the Lombok sill depth of ∼300 m located to the south of the Lom-East mooring (Figure 2.1) such that its characteristics are likely influenced by the sills presence. The sill would act to

block energy transmission from the Indian Ocean towards Makassar Strait for all oscillations occupying the water column below the sill depth. Correlation of the zonal velocity at 350 m in the EEIO with the along-channel flow at 350 m in Lombok Strait revealed that there is no significant coherence at 45-55 day periods for almost the entire observation period, except during the last 6 months in 2006 (Figure 2.13c). The effect of Lombok Strait sill coupled with the thermocline vertical motion at interannual timescales might explain the lower thermocline ISV modulation by ENSO. As discussed in Section 2.3.1.1 and shown in Figure 2.13b, the ISV signature in Lombok and Makassar Straits was markedly weaker in May-June 2006 during a weak La Niña period. The less energetic ISV is partly due to the increased effectiveness of Lombok Strait sill in blocking the incoming energy when the thermocline dips in a La Niña phase. In contrast, the effect of Lombok Strait sill would not be as strong when the temperature cools and the lower thermocline thickens during an El Niño phase such as in May/June 2005 when the coherence between Lombok and Makassar at 350 m depth is significant (Figure 2.13b). Therefore it is reasonable to argue that the sill in Lombok Strait acts as an obstacle for the energy from the Indian Ocean transmitted into the internal of Indonesian seas.

2.4 Summary

The intraseasonal variability [ISV] in the Makassar Strait thermocline and its linkage to the variability in the surrounding seas are investigated. The Makassar along-channel ISV as observed at the Mak-West and Mak-East moorings is characterized by 45-90 day oscillations, derived from either the local wind fluctuations in the surface layer or from more remote sources within the thermocline. Atmospheric ISV exhibits a substantial role in modulating or on some occasions fully over-riding the seasonal cycle. The oceanic ISV on the other hand exhibits western intensification, and is vertically and horizontally coherent with downward energy propagation speeds of 25 m/day. The stratification contributes substantially to the vertical distribution of the oceanic ISV signatures. For example, excessive buoyancy flux into Makassar Strait combined with a deeper thermocline characteristic of a La Niña period play a major role in inhibiting ISV momentum transfer from the base of the mixed layer to

deeper within the water column. We argue that local wind variability partly transfers its momentum to force ISV within the upper 25 m of Makassar Strait. However, the vertically coherent intraseasonal fluctuations within the thermocline are unlikely associated with the local atmospheric variation, but they are substantially related to the remotely perturbed forcing.

Investigating the relation between ISV in Makassar Strait thermocline and ISV in the Sulawesi Sea and Lombok Strait, it is inferred that in the upper thermocline, the first baroclinic mode of a Rossby Wave radiating from 50 m depth in Lombok Strait at a slight angle is suspected to force the variability at periods of 60-90 days in Makassar Strait. Adding further complexity, deep reaching 50-70 day oscillations originating in the Sulawesi Sea make up the full picture of the intraseasonal features recorded in the Makassar Strait thermocline. The nature of the ISV also reveals its dependence on ENSO and the monsoon phase. An El Niño episode dampens the strong shear that is confined to the upper thermocline, while the La Niña phase attenuates the energetic ISV during the monsoon-transition period in the lower thermocline. Upper thermocline and lower thermocline ISV are not synchronous with the ENSO phases: during El Niño, the ISV is suppressed in the upper thermocline and intensified in the lower thermocline. The nonconformity might indicate that the lower thermocline ISV draws some of its momentum from the equatorial Indian Ocean ISV transmitted through Lombok Strait.

How the ISV in Makassar Strait thermocline is dynamically related to the equatorial Kelvin waves in the Indian Ocean and its intricate interplay with the deep reaching features in the Sulawesi Sea that force variability in the sub thermocline is further addressed in ongoing studies.

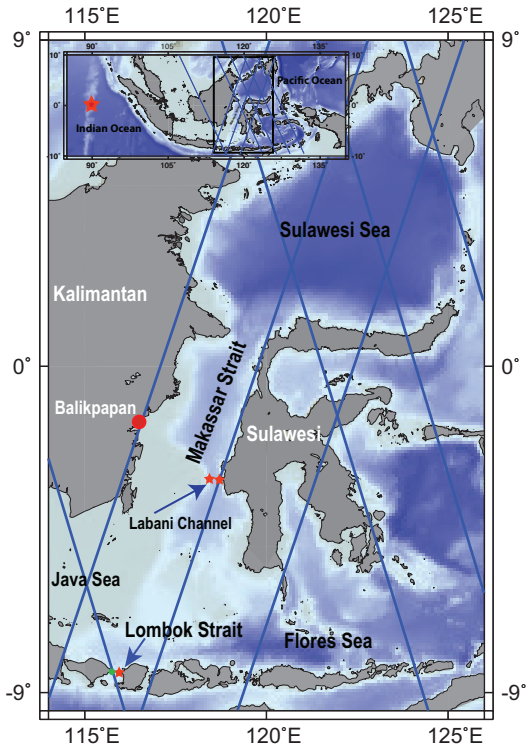

Figure 2.1: Mooring sites in Makassar Strait [Mak-West and Mak-East] and in Lombok Strait [Lom-East] are shown as red stars. Mak-West and Mak-East moorings were deployed in Labani channel, the narrowest deep passage in Makassar Strait, and separated by a distance of ∼19 km. The red circle indicates location of the Balikpapan airport where the local wind data were measured. The blue lines denote the JASON-1 satellite altimetry tracks, and the green circle the site of a JASON-1 derived Sea Level Anomaly time series used in this study. Location of the eastern equatorial Indian Ocean mooring is shown as the red star in the insert.

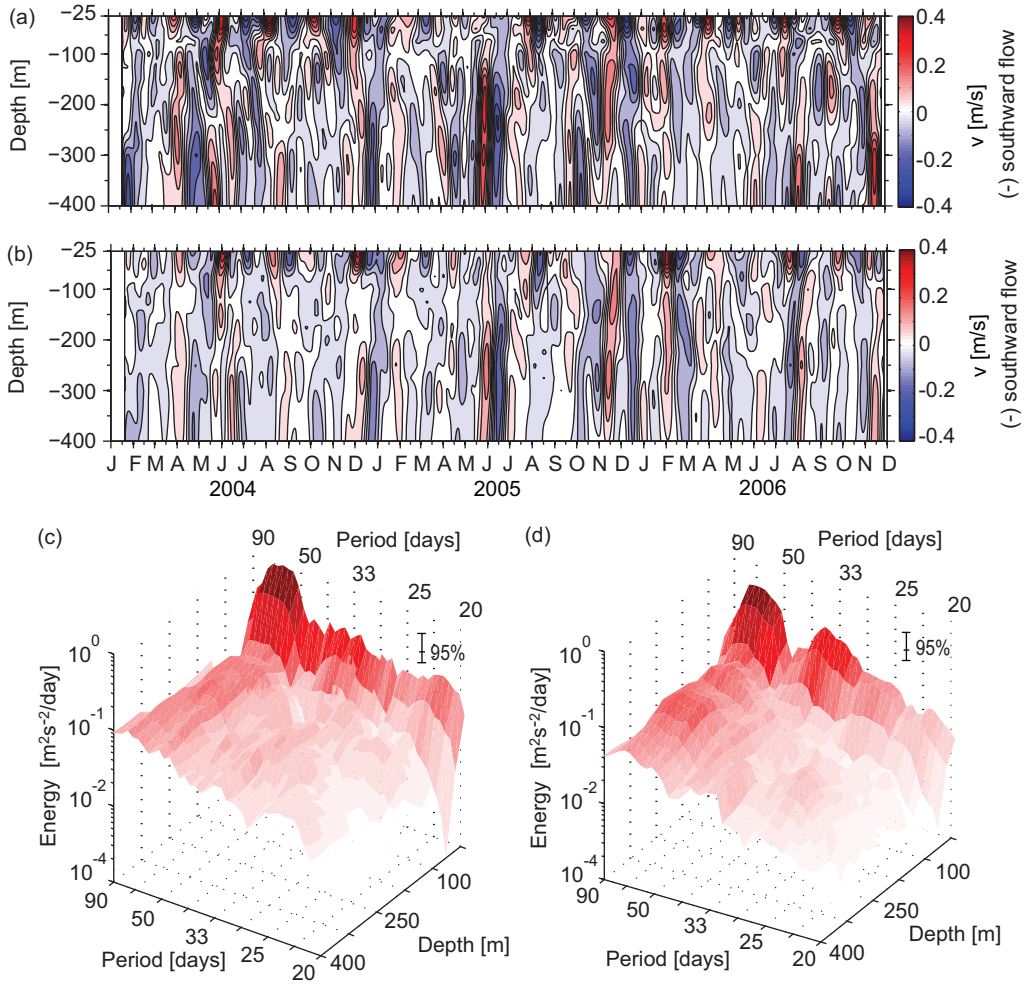

Figure 2.2: Along-channel flow thermocline flow at intraseasonal time scales observed at (a) Mak-West and (b) Mak-East. Negative values denote southward flow. (c,d) Spectral estimates of (a) and (b), respectively. Error bars on the spectral estimates mark the 95% confidence limits using power spectral confidence intervals.

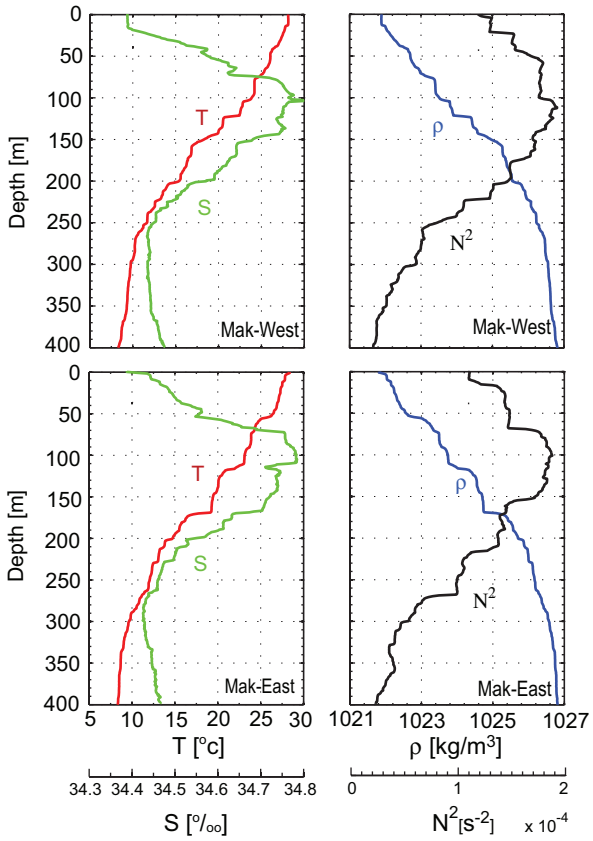

Figure 2.3: Temperature [red], Salinity [green], Density [blue], and Brunt-Väisällä [black] frequency profiles obtained from the CTD casts at the Mak-West [upper panel] and Mak-East [lower panel] mooring sites. The CTD data were collected in January 1994 during the Southeast monsoon.

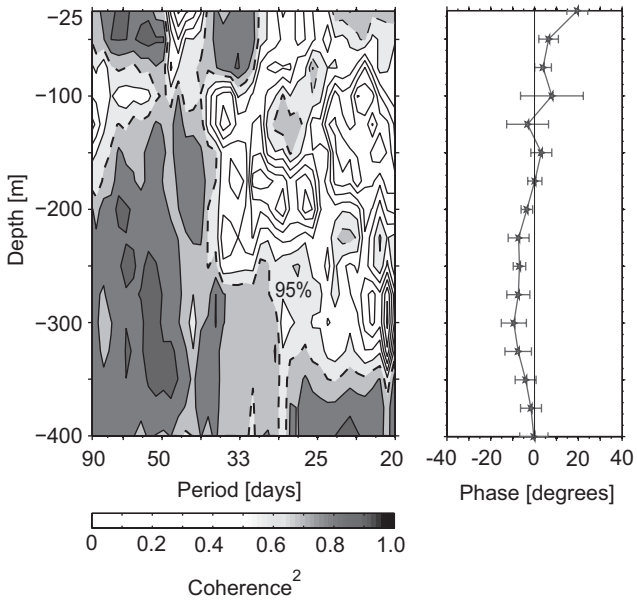

Figure 2.4: Coherence between the intraseasonal along-channel flow from Mak-West and Mak-East observed at the same depth. [Left panel]: Coherence squared. The dashed lines indicate the 95% significance level. [Right Panel]: Phase lags. Positive phases denote the intraseasonal along-channel flow at Mak-East leads the intraseasonal along-channel flow at Mak-West. Error bars show the 95% confidence limits for the phase lag estimates and are computed using a Monte-Carlo scheme.

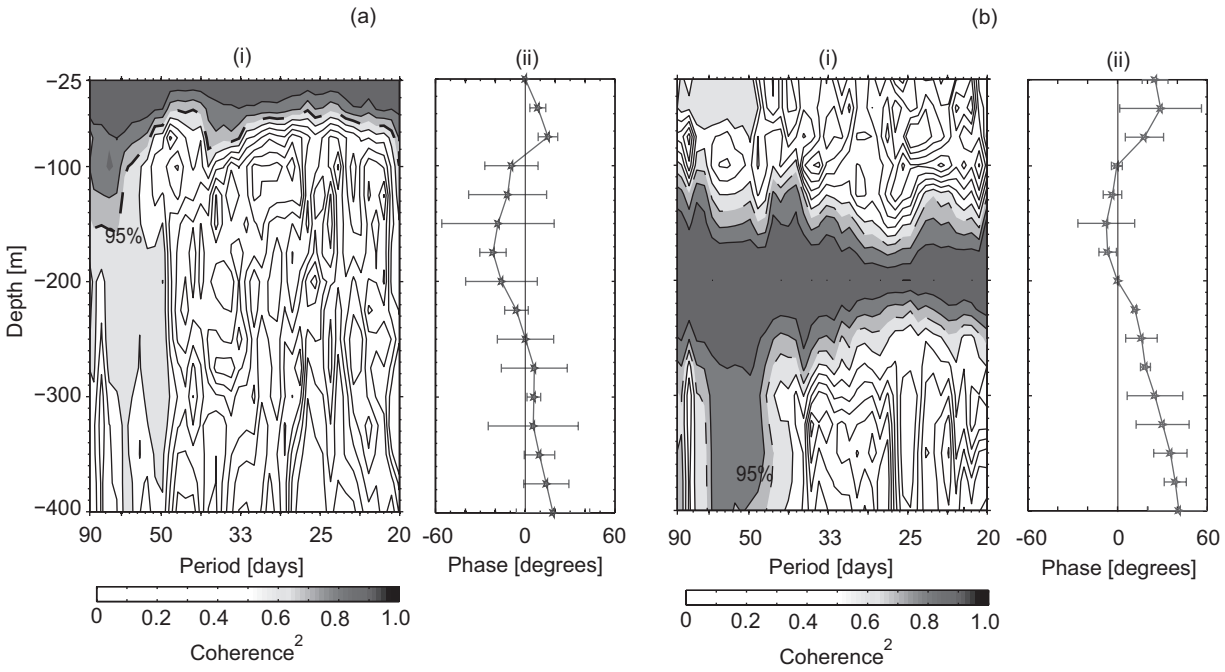

Figure 2.5: Coherence between the Mak-West intraseasonal along-channel flow at (a) 25 m and (b) 200 m, with the intraseasonal along-channel flow within the Mak-West thermocline. (i) Coherence squared. The dashed lines indicate the 95% significance level. (ii) Phase lags. Positive phases denote the intraseasonal along-channel flow at deeper layers lead the intraseasonal along-channel flow at a shallower depth. Error bars show the 95% confidence limits for the phase lag estimates were computed using a Monte-Carlo scheme.

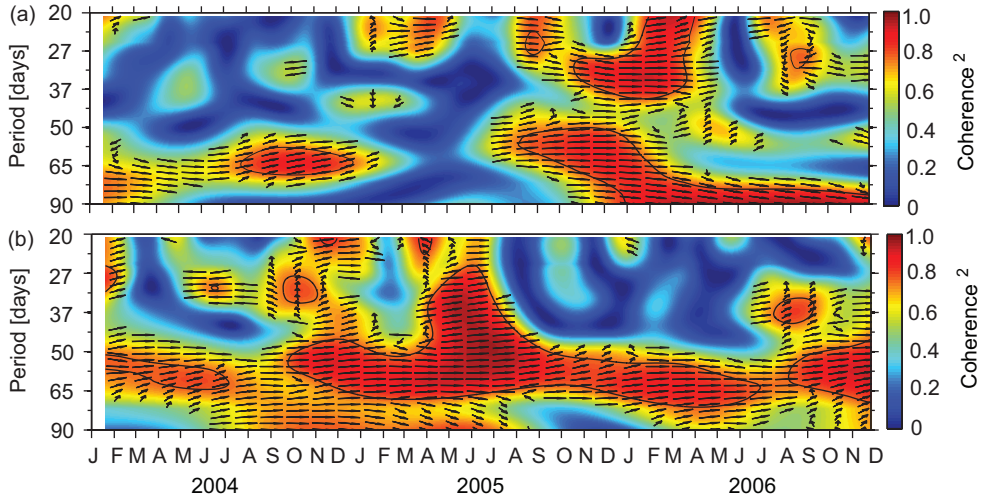

Figure 2.6: Wavelet coherence between the intraseasonal along-channel flow at 25 m and the intraseasonal along-channel flow at 50 m observed in the Mak-West thermocline. (b) Wavelet coherence between the intraseasonal along-channel flow at 200 m and the intraseasonal along-channel flow at 350 m observed in the Mak-West thermocline. The arrows indicate the phase lags. Pointing up signifies that the along-channel flow at 50 m (350 m) leads the along-channel flow at 25 m (200 m). Pointing right denotes that the along-channel flows at 50 m (350 m) and at 25 m (200 m) are in phase. Thin black lines denote the 95% significance level.

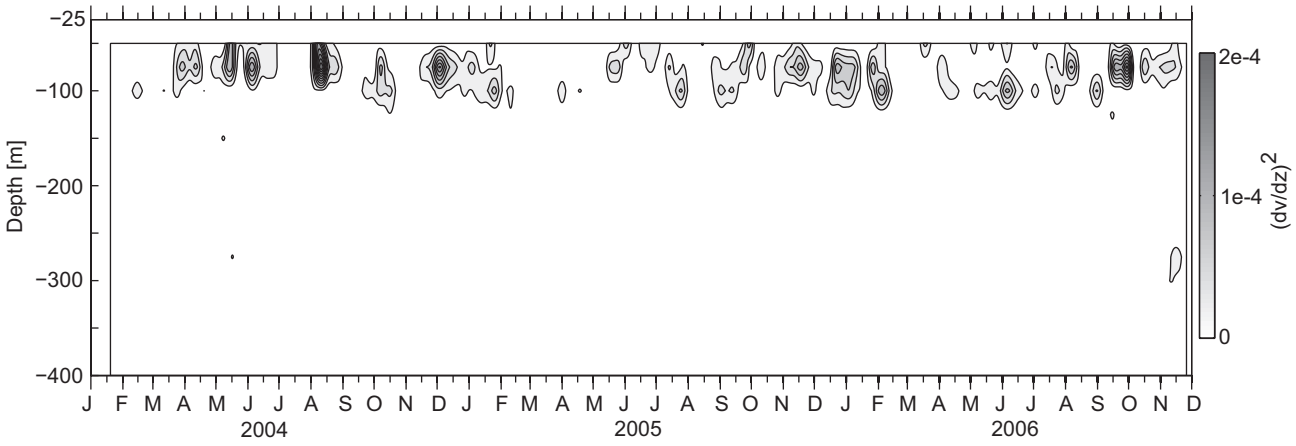

Figure 2.7: Squared vertical shear of interannual along-channel flow in the Mak-West thermocline.

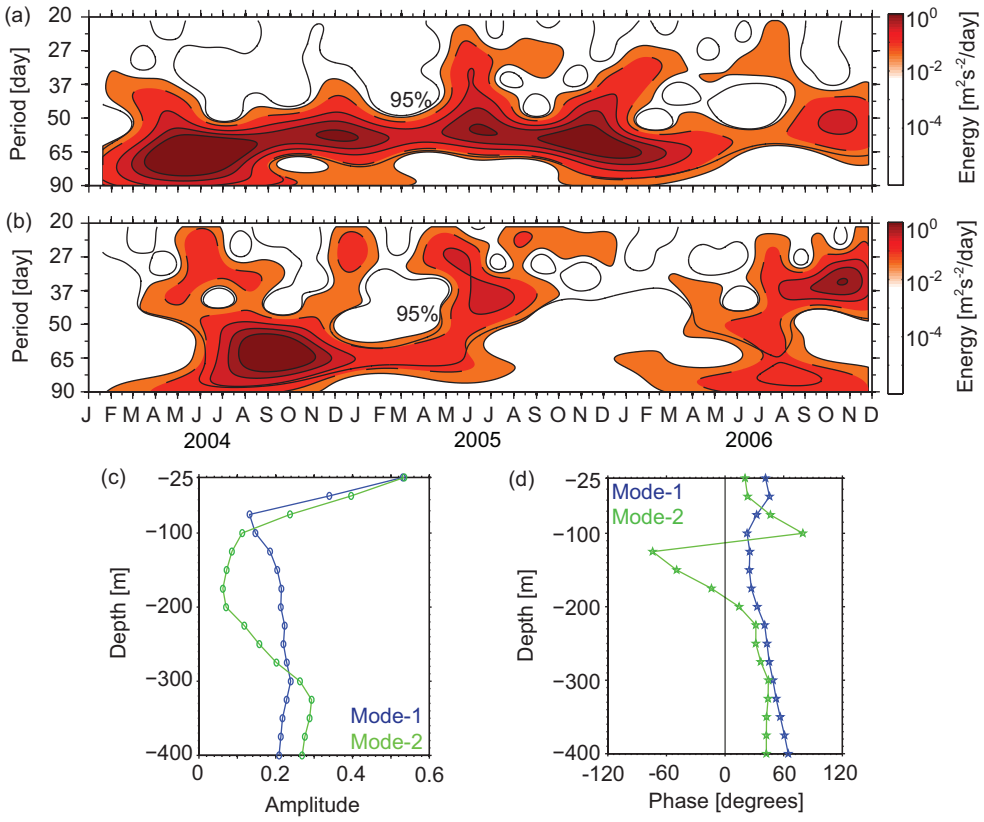

Figure 2.8: (a,b) Morlet Wavelet transform of the first two EOFs for the intraseasonal along-channel flow at Mak-West. The dashed lines indicate the 95% significance level. (c,d) Amplitude and phase of the first two EOFs for the intraseasonal along-channel flow at Mak-West. Modes 1 and 2 account for 70% and 20% of the variance, respectively.

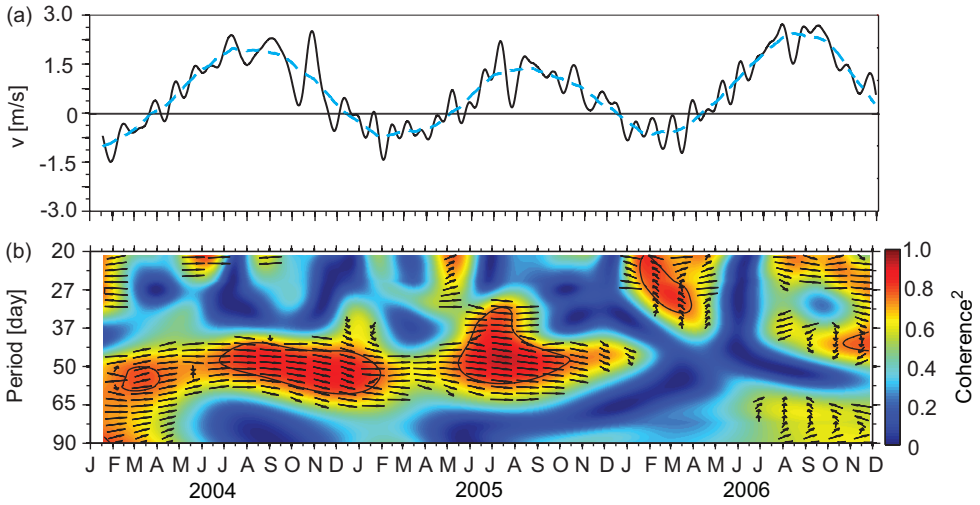

Figure 2.9: (a) The meridional wind monitored at the Balikpapan airport [see Figure 2.1 for location]. Intraseasonal component of the wind [black line] modulates the seasonal cycle of the wind [dashed blue line]. Negative values indicate Northerly wind. The seasonal wind was obtained by applying a 90-day running mean to the full data. (b) Wavelet coherence between the intraseasonal wind at the Balikpapan airport and the intraseasonal along-channel flow at 25 m in the Mak-West thermocline. The arrows indicate the phase lags. Pointing down indicates the intraseasonal wind leads the intraseasonal flow by 90°. Pointing right signifies the wind variability and the along-channel flow are in phase. Thin black lines denote the 95% significance level.

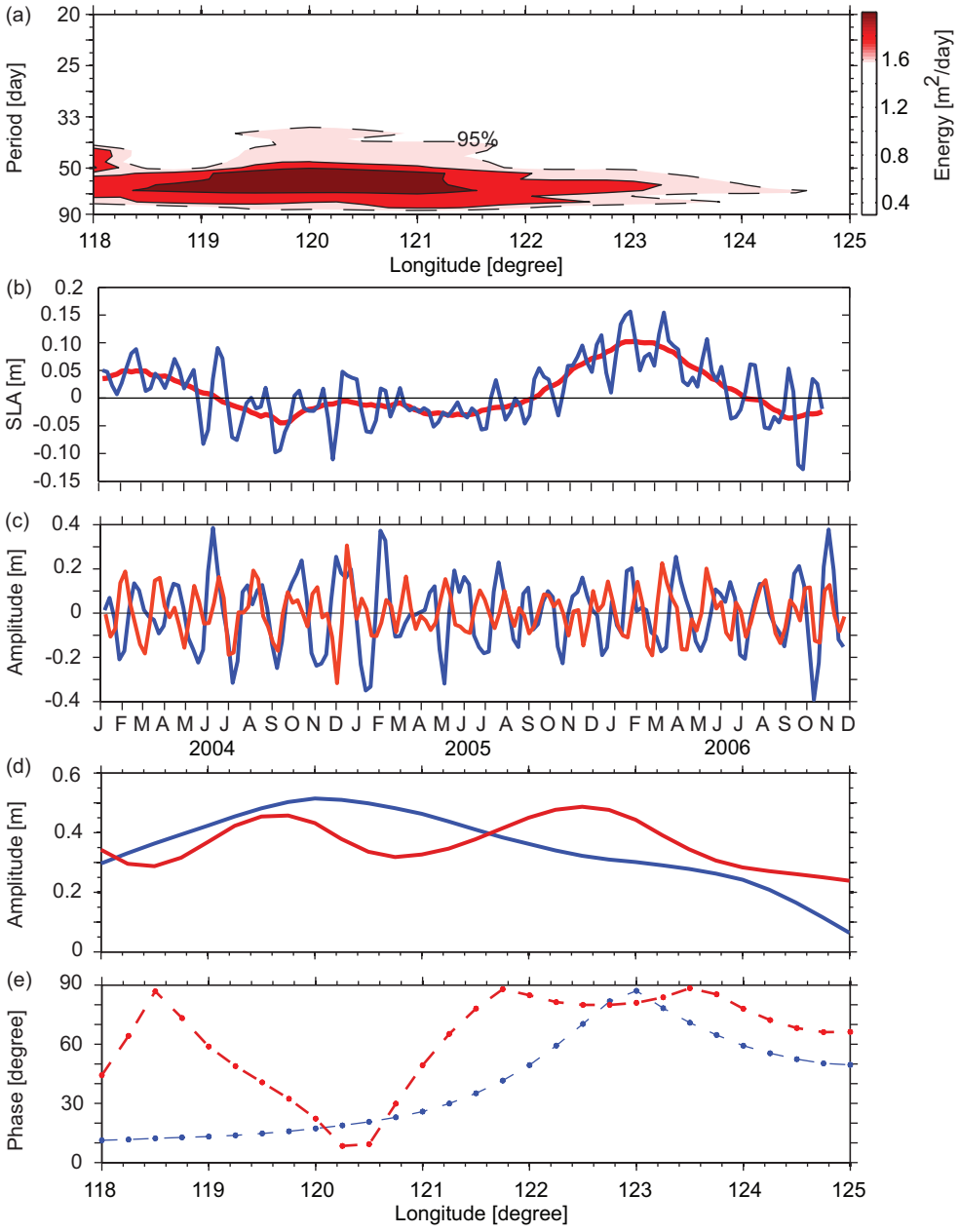

Figure 2.10: (a) Spectra for SLA at the intraseasonal time scales measured at 3°N; 118°E-125°E in the Sulawesi Sea. The dashed lines indicate the 95% significance level. (b) Intraseasonal [blue line] and seasonal [red line] SLA at 3°N; 120°E in the Sulawesi Sea. The seasonal SLA variability was obtained by applying a 90-day running mean to the full SLA data. (c,d,e) CEOF analysis for SLA at the intraseasonal time scales observed at 3N; 118°E-125°E in Sulawesi Sea. (c) Time series of the leading EOF modes. (d) Amplitude of the leading EOF modes. (e). Phase of the leading EOF modes. 1^{st} and 2^{nd} modes are in blue and red, respectively.

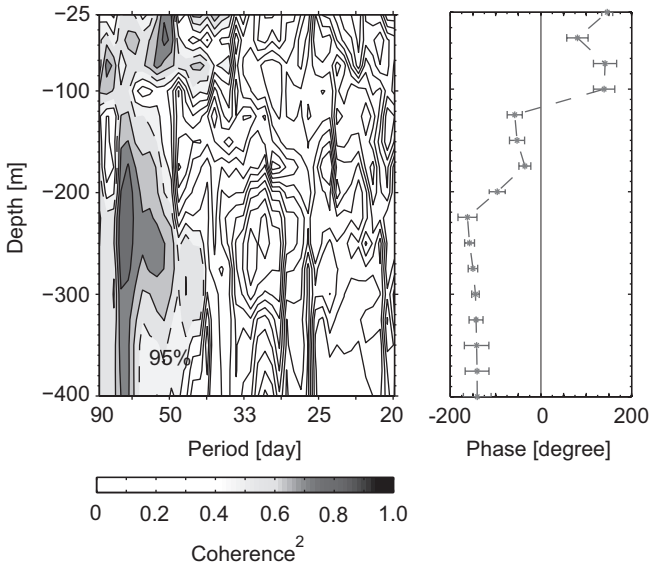

Figure 2.11: Coherence between the intraseasonal SLA in Sulawesi Sea and the intraseasonal along-channel flow from Mak-West. (Left panel): Coherence squared. The dashed lines indicate the 95% significance level. (Right panel): Phase lags. Negative phases denote the intraseasonal SLA leads the intraseasonal along-channel flow. Error bars show the 95% confidence limits for the phase lag estimates and were computed using a Monte-Carlo scheme.

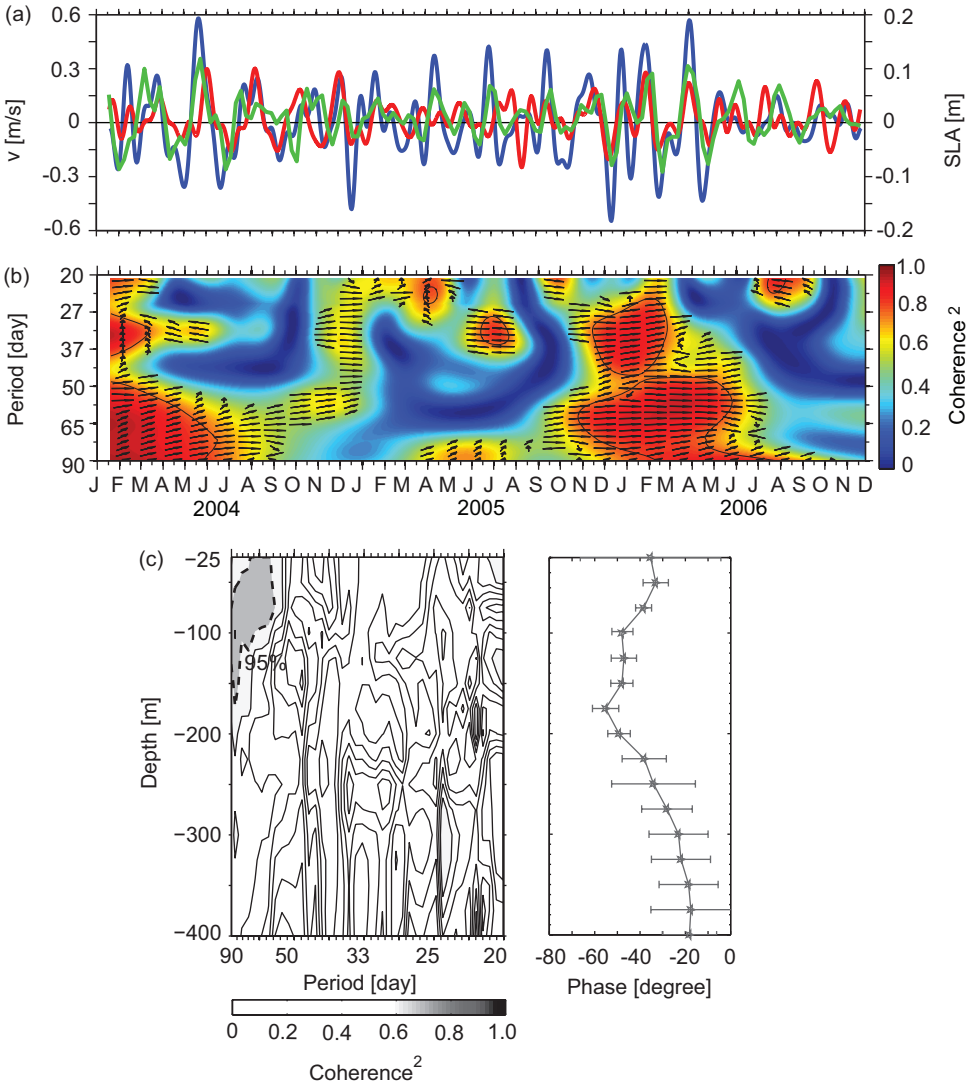

Figure 2.12: (a) Along-channel flow at the intraseasonal time scales measured at 50 m from Mak-West (red line) and from Lom-East [blue line], and SLA at the intraseasonal time scales from Lom-East [green line]. (b) Wavelet coherence between ISV at 50 m from Mak-West and ISV at 50 m from Lom-East. The arrows indicate the phase lags: Pointing up indicates ISV at Lom-East leads ISV at Mak-West by 90°. Pointing right signifies intraseasonal oscillations at Mak-West and at Lom-East are in phase. Thin black lines denote the 95% significance level. (c) Coherence between ISV at 50 m from Lom-East and ISV in the Mak-West thermocline. [Left panel]: Coherence squared. The dashed lines indicate the 95% coherence significance level. [Right Panel]: Phase lags. Negative phases denote ISV at Lom-East leads ISV at Mak-West. Error bars show the 95% confidence limits of the phase lag estimates and are computed using a Monte-Carlo scheme.

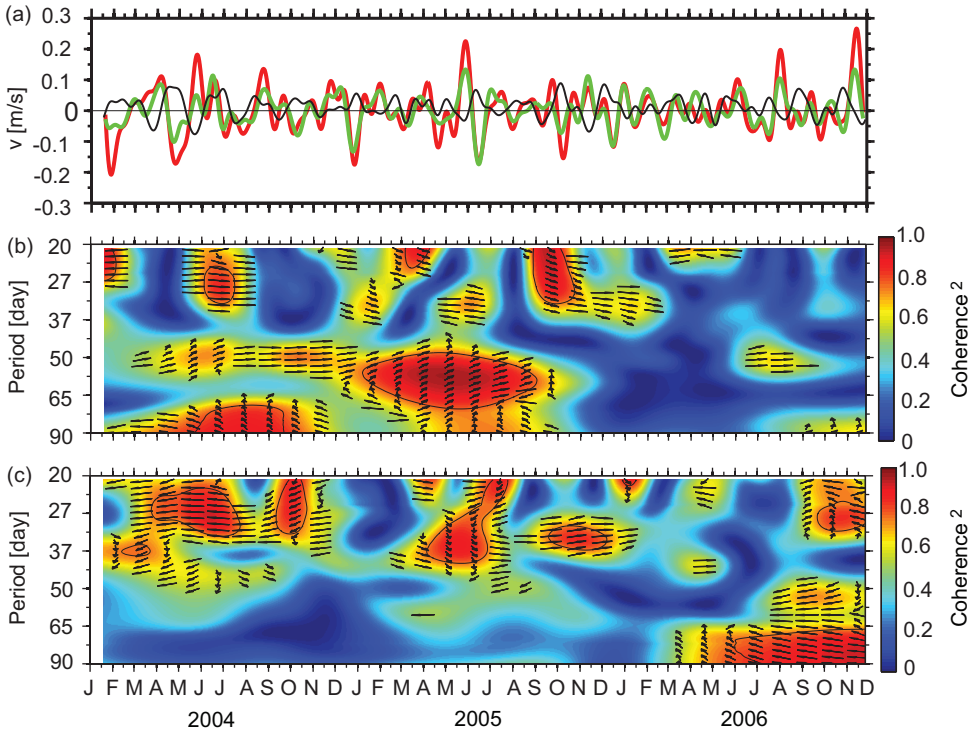

Figure 2.13: (a) Intraseasonal along-channel flow at 350 m from Lom-East [green line] and Mak-West [red line]. Black lines indicate the intraseasonal zonal velocity at 350 m from the EEIO mooring. (b) Wavelet coherence between ISV at 350 m from Lom-East and ISV at 350 m from Mak-West. The arrows indicate the phase lags: Pointing up means ISV at Lom-East leads ISV at Mak-West by 90°; Pointing right signifies intraseasonal oscillations at Mak-West and at Lom-East are in phase. (c) Wavelet coherence between ISV at 350 m from EEIO and ISV at 350 m from Lom-East. The arrows indicate the phase lags: Pointing up means ISV at EEIO leads ISV at Lom-East by 90°; Pointing right signifies ISV at Lom-East and ISV at EEIO are in phase. Thin black lines denote the 95% significance level

Chapter 3

Intraseasonal Kelvin Waves in Makassar Strait

Submitted as: Pujiana, K., Gordon, A. L., Sprintall, J., 2012. Intraseasonal Kelvin Waves in Makassar Strait. Journal of Geophysical Research-Oceans

Abstract Time series observations during 2004-2006 reveal the presence of 60-90 days intraseasonal events that impact the transport and mixing environment within Makassar Strait. The observed velocity and temperature fluctuations within the pycnocline reveal the presence of Kelvin waves including vertical energy propagation, energy equipartition, and non-dispersive relationship. Two current meters at 750 m and 1500 m provide further evidence that the vertical structure of the downwelling Kelvin wave resembles that of the second baroclinic wave mode. The Kelvin waves derive their energy from the equatorial Indian Ocean winds, including those associated with the Madden-Julian Oscillations, and propagate from Lombok Strait to Makassar Strait along the 100-m isobath. The northward propagating Kelvin Waves within the pycnocline reduce the southward Makassar Strait throughflow by up to 2 Sv and induce a vertical mixing rate of 1-5x10^{-5} m^2s^{-1}.

3.1 Introduction

The Makassar Strait (Figure 3.1) throughflow is a prominent component of the Indonesian Throughflow (ITF; Gordon and Fine, 1996; Gordon *et al.*, 2003; Gordon, 2005). Makassar Strait is not only the main inflow conduit for the ITF (Gordon *et al.*, 2008; Gordon *et al.*, 2010) but also part of a waveguide extending along the equatorial Indian Ocean to the southwestern coasts of Indonesia then to Makassar Strait, via Lombok Strait (Figure 3.1; Wijffels and Meyers, 2004). Previous modeling studies have discussed the role of the waveguide in connecting wind energy in the equatorial Indian Ocean to the Makassar Strait throughflow variability with timescales varying from semiannual to intraseasonal (Qiu *et al.*, 1999; Sprintall *et al.*, 2000; Schiller *et al.*, 2010). The study of Sprintall *et al.*(2000) argued that semiannual variations (180 day) in the equatorial Indian Ocean zonal winds induced a response in the South Java Current (SJC) through coastally trapped Kelvin waves (CTKWs). The semiannual CTKWs propagate farther east along the southern coasts of Indonesian archipelago into the Savu Sea, but part of the wave energy is transmitted through the narrow Lombok Strait, which then move equatorward to force northward Makassar Strait throughflow. At intraseasonal timescales (20-90 days), Qiu *et al.*(1999) and Schiller *et al.*(2010) modeled the intraseasonal variation in the Indo-Pacific region and proposed that the equatorial Indian Ocean wind-forced CTKWs also accounted for intraseasonal variability in the ITF passages. These modeling studies emphasized the ITF reversal event as an indicator of the CTKW passage in Makassar Strait but did not elaborate on the mechanism of the CTKW transmission from Lombok Strait to Makassar Strait.

Observations during December 1996 - June 1998 from two current meters (Figure 3.1) at depths of 250 m and 350 m in Makassar Strait revealed that the subinertial flow was marked with northward (positive) along-strait flow in May 1997, during which strong intraseasonal northward flow completely reversed the southward lower-frequency background flow (Figure 3.2). In addition to the May-June 1997 event, intraseasonal variabilitys most pronounced impact to attenuate the southward Makassar Strait throughflow was observed in December 1996 and 1997, September, October 1997, and January, February, March, April 1998 (Figure 3.2).

Analyzing along-strait flow data within the pycnocline in Makassar Strait and Lombok

Strait observed during the INSTANT 2004-2006 program (Gordon *et al.*, 2008; Gordon *et al.*, 2010; Sprintall *et al.*, 2009) and zonal current data from a mooring in the eastern equatorial Indian Ocean, Pujiana *et al.*(2009) found a coherent signal at intraseasonal timescales propagating from the equatorial Indian Ocean to Makassar Strait through Lombok Strait with the speed consistent with that of a baroclinic wave. Drushka *et al.*(2010), focusing their analyses on the vertical structure of along-strait flow at the outflow passages of the ITF, indicated that the intraseasonal along-strait motions at Lombok Strait had a vertical structure of a remotely wind-forced Kelvin wave.

In this study we utilize the 2004-2006 Makassar Strait dataset to investigate intraseasonal features consistent with the theoretical Kelvin wave characteristics, specifically those of the downwelling Kelvin waves forcing the northward along-strait flow events, and evaluate the likely pathway channeling the intraseasonal energy from Lombok to Makassar Straits. Moreover the Kelvin waves impact on the ITF variability and mixing environment in Makassar Strait are addressed.

The paper is organized as follows. The data description is given in Section 3.2, followed in Section 3.3 with a discussion of the evidence supporting the intraseasonal Kelvin wave variability. The waveguide pathway from Lombok Strait to Makassar Strait is discussed in Section 3.4. The Kelvin waves influence on the Makassar throughflow transport and mixing is evaluated in Section 3.5. A discussion and summary follow in Section 3.6.

3.2 Data

3.2.1 Makassar Strait Mooring in situ data

We employ the velocity and temperature datasets obtained during the INSTANT 2004-2006 program to identify intraseasonal Kelvin wave events in Makassar Strait. The INSTANT program monitored the ITF variability in Makassar Strait at two moorings: 2°51.9 S, 118° 27.3 E [Mak-West] and 2°51.5 S, 118° 37.7 E [Mak-East], within the 45 km wide Labani Channel (Gordon *et al.*, 2008; Figure 3.1). An upward-looking RD Instruments Long Ranger 75 kHz Acoustic Doppler Current Profiler [ADCP] at a depth of 300 m and three current meters at 200, 400, and 750 m on each mooring (the Mak-west mooring had an

additional current meter at 1500 m) recorded the velocity data with a sampling period of 0.5-2 hour. Both moorings fully resolve the vertical structure of the horizontal velocity across the pycnocline depths of 50-450 m almost continuously (other than a short gap between recovery and redeployment on 7-10 July 2005) for a ∼3-year long period from January 2004 to through November 2006. The horizontal current vectors are subsequently projected to the along (y) and across-strait (x) axis of the Labani Channel, which are oriented along -10° and 80° (relative to north and positive is clockwise) respectively (Figure 3.1), to yield gridded along (v) and across-strait (u) currents. In addition to the moored velocity datasets in Makassar Strait, we also use the hourly velocity data at pycnocline depth of 50-150 m from INSTANT moorings in Lombok Strait (Figure 3.1. For more information on the Lombok mooring configurations, see Sprintall *et al.*, 2009).

Temperature stratification from 100 to 400 m within the Makassar Strait pycnocline are resolved by the temperature and pressure sensors attached to Mak-West and Mak-East moorings. Mak-West mooring provided higher resolution with 17 sensors attached, while Mak-East mooring only had 5 sensors. Since the vertical structure of temperature variability is less well resolved at the Mak-East mooring, we will only analyze the temperature profile dataset from Mak-West. The sensors sampled temperature and pressure at 6-minute intervals over the entire 3 years INSTANT deployment period. The temperature datasets are linearly interpolated onto a 25-m depth grid for each two-hour time step to provide the gridded temperature data from 150 to 350 m of water column.

3.2.2 Shallow-pressure gauge and satellite-derived data

In addition to the moored data in Makassar and Lombok Straits, we also employ the sea level anomaly (SLA) data from two shallow pressure gauges (Pw and Pe) in Lombok Strait (Figure 3.1) and from the gridded SLA products (merged and delayed time products) of Archiving, Validation, and Interpretation of Satellite Oceanographic Data (AVISO, Ducet *et al.*, 2000). Here the daily shallow pressure gauge data are used, and more information on the pressure gauge setting can be found in Sprintall *et al.*(2004). The satellite-derived SLA has a horizontal resolution of 0.25° x 0.25° and temporal resolution of 7 days, and the emphasis of our analysis will be on the SLA variability in Lombok Strait and along the

southeastern coasts of Indonesia archipelago (Figure 3.1). Furthermore we will be focusing on the SLA variability during April-June 2004 (Figure 3.3), one of the events when both moorings in Makassar and Lombok Straits display strong northward flow. The northward flow observed in Makassar Strait on May 30th 2004 (Figure 3.4b-d) was preceded by mass pilling up ($+\eta$) against the southwestern coasts of Sumatra on 12 May, followed up by southeastward propagation of the $+\eta$ signal so that the southern coasts of Java was marked with $+\eta$ on 19 May (Figure 3.3). The occurrence of $+\eta$ signal extended from the southern coasts of Java to the mooring sites in Makassar Strait via Lombok Strait on 26 May although there are some concerns on the SLA data quality within the internal Indonesian seas.

3.3 Intraseasonal variability in Makassar Strait and Lombok Strait

3.3.1 Weakened ITF events at intraseasonal timescales

Focusing on the weakened or reversed southward flow in Makassar Strait, the v component at the base of the pycnocline at 450 m depth (Figure 3.4d) demonstrates that southward subinertial flow, v^s (low-passed v time series with cut off periods of 9 days) reversed to northward flow five times over the course of 2004-2006: May 2004 and 2005, September 2005 and 2006, and November 2006. Although no ITF reversal was observed at depths shallower than 250 m, the northward v^s phases in May 2004 and 2005 and in November 2006 were observed as shallow as 350 m. One feature consistently revealed within the along channel pycnocline flow is the strong influence of intraseasonal variability, v' (band-passed v timeseries with cut off periods of 20 and 90 days) on v^s: a northward v^s event always corresponds with a northward v' phase (Figure 3.4b-d).

Over the course of 2004-2006, there were 17 northward ($+v'$) events with recurring period of 2-3 months (Figure 3.4b-d). The $+v'$ during May 2004 and 2005 was the most energetic of all $+v'$ events, while other less energetic $+v'$ events peaked in February, March, August and December 2004; January, March, July, September, and November 2005; January, April, June, August, September, and November 2006. The $+v'$ episodes demonstrated a strong correlation with the zonal winds in the eastern equatorial Indian Ocean (not shown) and

those particularly occurring in March and May 2004; May, and September 2005 were preceded by significant MJO phases (Pujiana *et al.*, 2009, Figure 3.4a) with the $+v'$ events in Makassar Strait lagging the MJO by 19-25 days (Figure 3.4e). Zhou and Murtugudde(2010) conjectured that the MJO influenced the intraseasonal variability at Lombok Strait. They further suggested that the meridional currents were reversed from southward to northward at Lombok Strait 15 days after the day of a peak MJO index. Thus the lag of 19-25 days revealed by $+v'$ in Makassar Strait, with respect to a strong MJO event, suggests a link between the intraseasonal variability in Makassar Strait and MJO episodes. More discussion on the relationship between the $+v'$ events in Makassar Strait and the MJO significant phases are given in Section 3.6.

3.3.2 Subpycnocline intraseasonal variability

The v timeseries at 750 m and 1500 m also display significant intraseasonal variability with a diminished subinertial background flow marked with recurring intraseasonal oscillation with a 60-day period (Figure 3.5a,b). The intraseasonal variation explains ∼80% of the total variance of the subpycnocline current meters v timeseries. Aside from their energetic intraseasonal signatures, the v' at 750 m and 1500 m in Makassar Strait also displays a unique characteristic that is not expected to be observed at depths where the stratification frequency is quasi-homogeneous: the flows at 750 m and 1500 m are out of phase. A lagged correlation between the v' data at 750 m and that at 1500 m shows a statistically significant correlation with $r^2 = 0.8$, and a coherence analysis further indicates that the 60-day oscillation is the most coherent among the v' data at both depths with a phase shift of 180°(not shown).

The time series from the two subpycnocline current meters (Figure 3.5a,b) are used to analyze the vertical profiles of $+v'$ from 50-1500 m attributed to the $+v'$ events observed in the pycnocline depths (Figure 3.4b-d). With over the 17 $+v'$ episodes during 2004-2006, the $+v'$ data consistently exhibit a vertical structure which signifies a baroclinic structure with two zero crossing depths, indicative of a second baroclinic wave mode. Examples of the measured$+v'$ vertical structure in May, September and November of 2005 when the $+v'$ was maximum are shown in Figure 3.5c.

3.3.3 Kelvin Wave Signatures

As discussed above, intraseasonal motions account for a significant proportion of the variance of the Makassar Strait variability (Figure 3.4 and Figure 3.5) and are clearly evident in the datasets as $+v'$. In this subsection, we provide evidence linking the $+v'$ attributes to theoretical Kelvin wave characteristics such as a vertically propagating wave, normal mode approximation, energy equipartition, and semi-geostrophic balance.

3.3.3.1 Vertically Propagating Waves

Over the 17 occasions when v^s turned northward or was greatly attenuated during 2004-2006, one consistent feature was that the $+v'$ profile across the pycnocline indicated upward phase propagation as $+v'$ at deeper levels led that at shallower levels. The composites of the $+v'$ data, formed by isolating each $+v'$ event and then averaging over the set of events observed during 2004-2006, demonstrated weak flow at depths shallower than 100 m, with a velocity core in the lower thermocline at 200 m at Mak-East and 350 m at Mak-West (Figure 3.6). There is an upward phase tilt (dz/dt) associated with the $+v'$ of 50 m/day (Figure 3.6).

What ocean dynamics might force this upward phase propagation of $+v'$ events in Makassar Strait? We suggest that this trait is consistent with the dynamics of vertically propagating Kelvin waves. If a wind-forced Kelvin wave perturbed the surface of a stratified ocean, the energy attributed to the perturbation would not only propagate horizontally away from the perturbation point but also downward making a horizontal slope:

$$\theta = \frac{\omega}{N} = \frac{dz}{dx} \tag{3.1}$$

where ω is a wave frequency, N is stratification frequency, z is depth, and x is horizontal distance. As our composite plots are in depth and time domains, the slope equation can be equivalently written as

$$\frac{dz}{dt} = \frac{\omega.c}{N} \tag{3.2}$$

where c is a theoretical phase speed of a baroclinic wave mode and t is time. Thus an observer, stationed at a distance away from where a Kelvin wave is generated, would see the linear wave signature arrives deeper in the water column first.

To test whether the observed phase slope (Figure 3.6) inferred from the $+v'$ composite is consistent with the slope formula, we use an averaged stratification profile (N) from several CTD casts along the projected ray path (Figure 3.1). The phase speed (c) is inferred from the normal mode analysis of N (Figure 3.1). Given $\omega = 2\pi/(20-90)$days, c = 1.2-2.5 m/s (the phase speed for the first two wave modes), and $N = 0.0068\ s^{-1}$. Thus dz/dt varies within 15 - 115 m/day which agrees fairly well with the phase slope inferred from the v' composite (Figure 3.6). Thus the pattern of upward phase shift with a slope of 50 m/day observed in the v' composite consistently expresses a linear Kelvin wave signature.

A vertically propagating Kelvin wave can also be identified from how temperature fluctuations and velocity vectors associated with the wave are related. The pressure perturbation (p) and its corresponding vertical velocity (w) for a vertically propagating Kelvin wave are

$$p'(x,y,z,t) = \frac{2}{\pi}\int \hat{p}cos(mz)dm \tag{3.3}$$

$$w' = -\frac{N^2}{\rho_o}\frac{\partial^2 p'}{\partial z \partial t} \tag{3.4}$$

where m is vertical wavenumber and ρ_o is background density. Assuming density (ρ) fluctuations can be represented by temperature (T) fluctuations and vertical displacements of density surfaces are solely driven by the vertical velocity following $\frac{\partial p'}{\partial t} + w'\frac{\partial \bar{p}}{\partial z}$, it is implied that the highs and lows of T and p are separated by $\pi/2$. Since p' is in phase with the wave induced horizontal velocity vectors (u, v), it is also implied that T and (u, v) attributed to a theoretical Kelvin wave would have the same phase shift. Plots of the v and T timeseries for several depths, which focus on an episode of strong $+v$ in late May 2004, demonstrate that maximum northward along-strait flow occurs prior to maximum temperature oscillations with a lead of approximately 1/4 cycle (Figure 3.7) implying that T would lead v in a space domain by about $\pi/2$. This agrees well with the phase relationship required for an upward propagating Kelvin wave.

3.3.3.2 Energy Equipartition

As in the oscillation of a pendulum, a theoretical Kelvin wave also expresses equal partition between its corresponding kinetic and potential energies (Pedlosky, 2003). We use the v and T data to examine whether the energy equipartition in the wave field also characterizes the

intraseasonal motions observed in the Makassar Strait pycnocline. To estimate the potential energy (PE), the temperature timeseries over several depths ranging the pycnocline of the Mak-West mooring are converted to vertical displacements (η') using a heat equation

$$\eta'(z,t) = \frac{T'(z,t)}{\frac{\partial \bar{T}}{\partial z}} \tag{3.5}$$

in which horizontal advection, diffusion, and heat sources are neglected. We also remove the effect of static stability on the thermal field through normalizing η with the ratio between N and its corresponding vertical average N_o

$$\eta'_n(z,t) = \eta'(z,t)\frac{N}{N_o} \tag{3.6}$$

where z, t, and subscript n denote depth, time and normalized respectively. The PE per unit mass is computed as $0.5\rho_o N^2\overline{\eta'^2}$, where $\overline{\eta'^2}$ is the variance of vertical displacements averaged over intraseasonal frequency band and ρ_o is averaged density across pycnocline depths. Kinetic energy (KE) is inferred from the spectra of v and defined as $0.5\rho_o\overline{v'^2}$ where $\overline{v'^2}$ is variance attributed to v averaged over intraseasonal periods. Vertical structures of PE and KE (Figure 3.8) demonstrate that PE and KE have similar amplitudes, indicative of equipartition between PE and KE, which further supports our hypothesis that the Kelvin wave field contributes significantly to intraseasonal motion in the Makassar Strait thermocline.

3.3.3.3 Dispersion Relation

The dispersion relation for a Kelvin wave in Makassar Strait, a North-South oriented channel, would be $\omega = lc$, where l and c are wavenumber in the y direction and wave phase speed, signifying a constant phase speed or non-dispersive. We employ the v datasets at Lombok and Makassar Straits to investigate whether the coherent oscillation transmitting from Lombok Strait to Makassar Strait reported by Pujiana *et al.*(2009) exhibits a dispersion relationship consistent with a Kelvin wave.

The v time series at the upper 200 m of Lombok Strait and that at depths below 75 m of Makassar Strait are statistically coherent above the 95% significance level across the period band of 45-90 days, and the corresponding phase differences linearly decrease

with period. For example, v at 100 m in Lombok Strait and Makassar Strait are not only statistically coherent but also show a linear trend of decreasing phase difference with period (Figure 3.9), indicative of a propagating feature with a quasi-constant phase speed of 1.3 $\pm$ 0.01 m/s from Lombok Strait to Makassar Strait (a distance of 1240 km, the 100-m isobath length connecting the moorings at Lombok and Makassar Straits, is used in the computation). Thus the relationship between ω and l inferred from the coherence analysis exemplifies a non-dispersive wave.

In addition to the relation between ω and l, the relation between l and m (vertical wavenumber) is also useful to determine the wave classification. The equatorial wave dispersion relation, can be simplified as $k = -(2n+1)m\omega/N_o$, where k is zonal wavenumber, N_o is averaged stratification frequency over depths of 50-450 m, m is vertical wavenumber, β is beta effect, and n is meridional mode number (n = -1, 1, 2,). Because of the Makassar moorings proximity to the equator, we propose that the equatorial wave dynamics are suitable to explain any waveforms captured in the study area. Nevertheless the wave properties are now assumed to vary zonally because the main axis of the Makassar Strait is nearly parallel to the y-direction, so the corresponding dispersion relation is

$$l = \frac{-(2n+1)m\omega}{N_o} \tag{3.7}$$

The estimated l and m at obtained from coherence analyses of v at Lombok and Makassar Straits also approximate well the Kelvin wave dispersion curve (Figure 3.10).

3.3.3.4 Semi-geostrophic Balance and Increased Decay Scale

Observations and numerical experiments agree that the Kelvin wave energy originating in the equatorial Indian Ocean significantly influences the intraseasonal variability at Lombok Strait (Arief and Murray, 1996; Qiu *et al.*, 1999; Schiller *et al.*, 2010,Drushka *et al.*, 2010). Drushka *et al.*(2010) proposed that the vertical structure of the observed Lombok Strait throughflow at intraseasonal timescales was best explained by a baroclinic Kelvin wave. We will be discussing two other Kelvin wave attributes measured at Lombok Strait: semi-geostrophic balance and reflected Kelvin wave.

A simple wave equation and its boundary condition applicable for simplified Lombok

Strait, a channel bounded by vertical walls, are

$$\frac{\partial^2 \eta'}{\partial x^2} + (\frac{-\omega^2 - f^2 - l^2}{c^2})\eta' = 0 \tag{3.8}$$

$$\frac{\partial^2 \eta'}{\partial x^2} + (\frac{lf}{\omega})\eta' = 0; x = 0, W \tag{3.9}$$

where η' is sea level anomaly across the strait, l is wavenumber in the along-strait axis direction, and W is the strait width. The general solution, with $\omega = \pm lc$, is $\eta'(x,t) = \eta_o e^{\frac{-fx}{c}} cos(ly - \omega t)$, where c denotes Kelvin wave phase speed. Given the corresponding momentum equation is $v'(f^2 - \omega^2) - gf\frac{\partial \eta'}{\partial x} + g\frac{\partial^2 \eta'}{\partial x \partial y} = 0$, we can then obtain

$$v' = \frac{g}{f}\frac{\partial \eta'}{\partial x} \tag{3.10}$$

which implies a semi-geostrophic balance.

The u, v obtained from moorings, and η from the pressure gauges and altimeter are employed to examine the Kelvin wave signatures in Lombok Strait. We focus on the May 2004 event during which the instruments were all operational. Moorings and pressure gauges in Lombok Strait demonstrated that $+v$ and $+\eta$ characterized the Lombok Strait intraseasonal variability during May 2004 (Figure 3.11). We also identify that the across-strait SLA slopes down towards the east ($\partial\eta'/\partial x$), with higher sea level at Pw than Pe, when $v > 0$ during May 2004 (Figure 3.11), indicating a balance between $\partial\eta'/\partial x$ and zonal coriolis force. Meanwhile the along-strait sea surface tilt ($\partial\eta'/\partial y$), inferred from satellite-derived SLA measured at two locations in Lombok Strait (Pn and Ps; Figure 3.1), is not balanced by f in the y-direction as the sea surface slopes up towards the south ($\partial\eta'/\partial y < 0$) when $u > 0$ (Figure 3.11b,c; Figure 3.12a), indicative of ageostrophy. Moreover the estimated geostrophic $+v$ inferred from $\partial\eta'/\partial x$ does not differ significantly from $+v$ measured from moorings (Figure 3.12b), which confirms a partial geostrophic balance in the x-direction.

The two shallow pressure gauges at the zonal boundaries of Lombok Strait also indicated enhanced across-strait decay scale, another Kelvin wave attribute. The estimated η' variability at Pe

$$\eta'_{Pe} = \eta'_{Pw} e^{-W/R} \tag{3.11}$$

with $W = 0.3R$ the distance between the two pressure gauges and R is the Rossby radius of deformation, is less than the observed η'_{Pe} (Figure 3.12c). The discrepancy between the measured and estimated η'_{Pe} implies increased across-strait decay scale. Durland and Qiu(2003) connected a low-frequency Kelvin wave passage in a strait with enhanced across-strait decay scale, mainly forced by the formation of a reflected Kelvin wave whose direction was 180° out of phase with the incident wave. When a Kelvin wave in Lombok Strait reaches an entrance into a larger basin, it does not contain the required energy to force a wave of equal amplitude in that basin which leads to the genesis of a reflected wave in order to preserve the continuity of pressure at the strait mouth. Since the maximum amplitude of the reflected wave is on the opposite side of the strait to the maximum amplitude of the incident wave, the reflection subtracts more from the minimum amplitude of the incident wave than it does from the maximum amplitude. This likely results in an enhanced across-strait pressure gradient such as observed in Lombok Strait (Figure 3.12c).

3.4 Waveguide from Lombok Strait to Makassar Strait

We have demonstrated that observations at Makassar and Lombok Straits reveal intraseasonal motions with Kelvin wave signatures, which signify propagation from Lombok Strait to Makassar Strait. Discontinuous coastlines separate the moorings at both straits raising the question of the pathway guiding the wave from Lombok Strait to Makassar Strait. Given the averaged depth across section A (Figure 3.13a) is 145 m, a barotropic Kelvin wave with a deformation radius of 1900 km would overcome the gap of ∼475 km and force another barotropic Kelvin wave of reduced amplitude to propagate along the southern Kalimantan coasts into the Makassar Strait. In contrast the gap is too wide for the observed baroclinic Kelvin wave with a deformation radius of less than 100 km to jump over.

A route which extends for 5195 km and runs along the northern Bali and Java, and eastern Sumatra coasts, the equator (across the South China Sea) and southern Kalimantan coasts (Figure 3.13a) would serve as a viable waveguide for a baroclinic Kelvin wave originating in Lombok Strait because the gaps in Bali and Sunda Straits (Figure 3.13a) are less than the deformation radius. Nevertheless the first two modes of a baroclinic Kelvin wave

with a speed of 1.2-2.5 m/s would take at least 25 days to propagate along this waveguide, whereas the lags between the v at Makassar Strait and that at Lombok Strait vary from 12-16 days (Figure 3.13b), indicative of a shorter pathway connecting both Straits. The third mode of a baroclinic Kelvin wave with a speed of 0.8 m/s would take even longer.

A shorter pathway from Lombok Strait to Makassar Strait is along the isobaths, across the Sunda continental slope and at depths greater than 50 m (Figure 3.13a), where a slope-trapped baroclinic Kelvin wave may propagate towards Makassar Strait with shallower water to the left. The propagation of a baroclinic Kelvin wave along an isobath has been studied through both laboratory experiments and observations (Codiga *et al.*, 1999; Hallock *et al.*, 2009). Figure 3.13a depicts the 100-m isobath, which extends for ∼1240 km and links the moorings in Lombok and Makassar Straits. A baroclinic Kelvin wave with a speed of 0.8-1.2 m/s, equivalent with a speed of the second and third modes theoretical baroclinic Kelvin waves inferred from stratification, would take 12-18 days to reach Makassar Strait, which is in good agreement with the observations (12-16 days, Figure 3.13b). We thus speculate that the Kelvin wave propagates as the second and third baroclinic modes along the 100-m isobath directly linking Lombok to Makassar Strait.

3.5 Transport and Mixing Associated with Kelvin Wave in Makassar Strait

3.5.1 Transport

We have provided supportive evidence for Kelvin wave propagation from the velocity vectors, temperature and stratification datasets. We now address a question of the relevance of Kelvin waves to ITF studies, more specifically, what are the transport anomalies associated with the intraseasonal baroclinic Kelvin waves in Makassar Strait? To deduce the estimated transport anomalies, we use the v datasets at depths of 125-450 m from the Mak-West and Mak-East moorings. At each depth of z, we fit the v timeseries from both moorings using an exponential function

$$v' = v'_{Mak-west} e^{-x/b} \tag{3.12}$$

which results in the across-strait structure of v, $v(x,z,t)$, where b is the horizontal scale coefficient, and $x = 0 : L$ ($x = 0$ and $x = L$ correspond with the Mak-West and Mak-East mooring sites respectively). The transport is then computed as

$$\int_{z=-450}^{z=-150} \int_{x=0}^{x=L} v'(x,z,t)dxdz \tag{3.13}$$

The transport variability observed during 2004-2006 across the pycnocline (Figure 3.14) indicates that a downwelling intraseasonal Kelvin wave passage could drive northward mass transport of 0.75 $\pm$ 0.4 Sv (mean $\pm$ standard deviation) across depths of 125-450 m within the Makassar Strait pycnocline with a maximum northward transport of $\sim$2 Sv recorded in late May 2005 (Figure 3.14).

3.5.2 Mixing

Ffield and Gordon(1992), using an archive of CTD datasets and the 1-D advection and diffusion equation, characterized tidal currents as the main forcing for the strong vertical mixing with vertical diffusivity in excess of 10^{-4} $\mathrm{m}^{-2}/\mathrm{s}^{-1}$ in the Makassar Strait thermocline. At intraseasonal timescales, Figure 3.4b-d, Figure 3.5 and Figure 3.6 demonstrate that a Kelvin wave episode in Makassar Strait is marked with the vertically sheared v, which potentially yields unstable stratification through Kelvin-Helmholtz instability and contributes to the vertical mixing strength. In a steady, inviscid, non-diffusive, and stably stratified flow, small disturbances are stable provided the Richardson number, $\mathrm{Ri} = \mathrm{N}^2/(dv/dz)^2$, is greater than 1/4 everywhere in the fluid. The relationship between a Kelvin wave and Kelvin-Helmholtz instability arises from the Kelvins wave perturbation to v and T. Thus if a Kelvin wave were important to govern the v variation across the pycnocline depths in Makassar Strait, we would expect that the energetic wave episodes correspond with small Ri.

The Ri variability (Figure 3.15) across the Makassar Strait pycnocline is computed using the observed v and N at the Mak-West site, where N was computed by assuming ρ' is equivalent to T. Figure 3.15 demonstrates that the likelihood of unstable stratification within the lower pycnocline depths is greater during the period when observed Kelvin wave signatures are stronger in Makassar Strait (e.g. late May, August 2004, December 2004, June 2005, November 2005). Furthermore the corresponding eddy viscosity coefficient is

parameterized using, Kv = 5.6 x 10^{-8} $Ri^{-8.2}$, a formula appropriate in a region where density variations are dominated by those of temperature (Thorpe, 2004) such as in Makassar Strait, and the vertical diffusivity during strong Kelvin wave events varies from 1-5 x10^{-5} m^2/s^{-1}.

3.6 Discussion and Summary

We have described the characteristics of the 2-3 month oscillations measured in Makassar Strait during 2004-2006, marking the weakened ITF transport across the pycnocline and the vertically sheared v at the subpycnocline. A composite of the 17 $+v$ events found within the pycnocline depths exhibits an upward phase tilt, which implies a vertically propagating wave attribute with a non-local origin. The v and T data across the pycnocline show a quarter cycle of phase shift, which favors downward energy propagation, and also the kinetic-potential energy equipartition. Warmer pycnocline occuring during the $+v$ episodes is also evident from the relation between v and T. Furthermore a normal mode approximation is also applicable to explain the link between the vertical structure of v and stratification. We suggest that these characteristics pertinent to the 2-3 month variability observed in the Makassar Strait are in agreement with the theoretical downwelling Kelvin wave signatures.

The η', u and v data in Lombok Strait also demonstrate two Kelvin wave attributes in the semi geostrophic balance between v and $d\eta'/dx$ and in enhanced $d\eta'/dx$, which corroborates those reported by Drushka *et al.*(2010). The v data in Lombok Strait and that in Makassar Strait are coherent and yield a Kelvin wave dispersion relationship between the wavenumber and wave frequency. The waves propagate from Lombok Strait to Makassar Strait with a phase speed of ∼1.3 m/s, a 2nd mode baroclinic Kelvin wave speed. The 2^{nd} baroclinic wave mode inferred from the measured Kelvin wave phase speed affirms the baroclinic vertical structure attributed to the $+v$ events in Makassar Strait which exhibits two-zero crossing points over depths. Through the comparison of the $+v$ episodes in Lombok Strait and Makassar Strait, we suggest that the Kelvin waves navigate along the 100-m isobath and extends for ∼1240 km, to transmit its energy from Lombok Strait to Makassar Strait. Another shallower route, encompassing a distance of ∼5195 km along the coasts of Java, Sumatra, and Kalimantan, is too long a pathway for a baroclinic Kelvin wave to

propagate within 12-16 days, the lags that the $+v$ events in Makassar Strait display relative to that in Lombok Strait. Thus the intraseasonal Kelvin waves in Makassar Strait are linked to that in Lombok Strait.

Drushka *et al.*(2010) demonstrated that the model v data in Lombok Strait, simulated by a simple wind-forced model forced by zonal winds in the eastern equatorial Indian Ocean and along-shore winds along the Sumatra and Java coasts, showed a good agreement with observation. Because the intraseasonal motions in Makassar Strait and Lombok Strait are significantly correlated, the intraseasonal Kelvin waves in Makassar Strait derive their energy from the same southeastern Indian Ocean winds.

Significant MJO phases preceded the Kelvin wave episodes in Makassar Strait occurring in March and May 2004; May, and September 2005 with the maximum $+v$ at 150 m associated with the Kelvin wave trailing the peak of MJO by 19-25 days. Meanwhile the MJO leads $+v$ at 150 m by 6-11 days, implying that the MJOs footprint in Makassar Strait lags that in Lombok Strait by 13-14 days, consistent with the number of days a baroclinic Kelvin wave requires to propagate from the Lombok Strait moorings to the Makassar Strait moorings. Unlike the study of Zhou and Murtugudde(2010), which suggested that the MJO affected the intraseasonal variability only at the ITF outflow passages such as Lombok Strait, we propose that the MJO-related oceanic Kelvin wave is also observed in Makassar Strait.

The downwelling Kelvin wave passages affect the ITF transport anomalies, in which a wave episode results in an averaged northward anomaly of $\sim$0.75 Sv across the pycnocline depths of 100-450 m. The wave passages are also commensurate with the small Richardson number phases, during which dv'/dz is intensified amplifying the likelihood of Kelvin-Helmholtz instability resulting in a vertical mixing with Kz of 1-5x10^{-5} m^2s^{-1}.

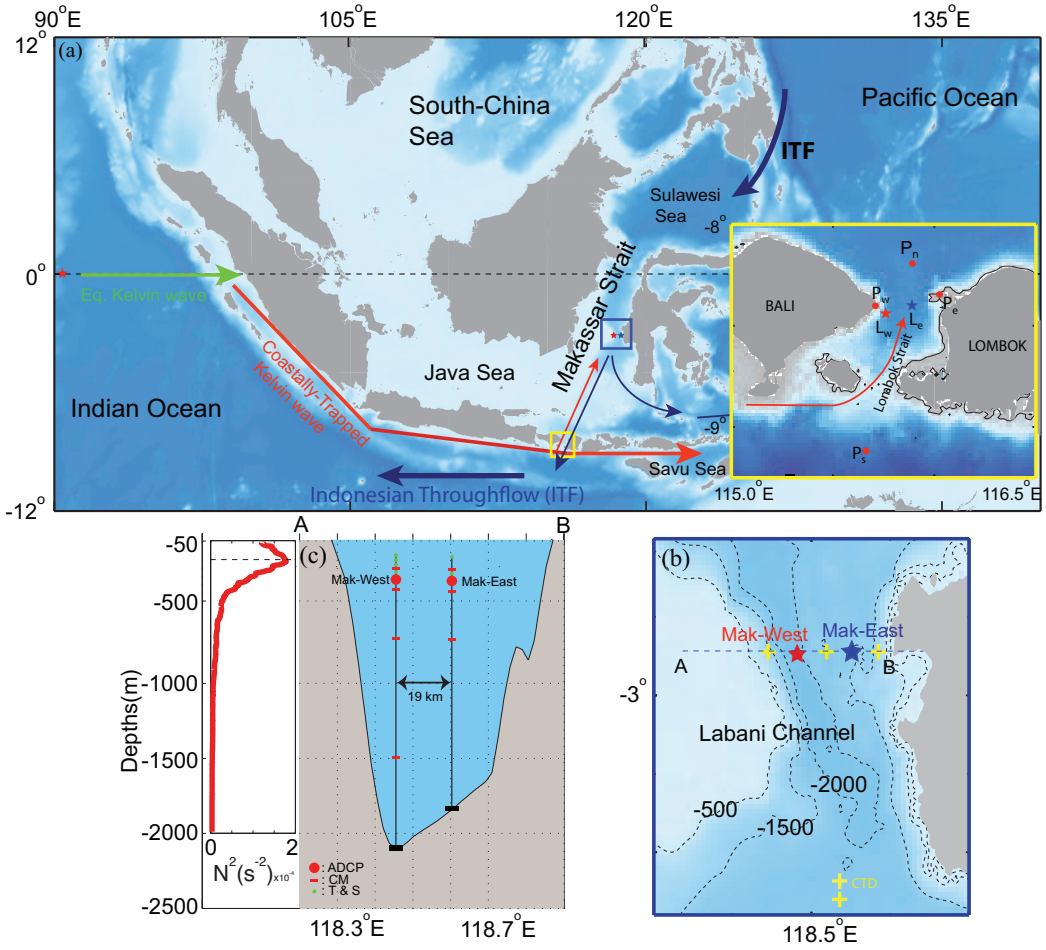

Figure 3.1: (a) The Makassar Strait location in the maritime continent, and the schematic of the waveguide for the Kelvin wave. Inset is an expanded view of Lombok Strait and the corresponding mooring [Lw and Le] and shallow pressure gauge sites [Pw and Pe] and location of altimeter measurement used for along-strait sea level anomaly [Pn and Ps]. (b) A blow-up of the blue box in (a) showing the Labani Channel, the narrowest passage within Makassar Strait where the moorings [Mak-West and Mak-East] were deployed. Yellow crosses denote CTD stations. (c) A bathymetric cross-section A-B [shown in (b)] in the Labani Channel, mooring configuration, and an averaged stratification profile obtained from the CTD stations.

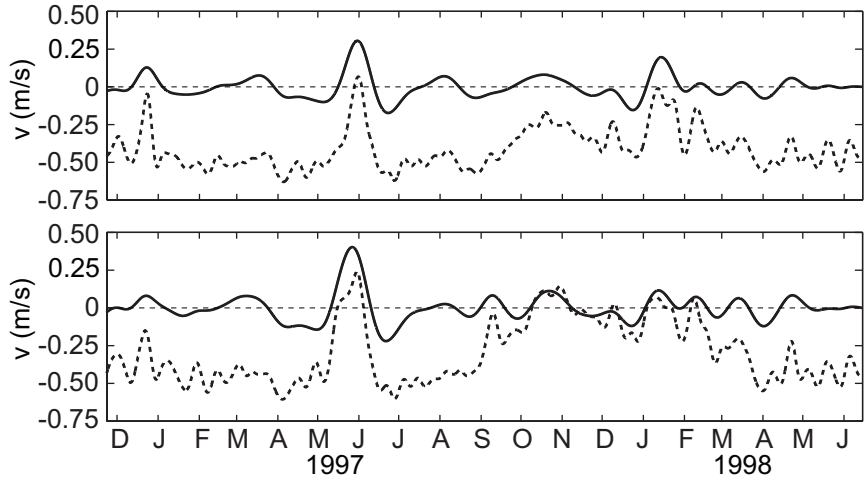

Figure 3.2: Timeseries of subinertial [dashed] and intraseasonal [solid] along-strait flow at 250 m [upper panel] and 350 m [lower panel] at the Mak-West site. Positive velocity indicates northward flow. The data were observed during late November 1996 - mid June 1998.

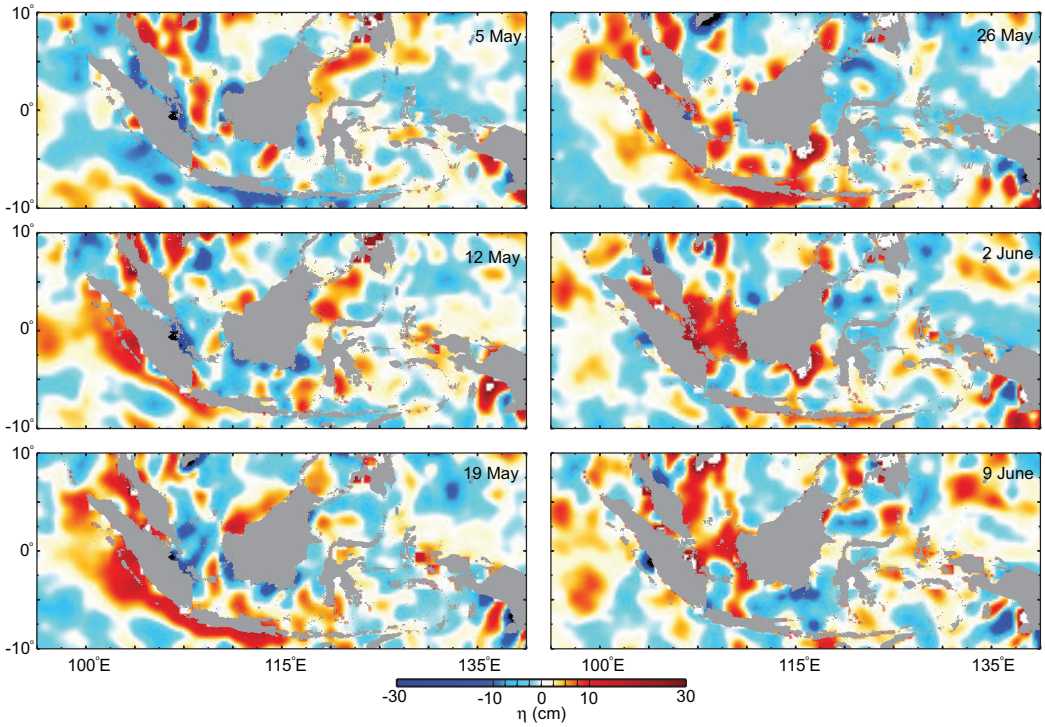

Figure 3.3: Snapshots of satellite altimetry-derived SLA [η] over the maritime continent during 5 May-9 June 2004. The η data vary at intraseasonal timescales.

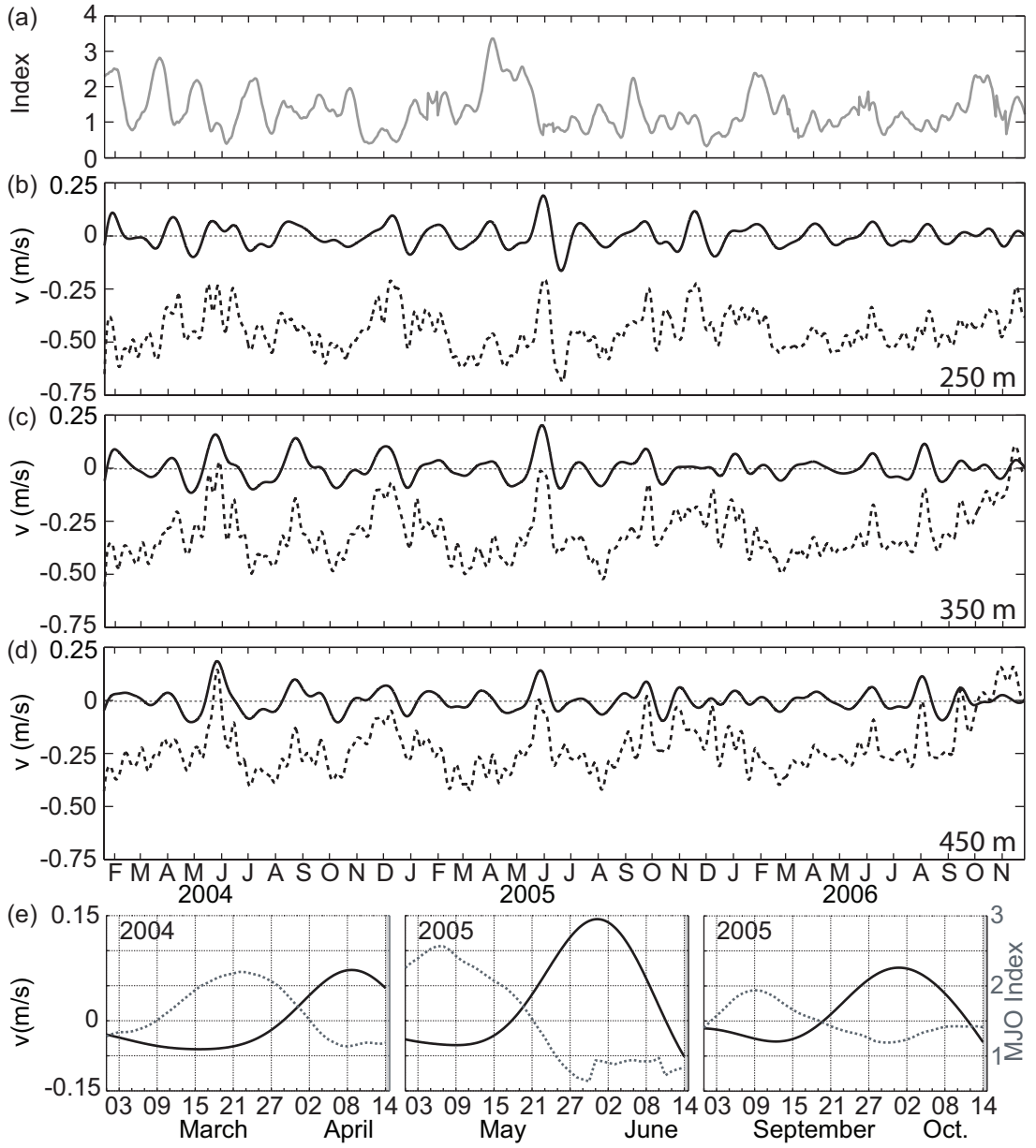

Figure 3.4: (a) Timeseries of Madden-Julian Oscillation index. Timeseries of subinertial [dashed] and intraseasonal [solid] along-strait flow at b) 250, c) 350, and d) 450 m. The MJO and velocity data were observed from 20 January 2004 to 26 November 2006. (e) Plots of the intraseasonal along-strait flow timeseries [solid] at 150 m and MJO index [dashed] during strong MJO phases.

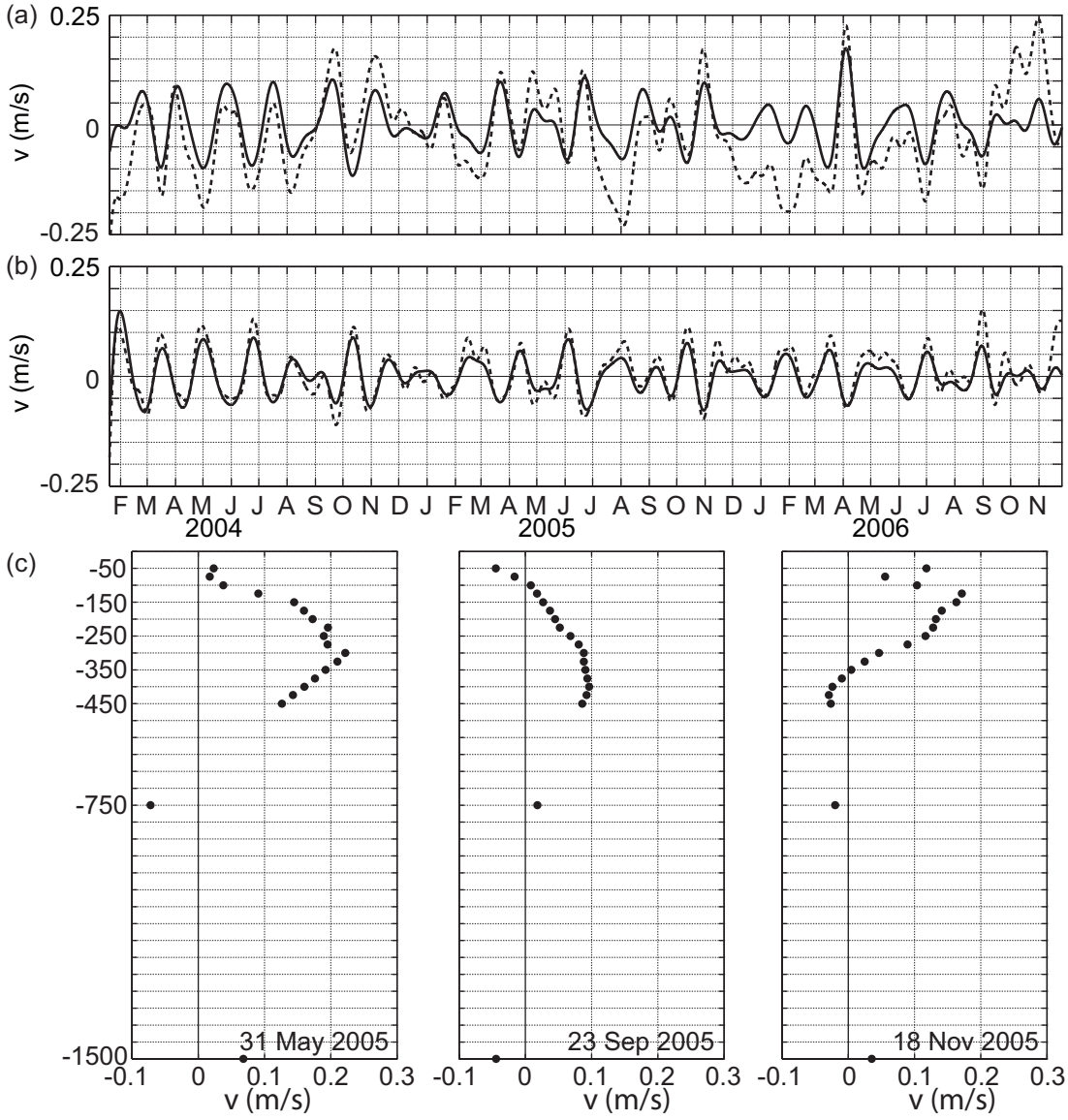

Figure 3.5: The along-strait flow timeseries varying at subinertial [dashed] and intraseasonal timescales [solid] observed at 750 m (a) and 1500 m (b) within the Mak-West subpycnocline. (c) Vertical structure of the intraseasonal along-strait flow data across the pycnocline and at two subpycnocline depths at three events when the intraseasonal along-strait flow at the pycnocline attains maximum value.

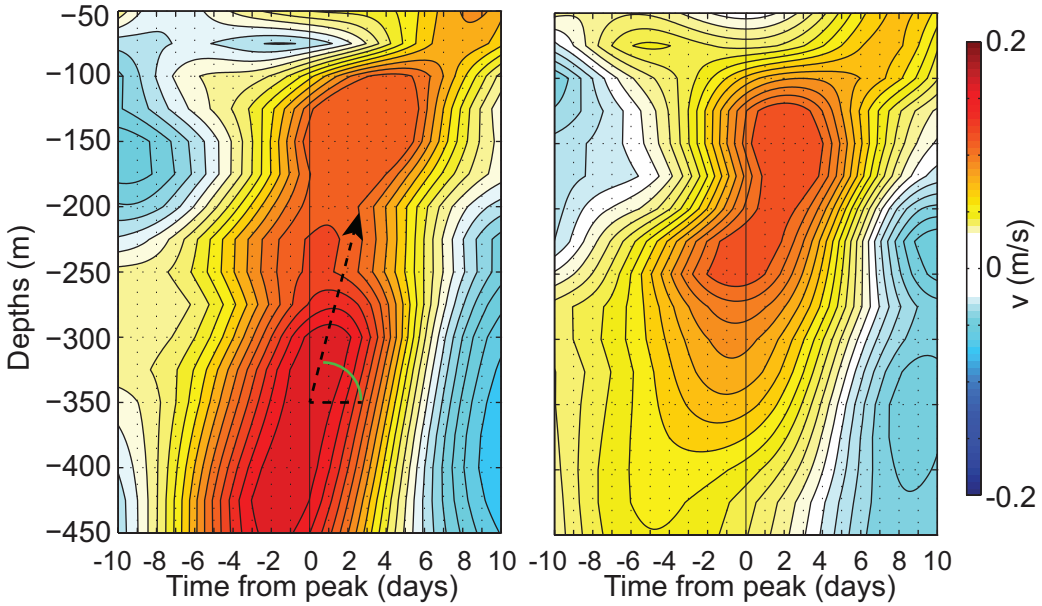

Figure 3.6: The composite of the northward along-strait flow at intraseasonal timescales observed at the Mak-West [left panel] and Mak-East [right panel] pycnocline. Day 0 was defined as the time of the peak northward flow at 350 m. The dashed line with an arrow denotes the phase line, and the angle [green curve] that the line makes with the horizontal dashed line indicates upward phase shift of 50 m/day.

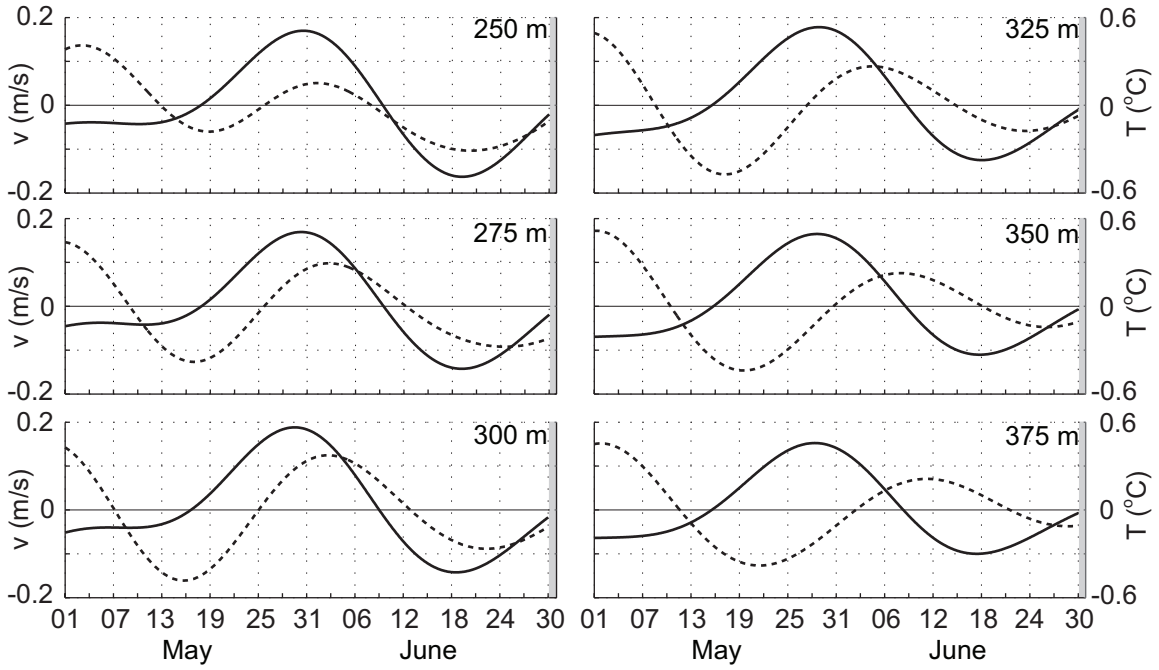

Figure 3.7: The along strait flow [solid] and temperature [dashed] timeseries varying at intraseasonal timescales observed at several depths within the Mak-West pycnocline during May-June 2004. Positive velocity indicates northward flow.

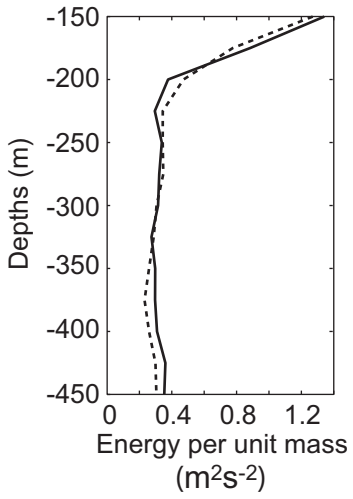

Figure 3.8: Vertical structure of potential [solid] and kinetic [dashed] energy across the lower pycnocline. The potential and kinetic energy are inferred from temperature and along-strait flow varying at intraseasonal timescales observed at the Mak-West.

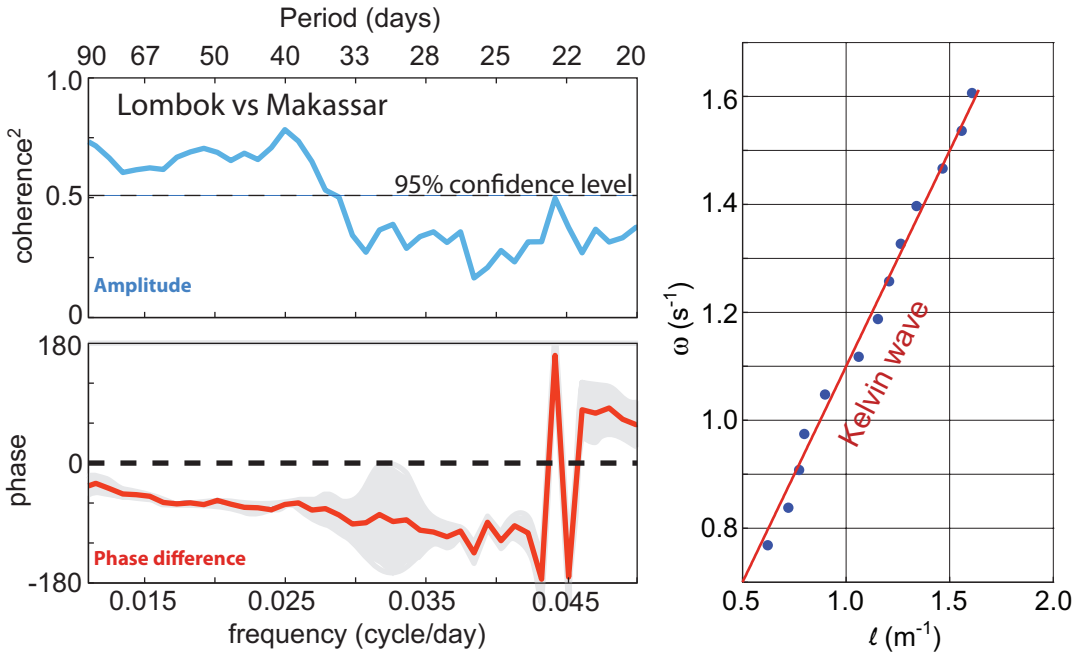

Figure 3.9: (Left) Coherence amplitudes and phases between the intraseasonal along-strait flow timeseries at 100 m in Lombok Strait [Lombok-East/Le] and that at 100 m in Makassar Strait [Mak-West]. (Right) Dispersion relation diagram inferred from the phase shift plot shown in the left panel.

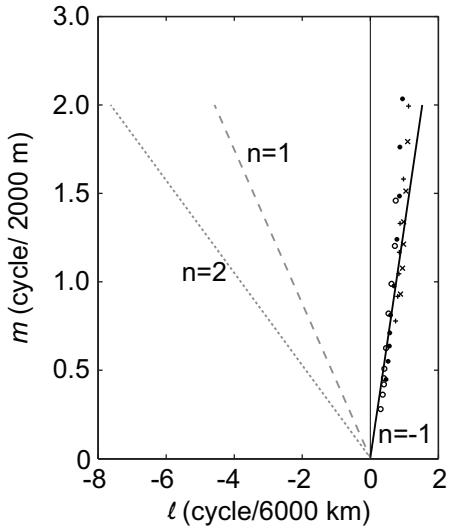

Figure 3.10: Dispersion diagram of horizontal versus zonal wavenumber at $\omega = 2\pi 60$ day^{-1}. The markers indicate the estimated values from the data, the solid black line demonstrates dispersion relation for a theoretical Kelvin wave, and the grey lines are the dispersion relation for the first two modes of theoretical Rossby waves.

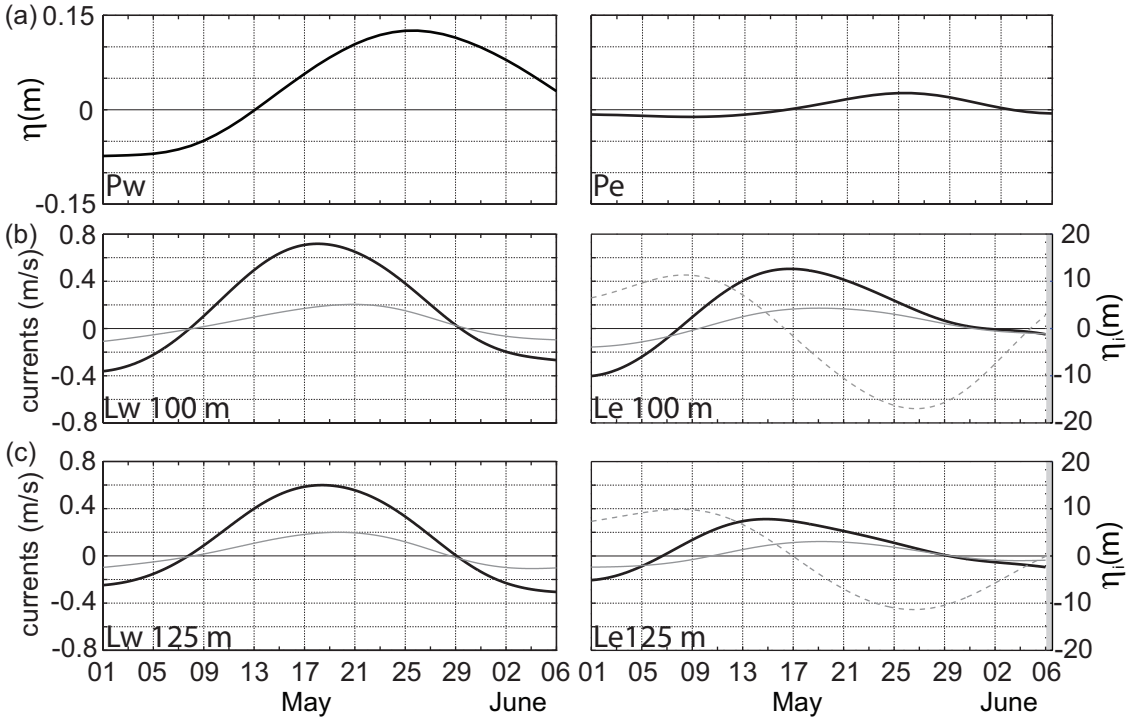

Figure 3.11: Time series of SLA at intraseasonal timescales during May - 6 June 2004 from two shallow pressure gauges deployed in Lombok Strait, Pw and Pe. (b and c) Time series of along-strait flow [solid black], across-strait flow [solid grey] and vertical isopycnal displacements [dashed gray] varying at intraseasonal timescales observed at Lombok moorings.

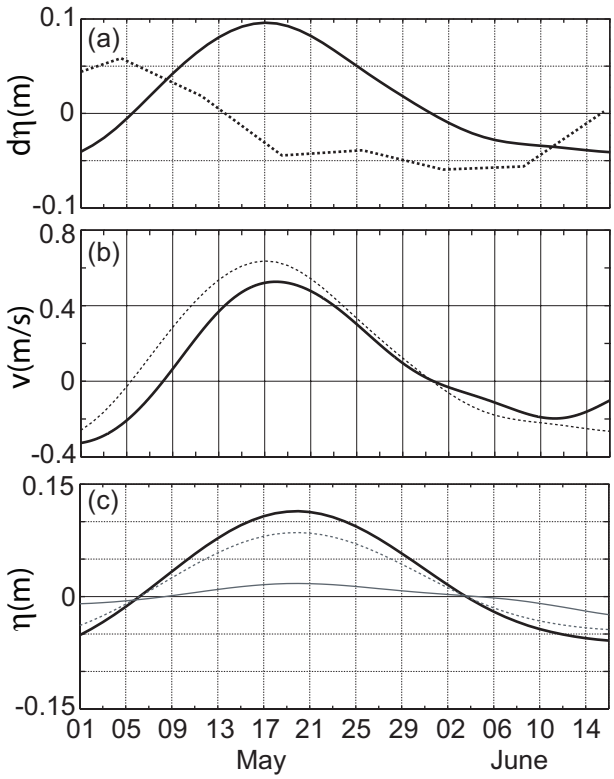

Figure 3.12: (a) Across-strait gradient of SLA (η_{Pw} - η_{Pe}, solid) computed from the shallow pressure gauges and along-strait gradient of satellite altimetry derived SLA [η_{Pn} - η_{Ps}, dashed] in Lombok Strait. (b) Geostrophic flow inferred from the moorings [solid] and pressure gauges [dashed]. (c) The observed η_{Pw} [black] and η_{Pe} [grey] and the estimated $\eta_{Pe} = \eta_{Pw}\mathrm{e}^{-w/R}$ [dashed grey]. (a,b, and c) demonstrate data from May-mid June 2004 which vary at intraseasonal timescales.

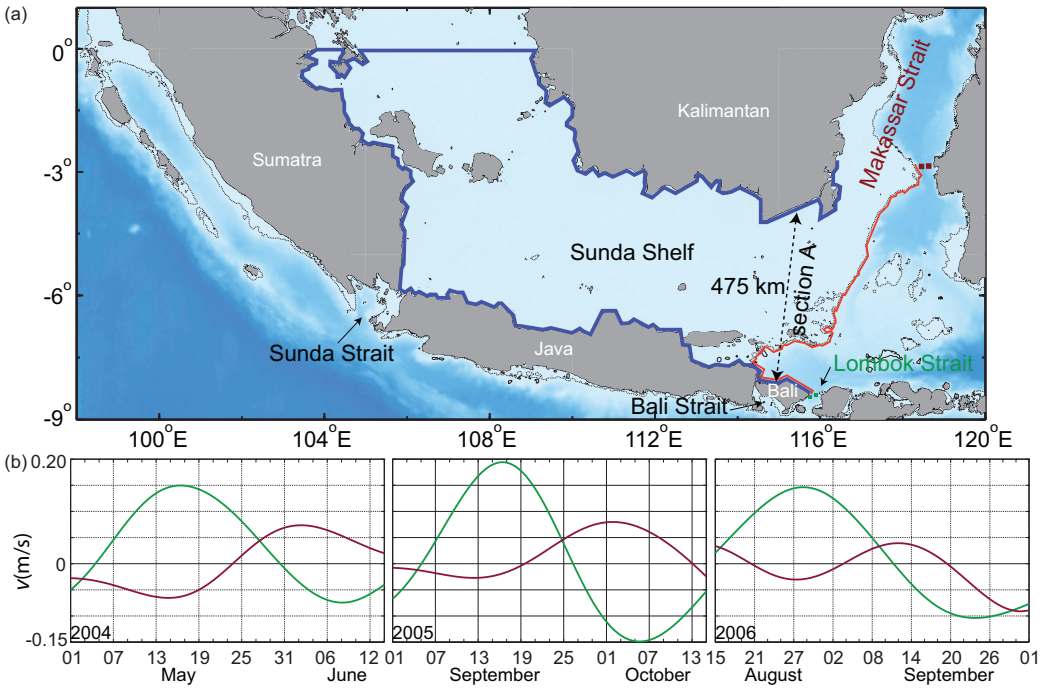

Figure 3.13: (a) Potential pathways, route-1 [blue] and route-2 [red] for a Kelvin wave propagating from Lombok Strait to Makassar Strait. Route-1 extends for 5195 km, while route-2 extends for 1271 km along the 100-m isobath. The colored boxes show the mooring sites, and the dashed contour depicts the 100-m isobath. (b) The intraseasonal along-strait flow data observed at 150 m of Lombok Strait [green] and Makassar Strait [purple].

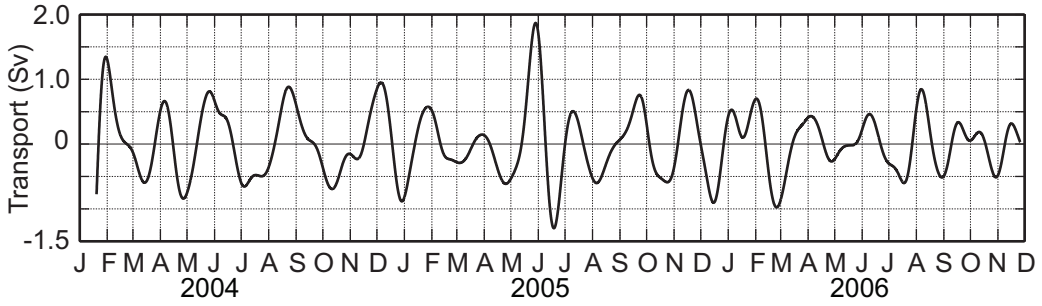

Figure 3.14: The along-strait transport magnitudes varying at intraseasonal timescales estimated across the Makassar Strait pycnocline. The magnitudes express the transport anomalies attributable to intraseasonal Kelvin wave passages.

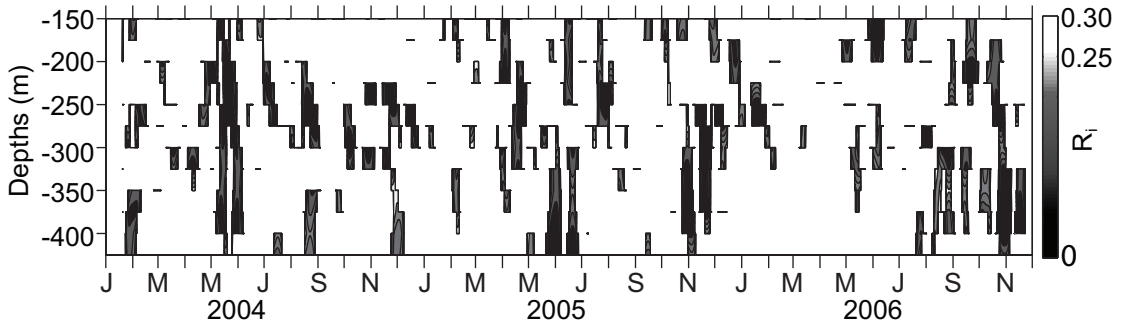

Figure 3.15: Time series of Ri obtained from the ratio between the vertical shear of intraseasonal along-strait flow $[dv/dz]$ and N in the Makassar Strait pycnocline. The dv/dz and N data are from the Mak-West mooring. Ri > 0.25 is given in white, while Ri < 0.25 is shown in grey/black.

Chapter 4

Intraseasonal Eddies in Makassar Strait

Published as: Pujiana, K., Gordon, A. L., Metzger, E. J., and Ffield, A, 2012. The Makassar Strait pycnocline variability at 20-40 days, Dynamics of Atmospheres and Oceans, 53-54, 17-35.doi: http://dx.doi.org/10.1016/j.dynatmoce.2012.01.001

Abstract The characteristics and plausible genesis of the 20-40 day variability observed within the Labani Channel, a constriction within the Makassar Strait, Indonesia, are described. The 20-40 day variability, trapped beneath the depth of the strongest stratification of the pycnocline, is most evident in the across-strait flow, and in the across-strait gradient of the along-strait flow as well as in the vertical displacements of isotherms. The 20-40 day energy distribution of the across-strait flow is identifiable as a blue spectrum, demonstrating downward phase propagation. The flow fields are approximated by a vortex velocity structure, and the corresponding isotherm displacements imply potential vorticity conservation. We propose that the 20-40 day features observed in the Labani Channel are expressions of cyclonic and anti-cyclonic eddies that are advected southward within the Makassar Strait throughflow. Analysis of simulated eddy kinetic energy from an eddy-resolving model further indicates that the upstream instability of the background flow within Makassar Strait is the energy source for the eddies which are dissipated within the Labani Channel.

4.1 Introduction

Makassar Strait is the primary Pacific water inflow gateway to the Indonesian Throughflow [ITF] (Figure 4.1a; Gordon and Fine, 1996). Observations made during 2004-2006 indicated that the Makassar Strait throughflow contributed 12 x 10^6 m^3/s to the ITF total of 15 x 10^6 m^3/s (Gordon *et al.*, 2008; Gordon *et al.*, 2010). The Makassar Strait throughflow is not steady but rich in interannual and seasonal variability as well as energetic fluctuations at tidal and intraseasonal [< 90 day period] timescales (Gordon *et al.*, 2010).

An earlier investigation of intraseasonal flow in Makassar Strait, using a 1.5 year (1996-1998) time series of along-channel speeds at 300 m and 450 m, showed two significant intraseasonal variability [ISV] peaks: 35-60 and 70-100 days (Susanto *et al.*, 2000). Estimates based on numerical experiments suggested that the two peaks were directly linked to remote forcing emanating in the Western Pacific and Indian Ocean, as well as baroclinic eddies originating in the Sulawesi Sea (Qiu *et al.*, 1999; Masumoto *et al.*, 2001). The *International Nusantara Stratification and Transport* [INSTANT] program from 2004 to 2006 (Sprintall *et al.*, 2004; Gordon and Kamenkovich, 2010) provides a longer time series with improved vertical resolution of the Makassar Strait throughflow. The Makassar along-strait flow observed by the INSTANT program reveal that the 45-90 days variability characterizes the intraseasonal motions in the Makassar Strait pycnocline, and the vertical structure of the motions resembles that of remotely forced baroclinic waves (Pujiana *et al.*, 2009).

In this study we investigate the 20-40 day signatures within the Makassar Strait pycnocline and focus the analysis on the across-strait flow (a parameter that has been overlooked in previous studies), relative vorticity derived from the along-strait flow at the two INSTANT moorings located across Makassar Strait and the temperature fluctuations. Although the across-strait mean flow in Makassar Strait is smaller than the along-strait mean flow (the maximum across-strait mean flow at the Labani Channel $\sim$O(0.25 cm/s)), its variance exhibits some interesting aspects. For example, the flow fields at periods of 20-40 days show that the variances in the across-strait component are comparable or larger than that in the along-strait direction at depths ranging from 100 to 300 m in the Makassar Strait pycnocline. We propose that the pronounced 20-40 day variability in the Makassar

Strait pycnocline derives its momentum from cyclonic and anti-cyclonic eddies, which are advected southward with the mean Makassar Strait throughflow. A better understanding on the 20-40 day features provides a fuller picture of Makassar Strait intraseasonal flow.

The presentation of this paper is organized as follows. We will first describe the data employed in section 4.2. Section 4.3 covers general descriptions of the 20-40 day variability and their corresponding eddy characteristics from several parameters observed in the Labani Channel. This is then followed by discussion on the eddy genesis in Makassar Strait as simulated by an eddy-resolving model in Section 4.4. The last section concludes the paper with discussion and summary.

4.2 Data

The INSTANT program observed the ITF by means of moorings with ADCPs, current meters, and temperature sensors, deployed at several Indonesian passages linking the Pacific to the Indian Ocean (Sprintall *et al.*, 2004). For this study we will be using the INSTANT data within Makassar Strait. We also utilize several Conductivity, Temperature, Depth [CTD] casts from the *Arus Lintas Indonesia* [ARLINDO] program of 1993-1998 (Gordon and Susanto, 1999) and simulated velocity vectors from the HYbrid Coordinate Ocean Model [HYCOM] (Metzger *et al.*, 2010).

4.2.1 ADCP and Current Meter

The INSTANT 2004-2006 program monitored the ITF transport in Makassar Strait from two moorings: 2°51.9 S, 118° 27.3 E [MAK-West] and 2°51.5 S, 118° 37.7 E [MAK-East], within the 45 km wide Labani Channel (Gordon *et al.*, 2008; Figure 4.1a). Each mooring consisted of an upward-looking RD Instruments Long Ranger 75 kHz Acoustic Doppler Current Profiler [ADCP] at a depth of 300 m and four current meters deployed at 200, 400, 750, and 1500 m. The Mak-West and Mak-East moorings recorded 3-year long datasets from 2004 to late 2006. The datasets, horizontal velocity vectors, are linearly interpolated onto a 25-m depth grid for each two-hour time step to produce gridded current vectors from 50 to 450 m of water column. The gridded horizontal current vectors are subsequently projected

to the along (y) and across-strait (x) axis of the Labani Channel, which are oriented along -10° and 80° (relative to north and positive is clockwise) respectively (Figure 4.1a), to yield gridded along (v) and across-strait (u) currents.

4.2.2 CTD

The CTD datasets used for this study are a compilation of several CTD casts collected within or near Labani Channel during ARLINDO 1993-1998 cruises (Figure 4.1a). For each station, a Neil Brown Instrument System Mark III [NBIS MK III] CTD measured conductivity, temperature and pressure within 12 hours period, yielding CTD casts or temporal variability of measured parameters. CTD was lowered at a rate of 1 ms^{-1}, and a 16 s^{-1} sampling rate was selected. A phase lagging filter is applied to the conductivity data as correction for the time constant mismatch. The data are then coarsely de-spiked and reduced to a 1-dbar pressure series by applying a 5-scan median filter around the target pressures.

A density profile inferred from several CTD casts within the Labani Channel shows that the pycnocline layer occupies a small fraction of water column from ∼25-450 m, with the strongest stratification at mid-pycnocline near 125 m separating the upper (25-100 m) and lower (150-450 m) pycnocline (Figure 4.1b).

4.2.3 Temperature Sensors

Several temperature and pressure sensors attached to Mak-West and Mak-East moorings measured the temporal variability of the temperature profile in Makassar Strait. Mak-West mooring provided better temperature profile resolution with 17 sensors attached at different levels from 100 m to 400 m; Mak-East mooring only had 5 sensors. The sensors sampled temperature and pressure at 6-minute intervals over a period of almost 3 years from January 2004 to November 2006. The temperature datasets are linearly interpolated onto a 25-m depth grid for each two-hour time step to provide the gridded temperature data from 150 to 350 m of water column. Since the vertical structure of temperature variability is less resolved at Mak-East mooring, we will only analyze the temperature profile datasets from Mak-West.

To investigate the vertical structure of thermal field, mooring sensor temperature data available in the lower pycnocline layer are converted to vertical displacement (η). Neglecting horizontal advection, diffusion, and heat sources, η is calculated using a heat equation, which is simply a ratio between the gridded temperature amplitudes and the vertical gradient of the averaged temperature, $\eta(z,t) = T(z,t)/\partial\bar{T}/\partial z$, where z and t denote depth and time respectively. The averaged temperature is a mean of the entire 3-year datasets. To remove the static stability effect from η, we normalize η with the ratio between stratification frequency structure (determined from the CTD data shown in Figure 4.1b) and its corresponding vertical average, $\eta_n(z,t) = \eta(z,t)[N/No]$, where subscript n and o are for normalized and vertically averaged respectively.

4.2.4 Simulated Data

Simulated velocity vectors and temperature variability from a numerical ocean model are also used in this study. HYCOM has a horizontal resolution of 1/12.5° cos(lat) x 1/12.5° and employs 32 hybrid vertical coordinate surfaces with potential density referenced to 2000 m. It has been shown to realistically simulate the circulation pathways of the Indonesian Seas, and specific model formulation details can be found in Metzger *et al.*, 2010. We examine daily data for a 3-year period from 2004 to 2006 within the Makassar Strait pycnocline, where the data are gridded vertically with a uniform resolution of 25 m from the surface to 450 m of water column.

4.3 Description of the Intraseasonal Velocity and Thermal Fields

In this section, general characteristics of the Labani Channel velocity and temperature profile variability measured are described. The statistical methods used to explore those characteristics are mainly spectral method, cross-correlation in frequency domain, and complex principal component analysis.

4.3.1 Observation

4.3.1.1 Horizontal and Sheared Flows

Gordon *et al.*(2008) using INSTANT data from 2004 to 2006 reported the vertical and horizontal profiles of the Makassar Strait mean flow for sub-tidal variability and found that $\bar{v}$ revealed a distinct maximum southward $(-y)$ speed at 140 m with western intensification. The average direction of the flow points slightly to the east of approximately north-south along-axis direction. Superimposed on the mean flow are the fluctuations (u' and v') across a broad spectrum from inertial to interannual time frame. Focusing on the intraseasonal variability and investigating the vertical profile of the variance attributed to across-strait and along-strait flow, $\overline{u'^2}$ and $\overline{v'^2}$, where over bar delineates integration over intraseasonal periods, we find that the profile exhibits: the maximum $\bar{u'^2}$ is found at mid pycnocline (Figure 4.2a), while $\overline{v'^2}$ attains maximum magnitude at depth closer to the sea surface (Figure 4.2b). The ratio between $\overline{u'^2}$ and $\bar{v'^2}$ suggests that the intraseasonal motions are anisotropic throughout the Mak-West pycnocline depths (Figure 4.2c), and $\overline{u'^2} > \overline{v'^2}$ for $75 \leq z \leq 225m$. If the ratio were derived for motions with periods of 20-40 days only, the depths where $\overline{u'^2} > \overline{v'^2}$ would then extend from 75 to 275 m (not shown). Meanwhile Mak-East mooring shows that $\overline{u'^2} > \overline{v'^2}$ is restricted to a thinner water column from 100 to 150 m (Figure 4.2c).

The structure of variances for both velocity components versus depths (Figure 4.2) likely reflects the dynamics of the intraseasonal motions at the Labani Channel. For example, a topographically trapped baroclinic Kelvin wave, a forcing that theoretically requires small transverse flow, may explain stronger signatures of $v(z)$ at depths beneath 225 m. An analysis of $v(z)$ at intraseasonal periods over pycnocline depths in Makassar and Lombok Straits suggests that remotely forced baroclinic waves propagate from Lombok to Makassar Strait in the lower pycnocline depths (Pujiana *et al.*, 2009). On the other hand, robust signatures of $u(z)$ at intraseasonal timescales over depths of 75-225 m may be driven by a topographic Rossby wave or an advected eddy whose dominant signal is expected to be in the normal component or x-direction at the Labani Channel.

A spectral analysis is applied to the datasets to examine which periods within intrasea-

sonal timescales dominate the flow field variances in the Makassar Strait pycnocline. The power spectrum is computed using the multi-taper method with adaptive weighing. Two distinct spectral peaks, 20-40 days and 45-90 days, generally characterize the intraseasonal flows in the Makassar Strait pycnocline. The 45-90 day variability is a dominant feature in $v(z)$ for throughout the pycnocline depths and extracts most of its energy from remotely forced baroclinic waves (Pujiana *et al.*, 2009).

As for the 20-40 day variability, $v(z)$ shows strong signature at 100-150 m of the Mak-West water column, where the flow is well defined by a spectral peak centered at 30-day (Figure 4.3a). A distinct monthly spectral peak is absent beneath 150 m of the Mak-West pycnocline although the 20-40 day variability energy does not change substantially with depth. Some discrepancies are found from the Mak-East pycnocline, however, in which the spectral peak centered at a shorter period of 25-day is more dominant and occurs deeper in the lower pycnocline from 225 to 300 m (Figure 4.3b). Furthermore, relative vorticity (ζ') computed from $v(z)$ of both moorings, shows significant variance associated with monthly variation. A broad spectral peak of 20-40 day centered at a period of 30-day characterizes ζ' at depths that extend from the base of the upper pycnocline to the lower pycnocline layer, and its energy is comparable or larger than that attributed to the 45-90 day variability (Figure 4.3c).

The signature of the 20-40 day variability over the Makassar Strait pycnocline is more pronounced in the u data. The vertical distribution of energy density of u at Mak-West across intraseasonal frequencies for several depths (Figure 4.4a) indicates that the spectrum shape transforms from red to blue spectrum as depth increases from 100 to 175 m; a blue spectrum with a distinct spectral peak centered at 25-day gains energy with depth. Deeper in the lower pycnocline, the spectral peak of the 20-40 day variability tends to be centered at a longer period of 30-day. The Mak-East mooring also shows a similar pattern of the 20-40 day variability in the lower pycnocline (Figure 4.4b). The 20-40 day variation observed from the Mak-East is also linked to that observed from the Mak-West as more than 80% of variance attributed to the 20-40 day variability from both mooring is statistically coherent. In addition to being coherent, the 20-40 day variability from the two moorings does not exhibit a significantly different from zero phase shift, a fact which may indicate that the 20-

40 day variability has its horizontal scale across the strait larger than the ∼19 km distance separating the moorings.

Distinct 20-40 day spectral peaks marking u and ζ' may express turbulent fluctuations on the mean flow that transports momentum across the strait. The instantaneous rate of along-strait momentum transfer in the across-strait direction is defined as $\rho_o(V+v)u$, where V is the mean flow, and u and v are velocity fluctuations in the across-strait and along-strait directions respectively. The average rate of flow of along-strait momentum in the across-strait direction is therefore $\rho_o\overline{(V+v')u'} = \rho_o V\overline{u'} + \rho_o\overline{v'u'} = \rho_o\overline{v'u'}$, as $\overline{u'} = 0$. The Reynolds stress, $\rho_o\overline{v'u'}$, is approximated with a cross-correlation between v' and u'. Structure of $\overline{v'u'}$, normalized by their variances and averaged over intraseasonal periods shows that $\overline{v'u'}$ (Figure 4.5a), which implies a westward (eastward) eddy flux of southward (northward) momentum. And the correlation coefficient in frequency domain (Figure 4.5b) indicates that the 20-40 day variability contributes substantially, particularly that in the lower pycnocline.

Another way to interpret $\overline{v'u'} < 0$ is in terms of the turbulence. The vertical structure of the mean flow (the time average of subinertial flow) observed at the Makassar Strait moorings indicates that the flow is directed southward and found with a maximum within the Mak-West pycnocline below 50 m (Figure 4.5c). More energetic Mak-West flow yields positive mean zonal shear and relative vorticity ($\partial\bar{v}/\partial x > 0$). Assume that a particle at a point between Mak-West and Mak-East sites instantaneously moves eastward ($u > 0$). The particle retains its original velocity during the migration, and when it arrives at Mak-East it finds itself in a region where a smaller velocity prevails. Thus the particle tends to speed up the neighboring fluid particles after it has reached the Mak-East site, and causes a more negative (southward) v. Conversely, the particles that travel westward ($u < 0$) tend to drag v down. In this way turbulence tends to diffuse and attenuate the across gradient of the mean flow, $\partial\bar{v}/\partial x > 0$.

Another unique feature from u varying at periods of 20-40 days, which is synonymously observed from both mooring, is a pattern of phase shift over depths: $u(z+dz)$ tends to flow slower than $u(z)$ with a constant lag. On a time and depth plot of u at a 20-40 day period band (Figure 4.6a), we draw lines, where each line connects the flow that has the

same phase, i.e. phase lines. And those lines are uniformly tilted downward at an almost constant angle, indicative of a downward phase propagating feature. This downward phase shift found from u differs from the phase shift of dominant variability in v. Pujiana et al. (2009) suggested that the most dominant period band of v observed in the Makassar Strait pycnocline exhibited upward phase propagation, which transferred energy downward to deeper depths at a speed of 25 m/day. A complex principal component (CPC) analysis of u varying at timescales of 20-40 days indicates that up to 90% of variances can be explained by the first three eigenvectors, where the first mode describes 50% variance and the next two modes denote 25% and 15% variance respectively. From the eigenvector profile, we learn how the amplitudes of u vary with depth. The first mode eigenvector reveals maxima at 175 m and at 250 m (Figure 4.6b) where two distinct spectral peaks of 25-day and 30-day are also observed: the energy associated with the spectral peak centered at 25-day is maximum at depth of 175 m, while the energy attributed to the 30-day variability is maximum at depth of 250 m. Therefore the vertical energy distribution for the 20-40 day across-channel flow is well resolved by the first eigenvector. Moreover, the relative phase inferred from the ratio between the imaginary and the real part of the first eigenvector signifies a phase increase with a rate of 1.7°/m towards greater depths (Figure 4.6b). The rate of phase shift implies that it would take around 20 days for the 25-day oscillation to propagate from 125 m to 300 m of water column. This relative phase structure is better understood from reconstructed data obtained through a multiplication between eigenvectors and their corresponding principal components (time series). A plot of reconstructed u based on eigenvector and principal component for the first mode captures the phase shift nature revealed by the eigenvector profile: periodic 20-40 day variability with phase lines titled downward at a uniform angle (Figure 4.6c). Thus the unique downward phase propagation feature contained in the filtered 20-40 day u data can be resolved and replicated by only the first mode.

4.3.1.2 Vertical Displacement

The vertical displacement of the isotherms within Makassar Strait is rich in intraseasonal features (Figure 4.4c). Figure 4.4c demonstrates that significant variance associated with 25-

day oscillation also characterizes temperature fluctuations at 150 m and greater depths. The vertical scale of the temperature variability within a period band of 20-40 days is likely larger than the lower pycnocline thickness, as the correlation between temperature variability at different depths shows that 70% temperature variance at 150 m is coherent with that at 300 m (not shown). Thermal field at intraseasonal timescales within Makassar Strait shares a similar power spectrum pattern with the across-strait flow data as the variability shows significant 20-40 day variation, and it is likely that the two parameters are physically linked.

4.3.1.3 Eddy-Like Features From Observation

In previous sections we have discussed general characteristics of the 20-40 day variability in the Makassar Strait pycnocline extracted from datasets obtained at the Labani Channel of Makassar Strait. At least three interesting features attributed to the 20-40 day variability were obtained from the datasets.

1. The u is more energetic than v at depths extending from 100 m to 250 m. Although inferring the two-dimensional motion from two points is inherently tricky, we suspect that a dominant across-strait flow at the Labani Channel may relate to an eddy advected by the ITF. Assume an eddy propagates along a mean flow, $U(t) + iV(t)$, that is spatially uniform but varying with time, the eddys path can be projected into a complex plane as $x(t) + iy(t) = r(t)e^{i\phi(t)}$. The currents observed by a mooring are then given as (Lilly and Rhines, 2002)

$$\xi(t) = V + iU - ie^{i\phi}\tilde{v}(r) \tag{4.1}$$

where $\tilde{v}(r)$ is the radial velocity of the eddy and r is the distance from the mooring to the eddy center. If the eddy dynamics is simplified as a Rankine vortex,$\tilde{v}(r)$ can be expressed in the following formula

$$\tilde{v}(r) = \begin{cases} VrR^{-1} & r < R \\ -Vr^{-1}R & r > R \end{cases} \tag{4.2}$$

where V is the maximum azimuthal velocity, and R marks the eddy core radius that has uniform potential vorticity. Since the ITF flows in the y-direction at the Labani

Channel, the observed eddy currents, by virtue of equations (4.1) and (4.2) , then are always perpendicular to the along-strait axis or in the across-strait component. Therefore, the observed flow associated with the eddy would be more dominant in u than in v.

2. There are 17 $+\zeta'$ and 18 -ζ' events over 3 year observation at which the v data in Mak-West and Mak-East moorings are in opposite directions: $+\zeta'$ occurs when -v at Mak-West and $+v$ at Mak-East are observed, while -ζ' appears when $+v$ at Mak-West and -v at Mak-East are observed (Figure 4.7, upper panel). Given the Mak-West and Mak-East moorings are separated by a distance of ∼19 km across a ∼60 km width channel (Figure 4.1b), the current vector in opposite senses that mark the positive and negative relative vorticity phases may imply that the moorings are located on different side of the passing eddies. To better visualize the relationship between the out of phase signature of v observed at the two moorings and an eddy, it is shown in Figure 4.7 (lower panel) an ideal vortex, whose azimuthal velocity structure is given in equation (4.2), has a core with radius presumably of 20 km and its center assumed on the median line of the Labani Channel. It thus can be inferred from Figure 4.7 (lower panel) that the out of phase nature shown by the v timeseries at 20-40 days (Figure 4.7, upper panel) may relate to eddies whose center likely occurs in between the two moorings.

3. The strongest $+\zeta'$ episodes, at which -v at both moorings is out of phase, are preceded with $+u$, while -ζ' events coincide with initially observed -u (Figure 4.8a,b). We argue that the relationship between u and ζ' measured in the Labani Channel consistent with what a mooring would observe from a passing eddy as suggested by Lilly and Rhines(2002): Normal component of eddy currents is initially positive (negative) for an anticlockwise (clockwise) eddy. To further examine whether the nature of u is linked to eddy footprint at the moorings, we examine a Rankine vortex on Eulerian current records, which the associated currents can be written as

$$\zeta'(t) = \begin{cases} -iR^{-1}V\chi \\ -i\chi^{*-1}VR \end{cases} \tag{4.3}$$

where χ is the distance from the mooring location to the eddy center. We assume that V (the peak azimuthal speed at the eddy edge) is 15 cm/s, the southward advection speed of the vortex is 20 cm/s, the eddy core radius is 20 km, and the eddy center is set at about 31 km to the north of the measurement points for the initial condition. Also the isobaths are presumably perpendicular to the mooring transect, and the moorings are placed across a 50 km-wide channel in a way that replicates mooring arrangements in the Labani Channel. We run the eddy model with the same eddy parameters for both anticlockwise and clockwise eddies but change the sign of V from positive to negative for the clockwise eddy case. The simulated eddy currents, either for anticlockwise or clockwise eddy, yield a decent agreement with observations: the passing of a clockwise eddy (-ζ') is initially marked with westward currents (-u) (Figure 4.8c), while the occurrence of an anti-clockwise eddy (+ζ') is preceded by the onset of eastward currents (+u) (Figure 4.8d). A good accordance between real and theoretical events further indicates that the rotational events observed from moorings in the Labani Channel are likely related to eddy motions.

4. The thermal field and relative vorticity are linked at the Labani Channel. The isopycnals in the lower pycnocline layer dip down when the flow field exhibits negative relative vorticity (Figure 4.9a). Meanwhile the isopycnals shoal as the relative vorticity observed in the Labani Channel lower pycnocline turns positive (Figure 4.9b). We suspect that the vertical displacements of isopycnals varying at periods of 20-40 day in the lower pycnocline of the Labani Channel are direct responses to water column squeezing or stretching attributed to cyclonic or anti-cyclonic eddies, attributable to potential vorticity conservation. Potential vorticity conservation suggests that $(\zeta_{to} + f)/h_{to} = (\zeta_t + f)/h_t$, where h is the isopycnal depth, and subscripts to and t denote initial condition (at rest) and time when an eddy passes the mooring sites. Assuming $\zeta_{to} = 0$, h_t at the mooring sites located in the southern hemisphere can be written as $h_t = h_{to}(1 - (\zeta_t/f))$, it can be inferred that the isopycnals are displaced upward (downward) when a motion with positive (negative) relative vorticity passes through the mooring sites or the pycnocline shoals (deepens) when an anticyclonic (cyclonic) eddy is advected through the observational sites.

After reviewing the observations discussed in previous sections, we hypothesize that the features attributed to the 20-40 day variability from the moorings at the Labani Channel are linked to eddy dynamics, and the next step is to describe where the eddies originate from. Several numerical experiments (Qiu *et al.*, 1999; Masumoto *et al.*, 2001) indicated that eddy activities at intraseasonal timescales are intense within the Sulawesi Sea, a basin located to the north of Makassar Strait (Figure 4.1a). Masumoto *et al.*(2001) estimated that eddies with a period of 40-day were internally generated in Sulawesi Sea and affected the ITF transport in Makassar Strait. However the Sulawesi eddies that the study of Masumoto *et al.*(2001) numerically estimated were not only trapped in the lower pycnocline but rather occupied a thick water column extending from the surface to 1000 m isobath. To investigate the generating mechanism of eddies at the Labani Channel, we analyze the output of an eddy resolving numerical models in Makassar Strait, and the discussion is given in the following section.

4.4 The 20-40 day Variability in an Eddy-Resolving Model

As described earlier, flow and thermal field from two moorings at the Labani Channel of Makassar Strait reveal clear 20-40 day variability features, which we propose are related to cyclonic and anti-cyclonic eddies. To further examine the spatial variation and origin of the 20-40 day variability, we investigate the model output of a global HYCOM experiment (Metzger *et al.*, 2010). We focus our analysis on the model flow at intraseasonal timescales in the Makassar Strait and Sulawesi Sea pycnocline. Comparison between the model output and observation at the Mak-West and Mak-East mooring sites indicates that the numerical experiment underestimates the Makassar Strait throughflow due to inaccurate model topography, where the Dewakang Sill (Figure 4.1a), located near the southern end of the strait, was introduced 195 m too shallow in the model (Metzger *et al.*, 2010). In addition to weaker simulated mean transport, the study of Metzger *et al.*(2010) also showed that shallower sill depth assigned in the model caused the maximum simulated southward flow in Makassar Strait to be $\sim$50 m deeper than observed.

The model u at intraseasonal timescales qualitatively agrees with observation at Mak-

West and Mak-East moorings: the 20-40 day variability has clearly larger energy than other intraseasonal periods, and the variability at Mak-West is more energetic than that at Mak-East (Figure 4.10a,b). It is also shown in Figure 4.10a,b that the distinct monthly spectral peak is well simulated at depths greater than 200 m, which is 50-75 m deeper than the depth where observation starts to record the monthly peak. The discrepancy is again due to inaccurate sill depth. Monthly variation also occurs in the model ζ' simulated at the mooring locations. Like the observation, the model ζ' and u at depths beneath 200 m are linked: positive relative vorticity correlates with eastward flow, while negative vorticity corresponds with westward flow (not shown). A coherence analysis between the model ζ' and u for several depths within the pycnocline layer of Mak-West site displays that both parameters varying at intraseasonal timescales are strongly coherent for a period band of 20-40 days, and the strongest correlation is found at depths greater than 200 m (not shown). Moreover the simulation not only qualitatively shows a good agreement with observation but also quantitatively explain significant variances of the recorded datasets. It is inferred from some cross-correlation analyses between the simulated and observed data at some select levels within the lower pycnocline depths that the model u explains 64-72% variances of the observed u varying at 20-40 days. Thus the numerical experiment is able to capture some general features of the 20-40 day variability, which are similarly revealed from observation at the mooring sites in the Labani Channel.

4.4.1 Eddy Signature and its Genesis in Makassar Strait

The next questions we explore within the model output are what causes the 20-40 day variability? Where does the forcing originate from? And why is the strong 20-40 day variability trapped within the lower pycnocline. To determine the ocean dynamics responsible for the pronounced 20-40 day fluctuations, the simulated flow field attributed to the period band of interest in the Makassar Strait is analyzed. We first want to gain insights on the space and time evolution of a motion that may drive the ζ' fluctuations in Makassar Strait. For example, an event of positive ζ' is inferred from two moorings at 250 m in the Labani Channel on 17 December 2005 (selected to be representative of positive ζ' events), and it is assumed that an anticlockwise eddy-like motion causes the ζ' field. The model agrees well

with observation to simulate positive ζ' at 250 m of the Labani Channel pycnocline on 17 December 2005, and the model flow field shows that the positive ζ' value does correspond with a counter clockwise vortex motion with a diameter of 40 km squeezed in the narrow Labani passage (Figure 4.11). Assume quasi-geostrophic dynamics govern the vortex observed and simulated in the Labani Channel, the vortex diameter will be approximately as large as the local internal radius deformation, which is function of N, coriolis acceleration (f), and water depth (H). The deformation radius for the first oceanic mode in the Labani Channel falls within O($\sim$275 km), substantially larger than the channel width itself. Therefore the eddy size in Makassar Strait is more likely topographically constrained. The model velocity and relative vorticity fields at the Labani Channel for over a period of $\sim$3 years (2004-2006) display 23 events of anti-cyclonic vortex motion and 17 episodes of cyclonic eddy-like features.

Furthermore, following the spatial and temporal eddy core variability, it can be inferred that the eddy-like motion is not locally generated at the Labani Channel but seems rather to propagate from the northern Makassar Strait into the Labani Channel. It is shown in Figure 4.11 that an anti-cyclonic eddy with a diameter of $\sim$100 km has its core located at latitude of 2°S and is simulated on 7 December 2005, and the eddy diameter is reduced as it propagates southward with a phase speed of 0.25 m/s before occupying the Labani Channel on 17 December 2005. After reaching the Labani Channel, the eddy dissipates and its signature is not simulated further south (not shown).

The model eddy occurs only within the lower pycnocline and is identifiable as a feature that has homogeneous ζ' over depths. A depth versus distance plot of ζ' along a transect given in Figure 4.1 shows that a homogeneous positive ζ' over depths extending from 200 to 350 m marks the event of an anti-cyclonic eddy on 17 December 2005 in the Labani Channel (Figure 4.12). Thus the eddy varying at periods of 20-40 days in Makassar Strait is trapped within the lower pycnocline. Several snapshots of simulated horizontal flow fields and structure of ζ' in Makassar Strait (Figure 4.11; Figure 4.12) provide spatial and temporal dimension of the motions that likely force the 20-40 day variability observed at the Labani Channel. It is shown that circular motions develop at 2°S or farther north and propagate southward in Makassar Strait. To better map out the source region of the

vortices, we analyze simulated eddy kinetic energy (EKE) budget over an expanded region including the Sulawesi Sea (Figure 4.1), a basin with robust intraseasonal activities (Qiu *et al.*, 1999; Masumoto *et al.*, 2001, Pujiana *et al.*, 2009). Although detecting energy radiation through EKE can be ambiguous, the intraseasonal variability can be characterized by a suitably specified EKE.

The EKE budget is deduced from the rapidly-varying segment of u and v, with an assumption that each variable has a slowly-varying part and a rapidly-varying part, labeled as (u, v) and (u', v') respectively. The rapidly-varying part oscillates at periods of 20-40 days, and the EKE density is therefore defined as $0.5(\rho_o(u^2 + v^2)$, where ρ_o is the background density, vertically averaged over depths from the potential density structure given in Figure 4.1. Comparison of the averaged EKE (Figure 4.13) at several depths clearly exemplifies the basins with the most pronounced EKE in the region: Sulawesi Sea (A), northern Makassar Strait (B), and Southern Makassar Strait (C), where the Labani Channel demarcates the separation between the northern and southern of Makassar Strait. Nevertheless we consider basins A and B as the only viable energy source areas for eddy activities at the Labani Channel as we expect the eddy to be advected, along with the ITF, southward into the channel. In area A, the eddy activity is significantly close to the surface and decays away from it, and the eddy likely does not extract its energy from the wind because the atmospheric perturbations over the area lacks a 20-40 days variability (not shown). The eddy might instead relate to instabilities of the Mindanao currents occurring on the eastern Mindanao coasts or be a Sulawesi basin scale response to the periodic Mindanao currents (Qiu *et al.*, 1999; Masumoto *et al.*, 2001). In contrast, the EKE vertical distribution in B shows a structure that is quite typical of the mean flow profile in the Labani Channel (Figure 4.5c), in which the maximum value is attained at the mid pycnocline depth, where the vertical shear of the mean flow is strongest. The EKE in B is strongest at 200 m and fades away with distance from that depth (Figure 4.14a).

Considering how the EKE is distributed in Makassar Strait and Sulawesi Sea, we propose that zone B, rather than area A in Sulawesi Sea, is the EKE source for generating eddies that are trapped in the lower pycnocline and propagate into the Labani Channel. If area B were the eddies source, southward dispersion of EKE should be well simulated by the

model. To detect if there is southward energy transfer from zone B, we evaluate the time evolution of EKE at a depth of 225 m, a depth that has the largest averaged EKE value (Figure 4.14a). The EKE temporal variability along a band of latitudes within zone B demonstrates a southward propagating with a phase speed of 0.2 m/s which closely matches the propagation speed of an eddy (Figure 4.14b). To a first approximation, it therefore can be proposed that the eddy observed in the Labani Channel is not generated in the Sulawesi Sea, but rather originating from just to the north of the channel in the Makassar Strait at latitudes varying from 0.5°S to 2°S.

The next questions are why the eddy-like motions are formed at latitudes which fall within range of 0.5°-2°S in the Makassar Strait lower pycnocline, and how are they initiated? As mentioned in the earlier discussion on eddies characteristics from observation, we argue that the eddy occurring at depths beneath the mid pycnocline layer of Makassar Strait extracts its energy from the sheared mean flow. To support the argument that the eddy generation may relate to the background flow, spatial variation of the time averaged speeds in Makassar Strait at several depths within the pycnocline, is studied. The background flow magnitudes at several different depths (Figure 4.15) synonymously display significant variations across Makassar Strait: the southward mean flow is simulated speediest at and south of the Labani Channel and at depths of 150-200 m. Figure 4.15 also demonstrates a clear across-strait gradient of the mean flow particularly at latitudes of 0.5°-2°S as weaker northward mean flow on the eastern end of the Makassar Strait features against the energetic western-intensified southward mean flow. And the across-strait gradient of the mean flow within that particular latitude band reveals its maximum at 200 m, a depth where the EKE is noticeably largest as shown in Figure 4.13. Given the sheared mean flow and the EKE equally exhibit strongest signature at depth of 200 m, we propose that the background flow supplies the eddy energy through a flow instability mechanism. Assuming the mean flow structure across the strait can be described as an inviscid parallel flow, the two necessary criteria for instability of the flow are: the basic background flow profile has at least a point of inflection (Rayleighs inflection point criterion), and the magnitude of vorticity of the background flow must have a maximum within the region of flow, not at the boundary (Fjortofts theorm). The imaginary part of the Rayleighs equation,

$c_i \int (\partial^2 V/\partial x^2 \left|\phi\right|^2 / \left|V-c\right|^2) dx = 0$, suggests that for the unstable case to hold ($c_i \neq 0$), $\partial^2 V/\partial x^2$) (the mean flow curvature) needs to change sign across the strait (x-direction). Focusing on the across-strait profile of the mean flow at 200 m within latitudes of 0.5°-2°S in Makassar Strait (Figure 4.16), the profile shows one inflection point at each latitude that marks the mean flow structure across the strait, which complies with the necessary criterion for instability required by the Rayleighs equation. Another criterion for instability derived from Fjortofts theorem, $\int (\partial^2 V/\partial x^2 (V - V_I) \left|\phi\right|^2 / \left|V-c\right|^2) dx < 0$, indicates that the mean flow must not only have at least one inflection point across the strait but also have maximum vorticity away from the boundary. And Figure 4.16 also demonstrates that the positive relative vorticity magnitude of the mean flow has a maximum within the region of flow, which provides another indication that the background flow instability simulated within latitudes of 0.5°-2°S in Makassar Strait potentially generate the eddies.

4.5 Summary

We have described the characteristics of the 20-40 day variability observed at the two INSTANT moorings deployed in the Labani Channel of Makassar Strait 2004-2006. The variability is well identified from the u datasets recorded below the central pycnocline depth of 125 m, as a distinct spectral peak, which resembles a blue spectrum shape over the intraseasonal timescales. Comparison between u and v demonstrates that the across-strait component of the 20-40 day variability intraseasonal feature is more energetic within the pycnocline. Additionally, the 20-40 day fluctuations of u reveal downward phase propagation with a speed of 25 m/day and vertical distribution of energy, in which the flow at the mid pycnocline depth oscillates at shorter period than it does at greater depths.

Apart from u, the 20-40 day variability is also evident from the temperature datasets as η' continuously show monthly periodicity. The magnitude of η' is larger than the lower pycnocline thickness, and η' move up and down in concert although a small phase difference is observed over the lower pycnocline layer. Although the 20-40 day variability is not prominent in v, it does typify the $\partial v'/\partial x$ variation over the lower pycnocline depths. The $\partial v'/\partial x$ time series exhibit strong correlations with u which leads us to propose that the

20-40 day variability is linked to eddy-like features. As discussed previously, the velocity structure of a theoretical vortex approximates well the observations and the relationship between the measured parameters. Moreover the link between ζ' and η', the isopycnals dip down (elevated) as the relative vorticity magnitudes turn negative (positive) may also signify the presence and role of an eddy to conserve the potential vorticity within the water column in the Labani Channel.

If an eddy forces the 20-40 day variability within the lower pycnocline layer, why does the variability at the top of the lower pycnocline has strongest energy at a period of 25-day while the variability at the base of the lower pycnocline attains maximum energy at a period of 30-day? In other word, the spectral peak attributed to the 20-40 day variability is centered at periods varying from 25-day at the mid pycnocline depth to 30-day at the base of the lower pycnocline depth. Here, we suggest a Doppler effect may better explain the pattern in question than the motions natural frequencies. Referring to the general dispersion relation for gravity waves, natural frequencies of motions that a strait inherently can sustain is inversely proportional to the straits width, $\omega = ((\pi g(n+1)L^{-1})tanh((n+1)\pi HL^{-1}))^{1/2}$ where H, L, g, and n denote water depth, straits width, gravity and mode number, respectively. The relationship between the natural frequency and the straits width thereby indicate that as straits width decreases with depth, natural frequencies (periods) would get larger (smaller) with depth as natural frequency is inversely proportional to straits width. However, this increasing natural frequency with narrower width relationship does not fit well in the Labani Channel because the dominating frequency gets smaller as the channels width decreases with depth. Another physical process that may explain increasing periods of fluctuations with depth is Doppler phase shift. If the 20-40 day event is advected southward with the background flow, the feature is advected into the mooring sites with varying speeds over depths, following the vertical structure of the mean flow (Figure 4.5c), which is maximum at the mid pycnocline depth and decays with distance from this depth. As consequence, the observed dominant period of oscillation at the mid pycnocline depth is shorter than that at deeper levels in which the 20-40 day variability propagates at a slower pace.

An eddy-resolving model further supports that the 20-40 day variability observed in the

Labani Channel of Makassar Strait is driven by eddies. The model horizontal flow and ζ' fields show that a positive (negative) ζ' event observed in the channel does correspond with an anti-cyclonic (cyclonic) eddy that originates in Makassar Strait at latitudes between 0.5°-2°S, just to the north of the mooring site, a region with the largest EKE. The EKE vertical distribution within this band of latitudes demonstrates strongest EKE magnitude at depths greater than 200 m. The area and depths with the largest EKE also coincides with the latitudes and levels at which the across-strait gradient of the model background flow may provide the necessary energy for the eddy formation in Makassar Strait.

To summarize, we suggest that a cyclonic or an anti-cyclonic eddy generated at latitudes between 0.5°-2°S in Makassar Strait explains strong signatures of the 20-40 day variability in the across-strait flow and the temperature fluctuations observed within the lower pycnocline of the Labani Channel. The generation mechanism of the eddy is likely through instability in which the required energy is supplied by the across-strait shear of along-strait flow, marking the ITF. The eddy is trapped in the lower pycnocline because those are depths the EKE and the sheared background flow is found most energetic. The eddy propagates southward along with the ITF and dissipates its energy in the Labani Channel.

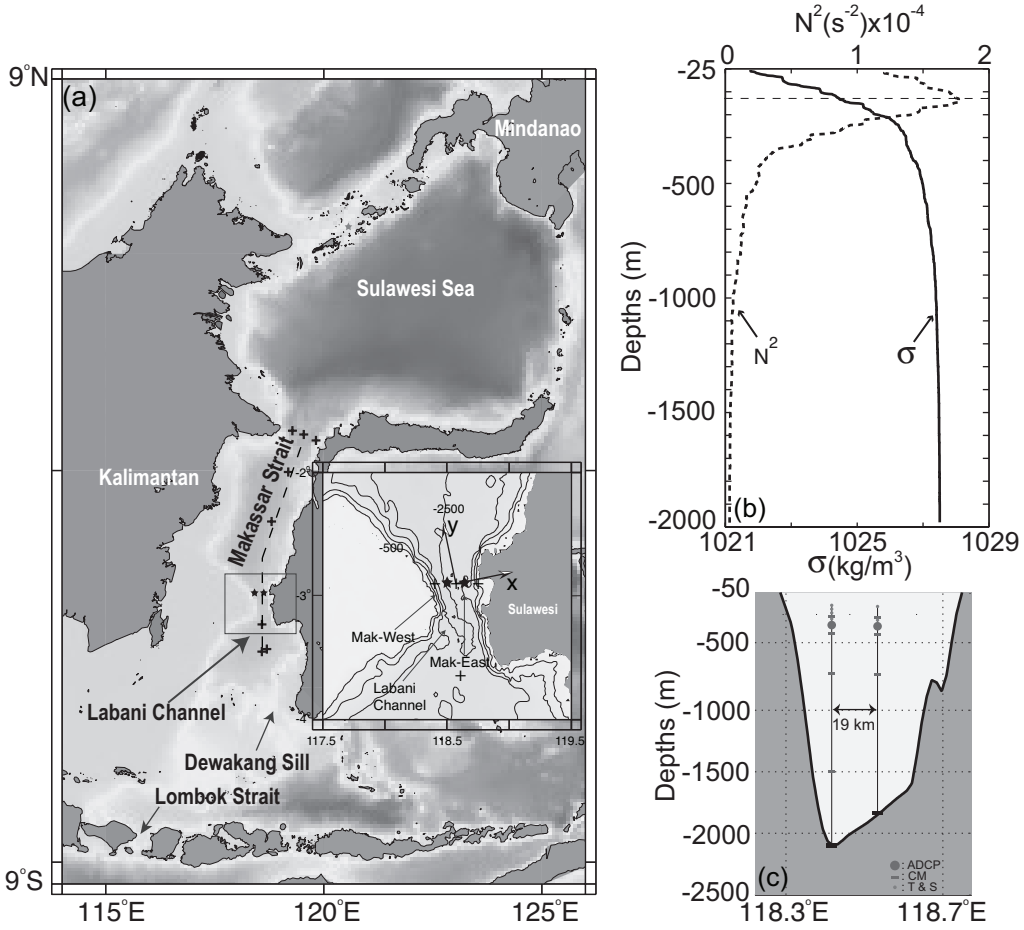

Figure 4.1: (a) Locations of point measurements in Makassar Strait. The moorings are shown as stars and are deployed in the Labani Channel, a constriction in Makassar Strait. Crosses denote CTD casts during 1996-1998. Inset displays an expanded view of the Labani Channel, the major and minor axes of the channel, and the mooring sites [Mak-West and Mak-East]. The along-strait axis [y] and across-strait axis [x] is tilted 10° counterclockwise relative to the geographic north and east respectively. (b) The average vertical structure of the interior Makassar Strait inferred from several CTD casts during 1993-1998 given in Figure 4.1a. The average of potential density [σ, solid line] and buoyancy frequency [N^2, dashed line]. (c) A schematic of the mooring configuration deployed across the Labani Channel

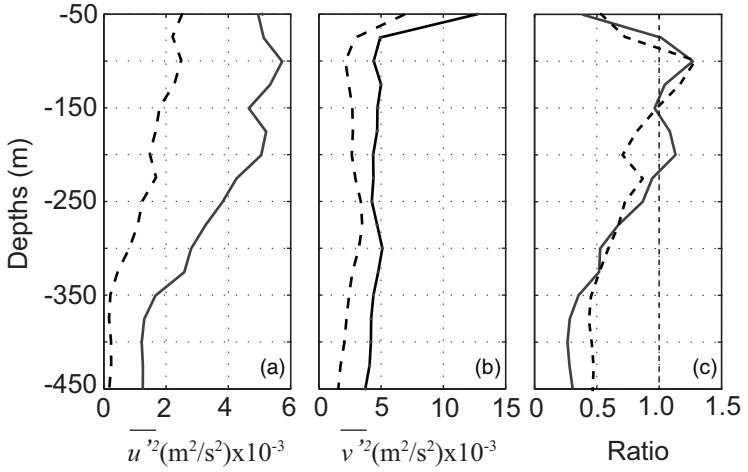

Figure 4.2: Profiles of variances attributed to u (a) and v (b) at intraseasonal timescales [20-90 days] within the Mak-West [solid line] and Mak-East [dashed line] thermocline. The corresponding ratio between u and v for each mooring [solid line: Mak-West; dashed line: Mak-East] is given in (c)

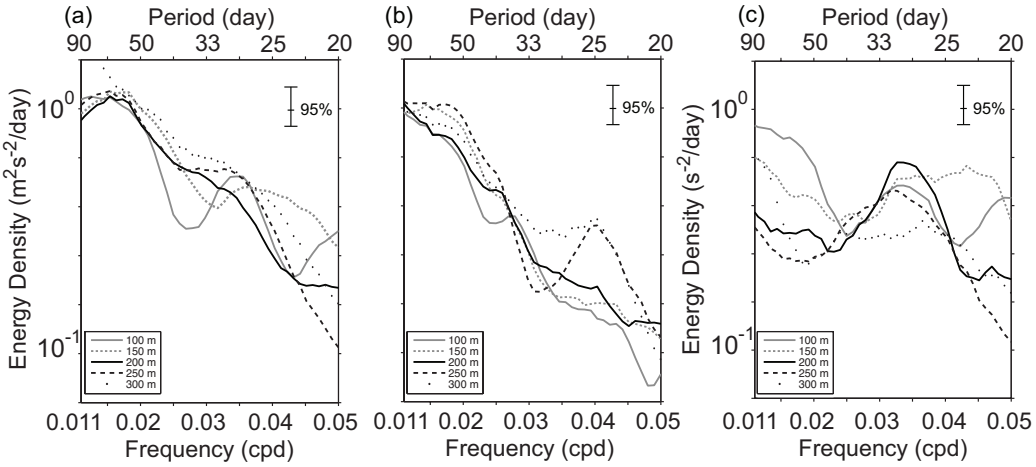

Figure 4.3: Multitaper spectral estimates of v observed at different levels in the Mak-West (a) and Mak-East (b) lower thermocline during 2004-2006. (c) displays spectral estimates of across-strait gradient of v, computed by subtracting v observed at Mak-East from that observed at Mak-West. Error bars on the spectral estimates mark the 95% confidence limits

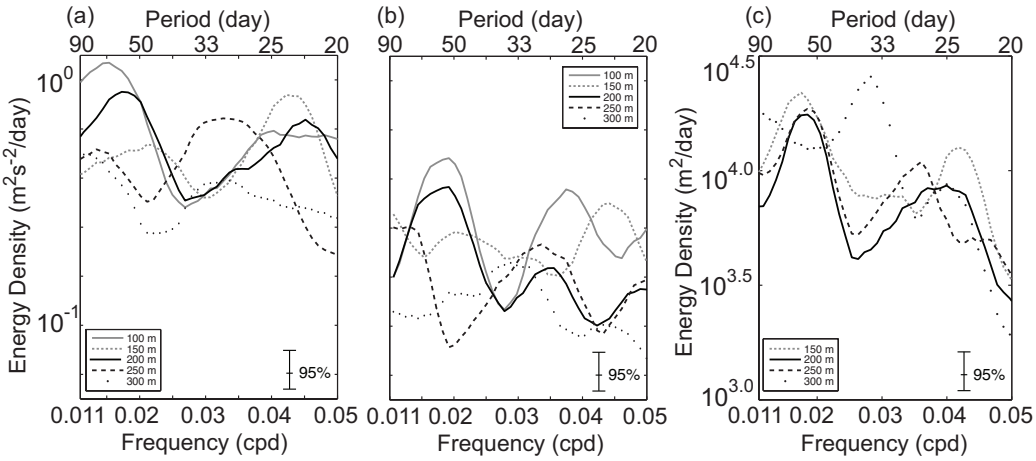

Figure 4.4: Multitaper spectral estimate of u and η at several levels from Mak-West and Mak-East moorings within the lower thermocline of Makassar Strait during 2004-2006. (a) and (b) illustrate spectral estimate of u for Mak-West and Mak-East respectively. (c) displays η spectral estimates of for Mak-West. Error bars on the spectral estimates mark the 95% confidence limits

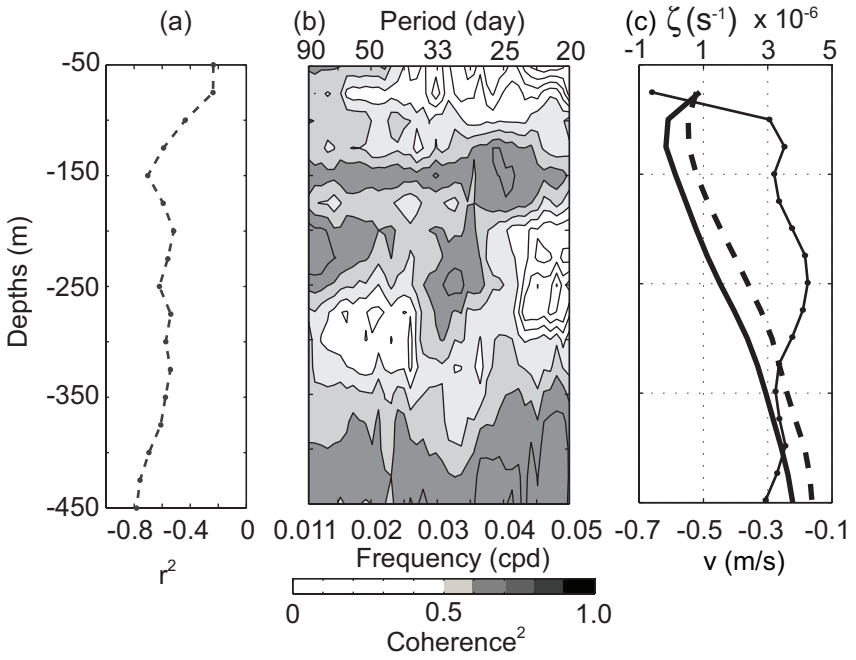

Figure 4.5: (a,b) The degree of correlation between v and u at intraseasonal timescales over the Mak-West thermocline. (a) Zero-lag coefficients are obtained from time-lagged cross correlation analysis. (b) Amplitudes of coherence squared are shaded for values larger than 95% significance level. (c) Vertical structure of the background flow observed at Mak-West [solid line] and Mak-East [dashed line] and its corresponding relative vorticity [dotted line]. The background flow at a certain depth is the time average of subinertial flow, which is obtained through applying a butterworth low-pass filter to the velocity field dataset with a cut-off period of 9.5-day

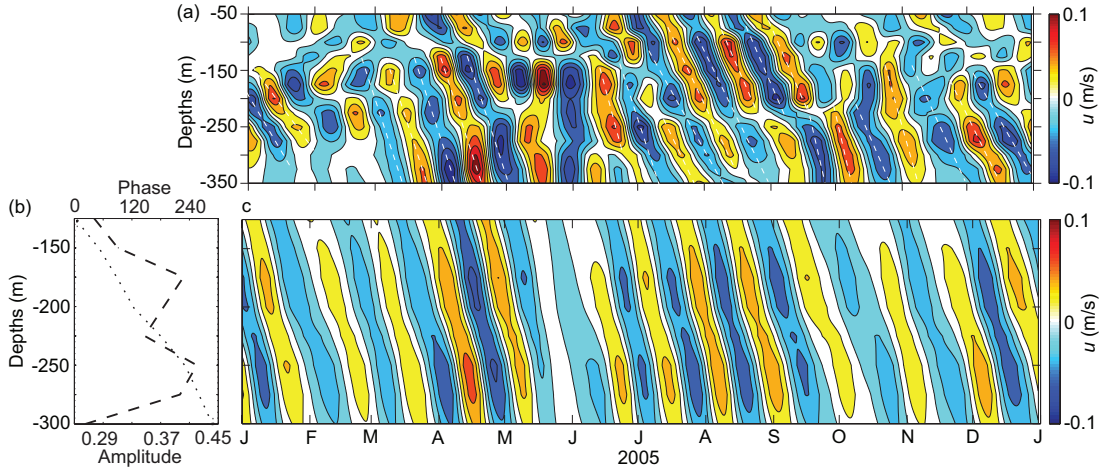

Figure 4.6: Across-strait flow varying at periods of 20-40 days observed at Mak-West mooring in 2005 (a) and its orthogonal function approximation (b, c). Dashed lines in (a) show phase lines. Dashed and dotted lines in (b) show the 1^{st} eigenvector and its relative phase that represents 50% variance of (a). (c): Reconstructed across-strait flow for the 1^{st} mode

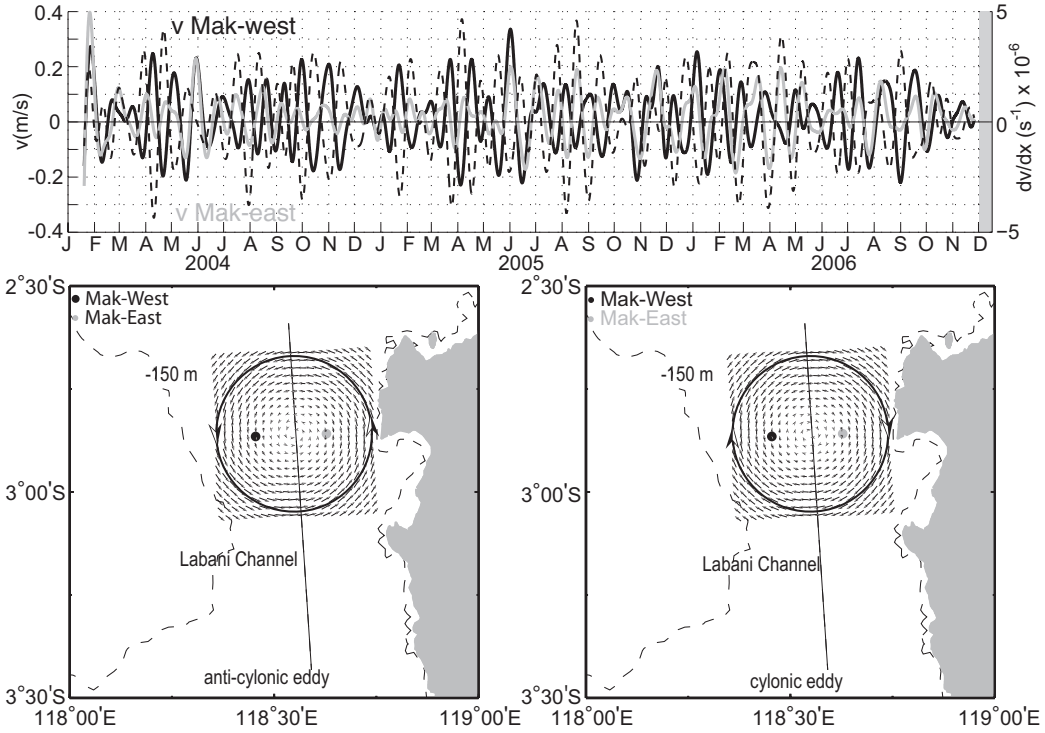

Figure 4.7: (Upper panel): Along-strait flow varying at 20-40 days and observed at depth of 150 m of the Mak-west [red] and Mak-East [blue] thermocline and the corresponding dv/dx [black dashed]. (Lower panel): Illustration of ideal anticyclonic and cyclonic eddy currents in the Labani Channel. Dashed red line denotes the median line of the Labani Channel

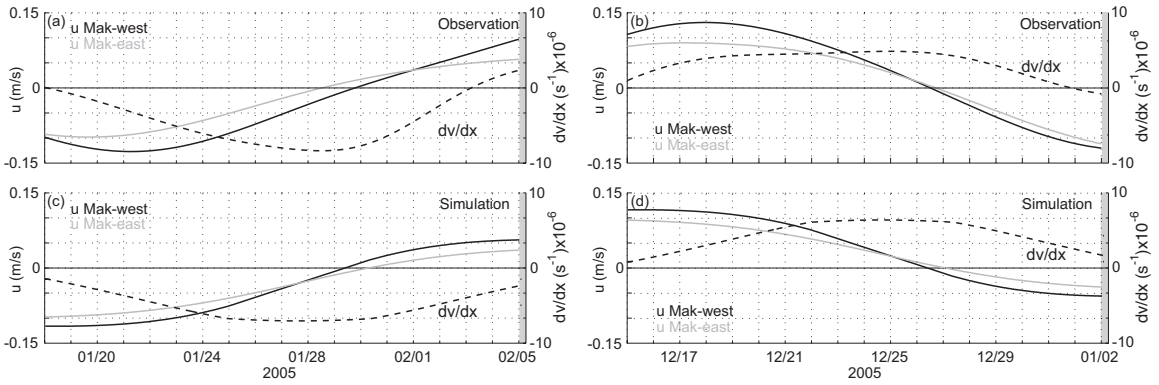

Figure 4.8: Observation and simulation of across-strait flow $[u]$ and relative vorticity $[dv/dx]$ varying at 20-40 days at Mak-West and Mak-East mooring sites, which corresponds with anticyclonic and cyclonic eddy currents. (a,c) displays temporal variability of real and theoretical anticyclonic eddy respectively, while (b,d) demonstrates time series of observed and modeled cyclonic eddy respectively

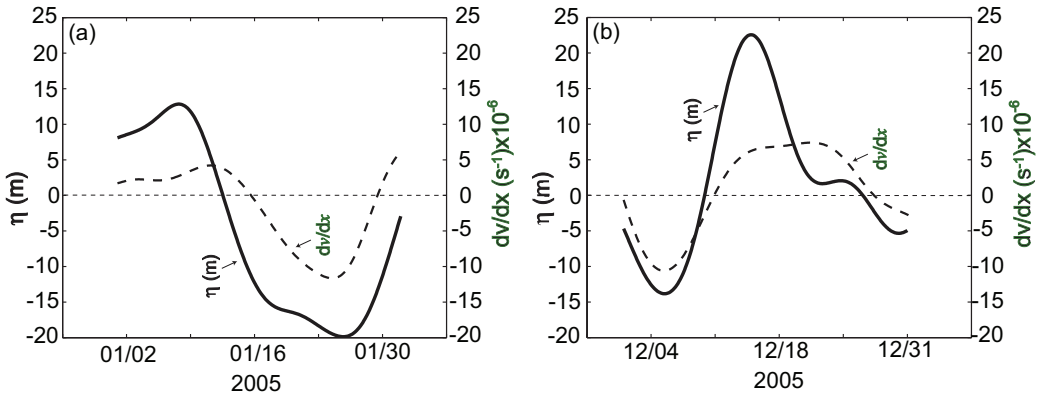

Figure 4.9: Temporal variability of relative vorticity (dv/dx) and isotherm vertical displacement (η) at depth of 150 m observed from the moorings in the Labani Channel. (a) demonstrates how a motion with -dv/dx corresponds with a minimum η on 24 January 2005, while (b) illustrates the relationship between a $+dv/dx$ motion and a maximum η on 17 December 2005

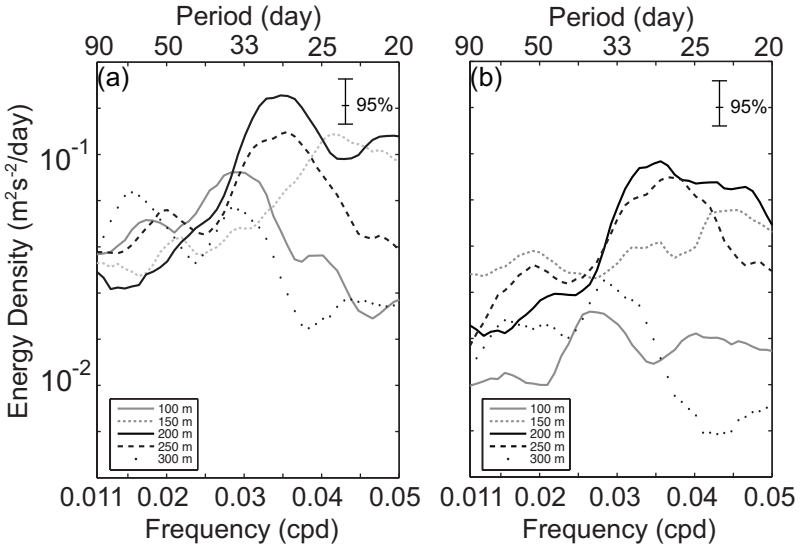

Figure 4.10: Multitaper spectral estimates of simulated u at intraseasonal timescales for several depths at the Mak-West (a) and Mak-East (b) locations in Makassar Strait. Error bars on the spectral estimates mark the 95% confidence level

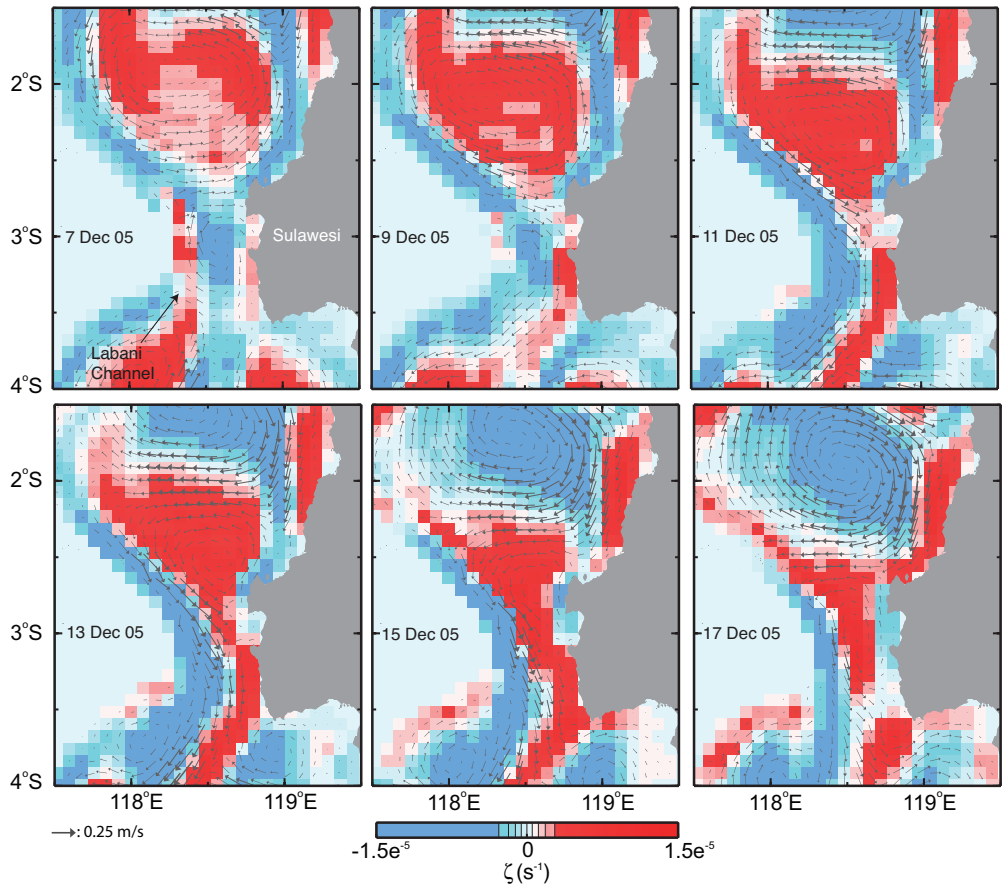

Figure 4.11: Snapshots of the model horizontal flow field [arrow] and its corresponding vorticity field [in color] at 250 m in the vicinity of the Labani Channel for several days in December 2005. The current vectors are for periods of 20-40 days. The stars denote the mooring sites

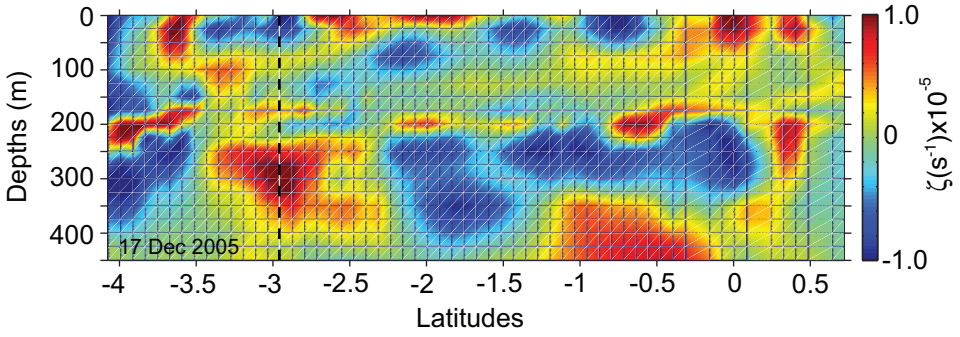

Figure 4.12: The model ζ' plot for several depths along a transect in Makassar Strait shown in Figure 4.1, simulated on 17 December 2005. The ζ' time series are computed using horizontal velocities for intraseasonal timescales. The dashed line indicates the latitude of the mooring location in the Labani Channel

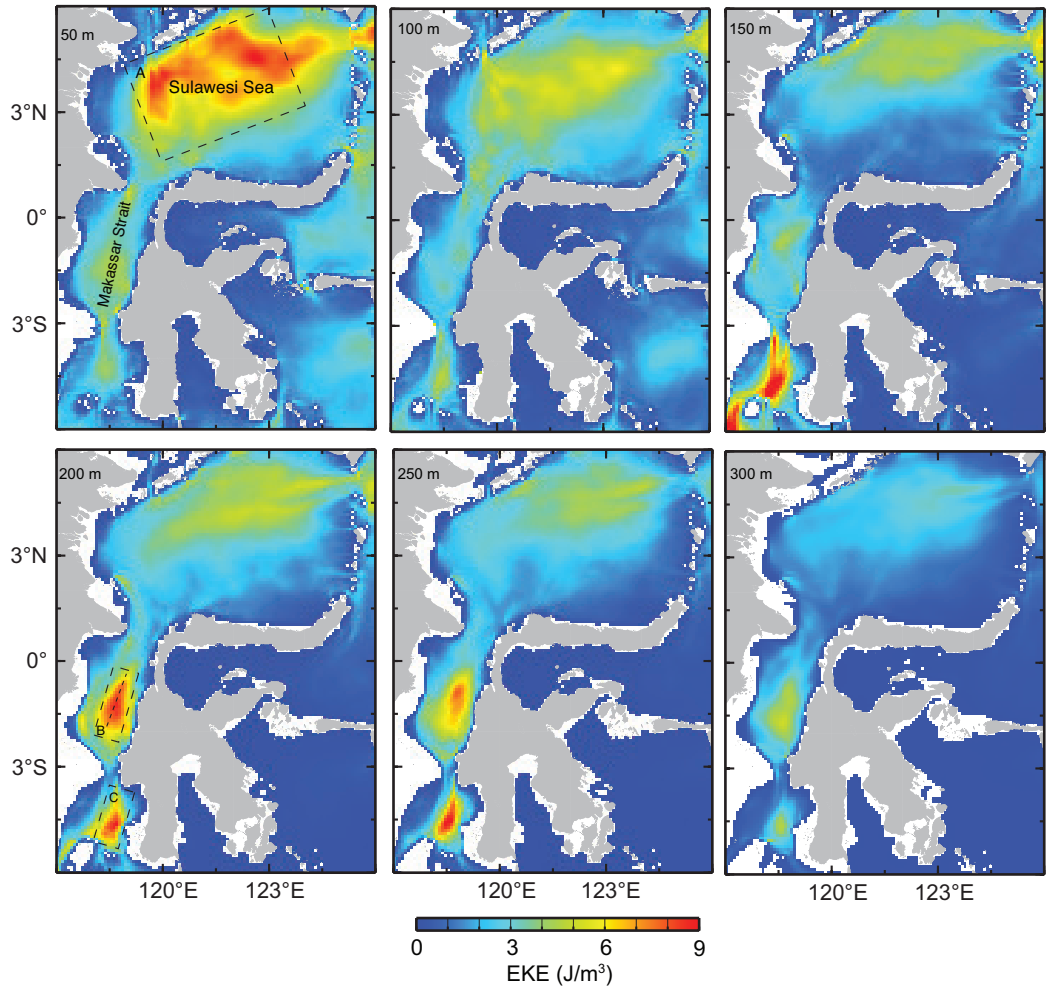

Figure 4.13: Plots of the averaged EKE simulated at several depths within the Makassar Strait and Sulawesi Sea thermocline. The mean EKE is computed for a 3-year period from 2004 to 2006. Dashed box represents a region with the most energetic EKE

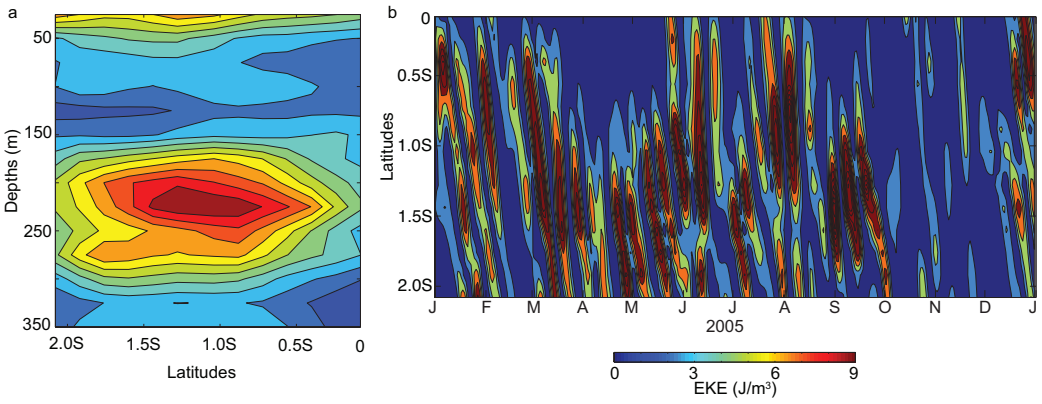

Figure 4.14: (a) A vertical distribution plot of the mean EKE simulated at several latitudes within zone B given in Figure 4.13. (b) The temporal variability of the model EKE at depth of 250 m for several latitudes along a transect within zone B

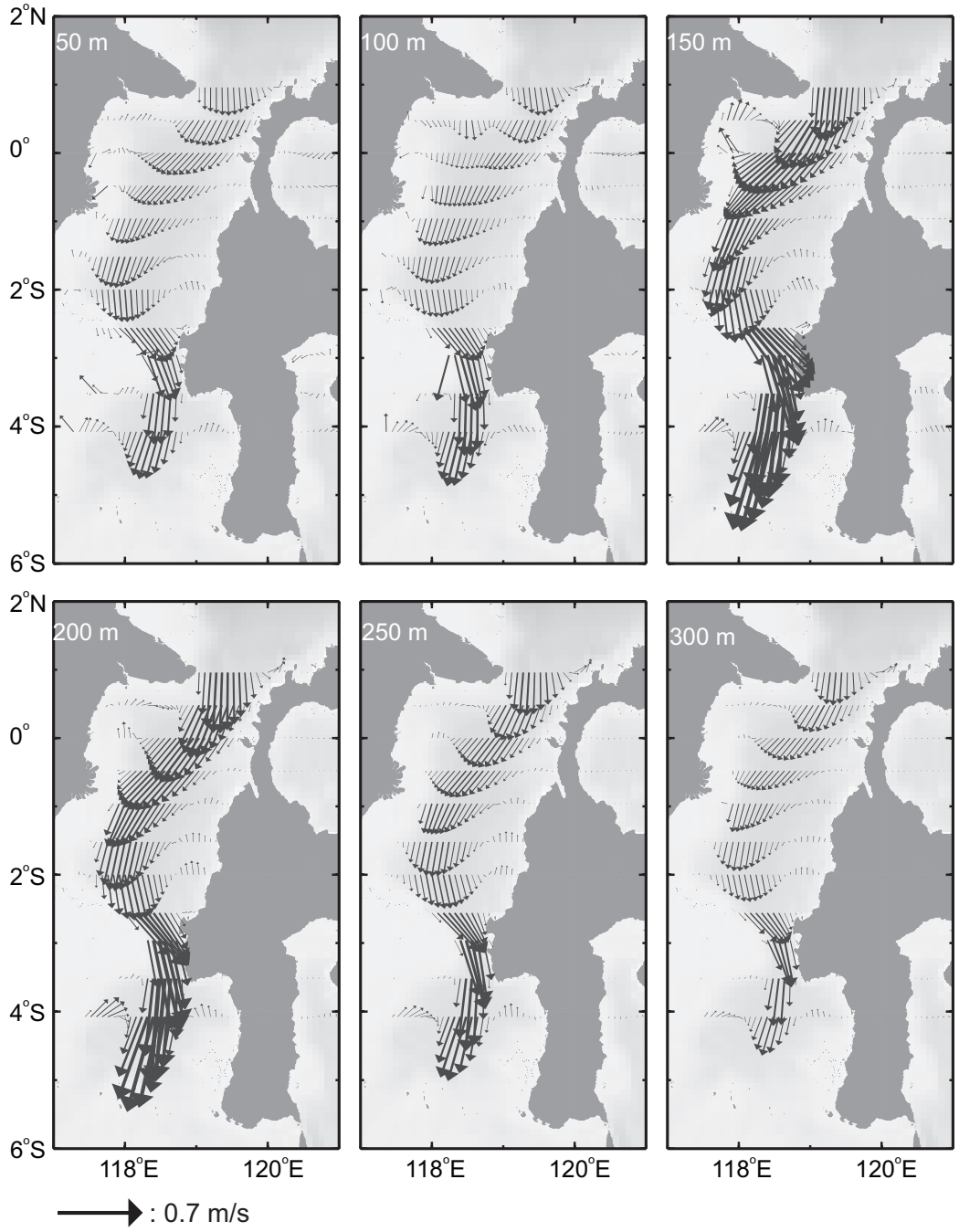

Figure 4.15: The model background flow at several depths simulated in the Makassar Strait thermocline. The mean flow is obtained through applying a butterworth low-pass filter to the model raw data with a cutoff period of 90-day

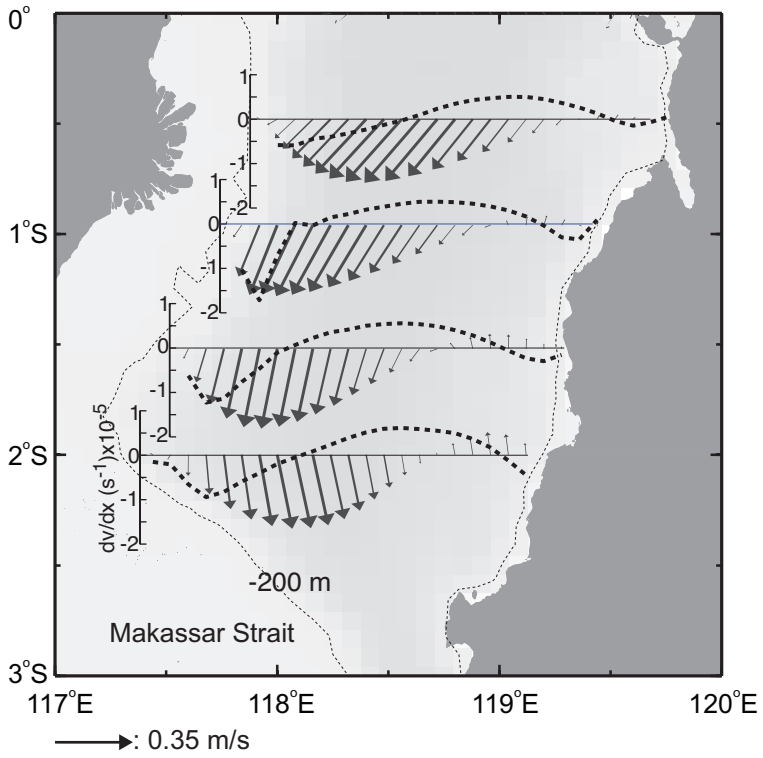

Figure 4.16: The model background flow and relative vorticity at depth of 200 m simulated within latitudes of 0.5°-2°S. The mean flow is obtained through applying a butterworth low-pass filter to the model raw data with a cutoff period of 90-day

Chapter 5

Summary and Future Work

Within this thesis we have identified and explained intraseasonal variability (ISV) in Makassar Strait observed during the INSTANT program of 2004-2006 (Sprintall *et al.*, 2004; Gordon *et al.*, 2008). ISV, a predominant feature in the Makassar Strait throughflow timeseries, is defined as oscillations varying at periods of 20-90 days.

The findings of the comprehensive analysis of various datasets, which consist of the moored velocity vector and temperature time series and of *insitu* and satellite-derived wind and sea level anomaly time series in Makassar Strait and the region, provide a general description on the intraseasonal features in Makassar Strait which can be summarized as follows:

- The ISV in Makassar Strait can be classified according into its energy origin: the locally generated and remotely forced variability. The locally generated ISV extracts its energy from the local winds and eddies, while the remotely forced ISV is linked to the Kelvin waves originating in the Indian Ocean and to the Sulawesi Sea eddies.

- The intraseasonal local wind energy is projected onto the Makassar Strait although it is confined only within the upper 50 m of the water column. Time series of the local wind and along-strait flow in the upper 50 m are found statistically coherent across the periods of 45-90 days with the 60-day oscillation shows the largest amplitude. The coherence is however significant only during 2004-2005 and the final half of 2006, and the reason why the along-strait flow is uncoupled to the wind in the first few months

of 2006 remains elusive. Nevertheless we suspect that it is due to the pycnocline deepening phase attributed to a mild La Niña phase occurring from November 2005 to May 2006, which may inhibit wind derived momentum transfer from the ocean surface to deeper levels.

- Another locally generated intraseasonal feature is observed in Makassar Strait varying at periods of 20-40 days, trapped at depths of 100-300 m and expressing the following eddy characteristics:

  ♢ The velocity vectors indicate that the across-strait flow is more energetic than the along-strait flow. The more energetic current in the across-strait direction is what one would measure if an ideal vortex were advected within a strait whose main axis is parallel with the along-strait axis.

  ♢ The 20-40 day variability distinctively characterizes the relative vorticity data inferred from the along-strait flow observed from two moorings separated by a distance of ∼19 km across a ∼60 km width channel. The relative vorticity data at 20-40 days over ∼3 years observation show 35 events at which the along-strait flow fluctuations in Mak-West and Mak-East moorings are in opposite direction, which suggests that the eddy center slices through in between the mooring.

  ♢ A positive (negative) relative vorticity phase is preceded with eastward (westward) across-strait flow, a relationship that observation and simulated velocity vector of a Rankine vortex agree on. This relationship illustrates that if a southward-advected eddy center were relatively to the north of a mooring site, the mooring would first record eastward (westward) across-strait flow for an anticlockwise (clockwise) eddy. The across-strait flow magnitude would then decrease, as the eddy center approached the mooring, and become zero if the mooring were right at the eddy center. As the eddy further moved southward, the corresponding across-strait flow turned westward (eastward) for an anticlockwise (clockwise) eddy and showed maximum speed if the mooring were positioned right at the eddys edge.

  ♢ The thermal field and relative vorticity are linked and signify potential vorticity

conservation as the isopycnals in the lower pycnocline shoal (dip down) when the flow field exhibits positive (negative) relative vorticity associated with an anticlockwise (clockwise) eddy.

- The model velocity vector data indicate that the eddies are likely generated in the northern Makassar Strait at latitudes of 0.5°-2° S and across depths of 100-300 m, where the eddy kinetic energy (EKE) associated with the 20-40 day variability is found most energetic. Furthermore the model data show that the maximum EKE in the northern Makassar Strait basin is attributed to the ITF instability.

- The Makassar Strait variability varying at periods of 45-90 days, displaying its strongest signatures at the pycnocline, is related to the ISV in the tropical Indian Ocean and Sulawesi Sea.

- The 60-90 day variation, notably marking the weakened ITF phases in the Makassar Strait pycnocline, shows the following Kelvin wave characteristics:

  ♢ Vertical energy propagation. The composite of the along-strait flow exhibits an upward phase tilt, indicative of downward energy propagation with a non-local origin. Moreover a quarter cycle of phase lag in temperature fluctuation with respect to along-strait flow fluctuation also favors downward energy propagation.

  ♢ Normal mode approximation. Vertical structure of the along-strait flow is well approximated by that of normal mode-derived velocity vector attributed to a Kelvin wave.

  ♢ Energy equipartition. Vertical structures of available potential energy and kinetic energy have similar amplitudes, which indicate that the intraseasonal energy is equally divided between kinetic and potential energy.

  ♢ Non-dispersive relation. The along-strait flow data in Makassar and Lombok Strait demonstrate a dispersion relation consistent with a Kelvin wave.

  ♢ Semi-geostrophic balance and enhanced decay scale. During a Kelvin wave passage, the across-strait gradient of sea level anomaly is balanced by the across-strait component of coriolis force, while the along-strait gradient of sea level

anomaly is not balanced by the along-strait component of coriolis, which suggests a partial geostrophic balance attributed to a Kelvin wave. The observed increased across-strait decay scale during an incoming Kelvin wave passage might indicate the presence of a reflected Kelvin wave, a necessary element to preserve the continuity of pressure at the strait mouth.

- The 60-90 day Kelvin waves in Makassar Strait emanate from the tropical Indian Ocean as wind-forced equatorial Kelvin waves impinging upon the west coast of Sumatra propagating along a waveguide extending from the southwestern coasts of the Indonesian archipelago to Makassar Strait, via Lombok Strait. From Lombok Strait to Makassar Strait, the Kelvin wave navigates along the 100-m isobath with a vertical structure resembling that of the 2nd baroclinic Kelvin wave.

- The intraseasonal Kelvin wave episode in Makassar Strait induces increased vertical shear of the along-strait flow across the pycnocline, which potentially leads to instability with a vertical mixing rate of 1-5x10^{-5} m^2/s. The Kelvin waves also force the ITF transport anomalies in the Makassar Strait. A downwelling Kelvin wave reduced the southward Makassar Strait throughflow by up to 2 Sv in May 2005.

- The 45-90 day oscillations in Makassar Strait are also likely forced by the intraseasonal eddies in Sulawesi Sea. The satellite-derived SLA and their corresponding geostrophic currents in Sulawesi Sea show the basin-sized eddies periodically generated at 50-70 days. The satellite-derived data also indicate that the intraseasonal eddies in Sulawesi Sea are not stationary but display westward propagation at a speed of 0.2 m/s towards the east Kalimantan coast, before being squeezed into Makassar Strait. Due to some concerns on the SLA data quality in Makassar Strait, the data are not further used to track southward advection of the eddy within Makassar Strait. However the SLA in Sulawesi Sea and the along-strait flow in Makassar Strait are significantly coherent at periods of 50-70 days with a phase lag that implies propagation into Makassar Strait. Thus the ISV in Sulawesi Sea might contribute to that in Makassar Strait.

The INSTANT program has improved our understanding of the intraseasonal processes in Makassar Strait and the region through providing spatially and temporally better mea-

sured datasets. Unlike the ARLINDO measurement sites that collected ∼1.5 year datasets (Gordon *et al.*, 1999), the INSTANT moorings recorded ∼3-year data and identify, with an improved statistical confidence, the dominant variability at intraseasonal timescales. The INSTANT data also well resolve the vertical and zonal structures of the intraseasonal eddies and Kelvin waves in Makassar Strait, intraseasonal features which the ARLINDO data could not demonstrate.

Moreover the INSTANT program simultaneously monitored the Indonesian Throughflow (ITF) variability at the main throughflow passages including Lombok Strait (Sprintall *et al.*, 2004; Gordon *et al.*, 2010), which provides a synoptic picture of the ITF and enables us to estimate the pathway guiding the Kelvin wave from Lombok Strait to Makassar Strait. Nevertheless there is always more to do and we hope that the findings of this study can be used to guide future work as well. We consider the following open questions would benefit from additional study:

- Mooring observations indicate that the footprint of the eastern tropical Indian Ocean Kelvin wave is detected along the southern coasts of Indonesian archipelago (Drushka *et al.*, 2010) and within the internal Indonesian seas at Makassar Strait. Moreover, Sections 3.3.3.1 and 3.3.3.2 demonstrate a significant relationship between a Kelvin wave event and temperature fluctuation within the pycnocline, but the impact of the event on the sea surface temperature (SST) has not been discussed. Because the SST variability across the Indonesia region is of paramount importance to convective distribution (Qu *et al.*, 2005), it is hence interesting to investigate the influence of Kelvin wave passage on modulating the SST and precipitation variability over Indonesia. Satellite-derived SST and precipitation data across the maritime continent region would be useful for the analysis.

- The ecological consequence of Kelvin wave passage across the Indonesian seas needs to be investigated. Chapter 3 demonstrates that the northward along-strait flow observed within the Makassar Strait pycnocline depths and occurring at timescales of 2-3 months is linked to a downwelling Kelvin wave propagating along the southern coasts of Indonesia archipelago, which is forced by westerlies along the tropical eastern Indian Ocean. Warmer SST, characterizing a downwelling Kelvin wave event, is not

suitable for increased biological activity such as phytoplankton bloom. Elevated surface chlorophyl, on the other hand, could be attributed to an upwelling Kelvin wave. Murtugudde *et al.*1999 proposed that the anomalously increased surface chlorophyl in the tropical Indo-Pacific basin, which signaled the end of the 1997-1998 El Niño, was related to persistent northerly anomalies resulting in an upwelling Kelvin wave. Drushka *et al.*(2010) argued that both downwelling and upwelling intraseasonal Kelvin waves, originating in the equatorial Indian Ocean, forced the intraseasonal variability in the outflow passages of the ITF. Thus impact of an upwelling Kelvin wave on phytoplankton productivity within the Indonesian waters is still an open question, and analyses of high resolution ocean color data provided by the Sea-viewing Wide Field of view Sensor (SeaWiFs) satellite would be practical for the study .

- What is the fate of Kelvin wave transient beyond the Makassar mooring in the Labani Channel? How is the wave interaction with the ITF as the background flow? Do the monthly eddies in Makassar Strait play a role in Kelvin wave dissipation? The answers would help determine whether Kelvin wave energy is completely dissipated within Makassar Strait or preserved to perturb temperature fluctuation in the Western Pacific region. Kessler *et al.*(1995) suggested that the MJO-generated Kelvin waves in the equatorial Pacific Ocean contribute to the onset of the El Niño 1991-1992. This study would require some numerical experiments since no useful data are available in Makassar Strait besides those from the INSTANT program.

- The impact of El Niño-Southern Oscillations (ENSO) and Indian Ocean Dipole (IOD) on the Makassar Strait ISV. Chapter 2 discusses the dependence of the Makassar Strait ISV on ENSO: the lower thermocline ISV is intensified (weakened) during El Niño (La Niña). Chapter 2 discusses a strong northward flow associated with a Kelvin wave passage was not observed in Makassar Strait in May 2006, following a mild La Niña between November 2005 and April 2006, although the wave was strongly observed in May 2004 and 2005. Sustained southward ITF transport in May 2006, however, may also be linked to anomalously weaker intraseasonal Kelvin wave signature in the equatorial Indian Ocean. Horii *et al.*(2008) reported that the upper 100-meter zonal

current along the tropical Indian Ocean was westward in May-June 2006 preceding the positive IOD period in the fall of 2006 although the zonal current climatology over the equatorial Indian Ocean region during the monsoon transition months is eastward. Thus both ENSO and IOD could control the strength of the ISV in Makassar Strait, but which one is more influential? To address this question, longer time series both in Makassar Strait and in the equatorial Indian Ocean are required. The research moored array for African-Asian-Australian monsoon analysis and prediction (RAMA; McPhaden *et al.*, 2009) and Makassar-ITF (Gordon *et al.*, 2012) mooring datasets might be utilized in future studies.

Bibliography

[Allen and Romea, 1980] J. S. Allen and R. D. Romea. On coastal trapped waves at low latitude in a stratified ocean. *Journal of Fluid Mechanis*, 98(3):555–585, 1980.

[Arief and Murray, 1996] D. Arief and S. P. Murray. Low frequency fluctuations in the indonesian throughflow through lombok strait. *Journal of Geophysical Research*, 101:12455–12464, 1996.

[Byrden and Imawaki, 2001] H.L. Byrden and S. Imawaki. Ocean transport of heat. in: ocean circulation and climate, g. seidler, j. church and j. gould. *Academic Press, Inc., London, U.K.*, 2001.

[Codiga *et al.*, 1999] D.L. Codiga, D. P. Renouard, and A. Fincham. Experiments on waves trapped over the continental slope and shelf in a continuously stratified rotating ocean, and their incidence on a canyon. *Journal of Marine Research*, 57:585–612, 1999.

[Cravette *et al.*, 2004] S. Cravette, J. Boulanger, and J. Picaut. Reflection of intraseasonal equatorial rossby waves at the western boundary of the pacific ocean. *Geophysical Research Letters*, 31:L10301, 2004.

[Drushka *et al.*, 2010] K. Drushka, J. Sprintall, S. Gille, and I. Brodjonegoro. Vertical structure of kelvin waves in the indonesian throughflow exit passages. *Journal of Physical Oceanography*, 40:1965–1987, 2010.

[Ducet *et al.*, 2000] N. Ducet, P. Y. Le Traon, and G. Reverdin. Global high-resolution mapping of ocean circulation from topex/poseidon and ers-1 and -2. *Journal of Geophysical Research*, 105:19477–19498, 2000.

[Durland and Qiu, 2003] T. Durland and B. Qiu. Transmission of subinertial kelvin waves through a strait. *Journal of Physical Oceanography*, 33:1337–1350, 2003.

[Ffield and Gordon, 1992] A. Ffield and A. L. Gordon. Vertical mixing in the indonesian thermocline. *Journal of Physical Oceanography*, 22:184–195, 1992.

[Ffield *et al.*, 2000] A. Ffield, K. Vranes, A. L. Gordon, R. D. Susanto, and S. L. Garzoli. Temperature variability within makassar strait. *Geophysical Research Letters*, 27:237–240, 2000.

[Fisher *et al.*, 1987] N. I. Fisher, T. Lewis, and B. J. J. Embleton. *Statistical Analysis of Spherical Data*. Cambridge University Press, 1987.

[Gill, 1982] A. E. Gill. *Atmosphere-Ocean Dynamics*. Academic press, New York, 1982.

[Gordon and Fine, 1996] A. L. Gordon and R. A. Fine. Pathways of water between the pacific and indian oceans in the indonesian seas. *Nature*, 379:146–149, 1996.

[Gordon and Kamenkovich, 2010] A. L. Gordon and V. M. Kamenkovich. Modelling and observing the indonesian throughflow. a special issue of dynamics of atmosphere and oceans. *Dynamics of Atmosphere and Oceans*, 50:113–114, 2010.

[Gordon and Susanto, 1999] A. L. Gordon and R. D. Susanto. Makassar strait transport: initial estimate based on arlindo results. *Marine Technology Society*, 26:34–45, 1999.

[Gordon *et al.*, 1999] A. L. Gordon, R. D. Susanto, and A. Ffield. Throughflow within makassar strait. *Geophysical Research Letters*, 26:3325–3328, 1999.

[Gordon *et al.*, 2003] A. L. Gordon, R. D. Susanto, and K. Vranes. Cool indonesian throughflow as a consequence of restricted surface layer flow. *Nature*, 425:824–828, 2003.

[Gordon *et al.*, 2008] A. L. Gordon, R. D. Susanto, A. Ffield, B. A. Huber, W. Pranowo, and S. Wirasantosa. Makassar strait throughflow 2004 to 2006. *Geophysical Research Letters*, 35(L24605), 2008.

[Gordon *et al.*, 2010] A. L. Gordon, J. Sprintall, H. M. Van Aken, R. D. Susanto, S. Wijffels, R. Molcard, A. Ffield, W. Pranowo, and S. Wirasantosa. The indonesian throughflow

during 2004-2006 as observed by the instant program. *Dynamics of Atmosphere and Oceans*, 50:115–128, 2010.

[Gordon *et al.*, 2012] A. L. Gordon, B. A. Huber, E. Joseph Metzger, R. D. Susanto, Harley. E. Hurlburt, and T. Rameyo Adi. South china sea throughflow impact on the indonesian throughflow. *Geophysical Research Letters*, 39(L11602), 2012.

[Gordon, 2005] A. L. Gordon. Oceanography of the indonesian seas and their throughflow. *Oceanography*, 18(4):14–27, 2005.

[Grinsted *et al.*, 2004] A. Grinsted, J. C. Moore, and S. Jevrejeva. Application of the cross-wavelet transform and wavelet coherence to geophysical time series. *Nonlinear Processes in Geophysics*, 11(5), pages = 561-566,), 2004.

[Hallock *et al.*, 2009] Z. R. Hallock, W. J. Teague, and E. Jarosz. Subinertial slope-trapped waves in the northeastern gulf of mexico. *Journal of Physical Oceanography*, 39(1474-1485), 2009.

[Horii *et al.*, 2008] T. Horii, H. Hase, I. Ueki, and Y. Masumoto. Oceanic precondition and evolution of the 2006 indian ocean dipole. *Geophysical Research Letters*, 35(L03607), 2008.

[Iskandar *et al.*, 2005] I. Iskandar, W. Mardiansyah, Y. Masumoto, and T. Yamagata. Intraseasonal kelvin waves along the southern coast of sumatra and java. *Journal of Geophysical Research*, 110:C04013, 2005.

[Kashino *et al.*, 1999] Y. Kashino, H. Watanabe, B. Herunadi, M. Aoyama, and D. Hartoyo. Current variability at the pacific entrance of the indonesian throughflow. *Journal of Geophysical Research*, 104:11021–11035, 1999.

[Kessler *et al.*, 1995] W. S. Kessler, M. J. McPhaden, and K. M. Weickmann. Forcing of intraseasonal kelvin waves in the equatorial pacific. *Journal of Geophysical Research*, 100(C6):10613–10631, 1995.

[Lilly and Rhines, 2002] J. M. Lilly and P. B. Rhines. Coherent eddies in the labrador sea observed from a mooring. *Journal of Physical Oceanography*, 32:585–598, 2002.

[Madden and Julian, 1971] R. A. Madden and P. R. Julian. Detection of a 40-50 day oscillation in the zonal wind in the tropical pacific. *Journal of Atmospheric Sciences*, 28:702–708, 1971.

[Masumoto *et al.*, 2001] Y. Masumoto, T. Kagimoto, M. Yoshida, M. Fukuda, N. Hirose, and T. Yamagata. Intraseasonal eddies in the sulawesi sea simulated in an ocean general circulation model. *Geophysical Research Letters*, 28:1631–1634, 2001.

[Masumoto *et al.*, 2005] Y. Masumoto, H. Hase, Y. Kuroda, H. Matsuura, and K. Takeuchi. Intraseasonal variability in the upper layer currents observed in the eastern equatorial indian ocean. *Geophysical Research Letters*, 32:L02607, 2005.

[Mcbride and Frank, 1996] J. L. Mcbride and W. M. Frank. Relationships between stability and monsoon convection. *Journal of Atmospheric Sciences*, 56:24–36, 1996.

[McCreary, 1984] J. McCreary. Equatorial beams. *Journal of Marine Research*, 42:395–430, 1984.

[McPhaden *et al.*, 2009] M. J. McPhaden, G. Meyers, K. Ando, Y. Masumoto, V. S. N. Murty, M. Ravichandran, F. Syamsudin, J. Vialard, L. Yu, and W. Yu. Rama: The research moored array for african-asian-australian monsoon analysis and prediction. *Bulletin of American Meteorological Society*, 90:459–480, 2009.

[Metzger *et al.*, 2010] E.J. Metzger, H. E. Hurlburt, X. Xu, J. F. Shriver, A. L. Gordon, J. Sprintall, R. D. Susanto, and H. M. Van Aken. Simulated and observed circulation in the indonesian seas: $1/12^\circ$ global hycom and the instant observations. *Dynamics of Atmospheres and Oceans*, 57:275–300, 2010.

[Murtugudde *et al.*, 1999] R. G. Murtugudde, S. R. Signorini, J. R. Christian, A. J. Busalacchi, C. R. McClain, and J. Picaut. Ocean color variability of the tropical indo-pacific basin observed by seawifs during 1997-1998. *Journal of Geophysical Research*, 104(C8):18351–18366, 1999.

[Pedlosky, 2003] J. Pedlosky. *Waves in the ocean and atmosphere*. Springer-Verlaag, 2003.

[Percival and Walden, 1993] D. B. Percival and A.T. Walden. Spectral analysis for physical applications, multitaper and conventional univariate techniques. *Cambridge University press*, 1993.

[Pujiana *et al.*, 2009] K. Pujiana, A. L. Gordon, J. Sprintall, and R. D. Susanto. Intraseasonal variability in the makassar strait thermocline. *Journal of Marine Research*, 67:757–777, 2009.

[Qiu *et al.*, 1999] B. Qiu, M. Mao, and Y. Kashino. Intraseasonal variability in the indo-pacific throughflow and the regions surrounding the indonesian seas. *Journal of Physical Oceanography*, 29:1599–1618, 1999.

[Qu *et al.*, 2005] T. Qu, Y. Du, J. Strachan, G. Meyers, and J. Slingo. Sea surface temperature and its variability in the indonesian region. *Oceanography*, 18:50–61, 2005.

[Qu *et al.*, 2008] T. Qu, J. Gan, A. Ishida, Y. Kashino, and T. Tozuka. Semiannual variation in the western tropical pacific ocean. *Geophysical Research Letters*, 35:L16602, 2008.

[Schiller *et al.*, 2010] A. Schiller, S. E. Wijffels, J. Sprintall, R. Molcard, and P. R. Oke. Pathways of intraseasonal variability in the indonesian throughflow region. *Dynamics of Atmospheres and Oceans*, 50:174–200, 2010.

[Schneider, 1998] N. Schneider. The indonesian throughflow and the global climate system. *Journal of Climate*, 11:678–689, 1998.

[Schoellhamer, 2001] D. H. Schoellhamer. Singular spectrum analysis for time series with missing data. *Geophysical Research Letters*, 28(16):3187–3190, 2001.

[Sprintall *et al.*, 2000] J. Sprintall, A.L. Gordon, R.Murtugudde, and R.D. Susanto. A semiannual indian ocean forced kelvin wave observed in the indonesian seas in may 1997. *Journal of Geophysical Research*, 105(C7):17217–17230, 2000.

[Sprintall *et al.*, 2004] J. Sprintall, S. Wijffels, A.L. Gordon, A. Ffield, R. Molcard, R.D. Susanto, I. Soesilo, J. Sopaheluwakan, Y. Surachman, and H. Van Aken. A new international array to measure the indonesian throughflow. *EOS Trans. AGU*, 85(39), 2004.

[Sprintall *et al.*, 2009] J. Sprintall, S. Wijffels, R. Molcard, and I. Jaya. Direct estimates of indonesian throughflow entering the indian ocean: 2004-2006. *Journal of Geophysical Research*, 114:C07001, 2009.

[Susanto *et al.*, 2000] R.D. Susanto, A.L. Gordon, J. Sprintall, and B. Herunadi. Intraseasonal variability and tides in makassar strait. *Geophysical Research Letters*, pages 1499–1502, 2000.

[Syamsudin *et al.*, 2004] F. Syamsudin, A Kaneko, and D. B. Haidvogel. Numerical and observational estimates of indian ocean kelvin wave intrusion into lombok strait. *Geophysical Research Letters*, 31:L24307, 2004.

[Thorpe, 2004] S. A. Thorpe. Recent developments in the study of ocean turbulence. *Annual Review of Earth and Planetary Sciences*, pages 91–109, 2004.

[Tillinger and Gordon, 2010] D. Tillinger and A. L. Gordon. Fifty years of the indonesian throughflow. *Journal of Climate*, 22:6342–6355, 2010.

[Torrence and Compo, 1998] C. Torrence and G. P. Compo. A practical guide to wavelet analysis. *Bulletin of the American Meteorological Society*, 79:61–78, 1998.

[Wheeler *et al.*, 2000] M. Wheeler, G.N. Kiladis, and P. J. Webster. Large-scale dynamical fields associated with convectively coupled equatorial waves. *Journal of Atmospheric Sciences*, 57:613–640, 2000.

[Wijffels and Meyers, 2004] S. Wijffels and G. Meyers. An intersection of oceanic waveguides: Variability in the indonesian throughflow region. *Journal of Physical Oceanography*, 34:1232–1253, 2004.

[Zhou and Murtugudde, 2010] L. Zhou and R. Murtugudde. Influences of madden-julian oscillations on the eastern indian ocean and the maritime continent. *Dynamics of Atmospheres and Oceans*, 50:257–274, 2010.